

# Measurement report: Stoichiometry of dissolved iron and aluminum as an indicator of the factors controlling the fractional solubility of aerosol iron: Results of the annual observations of size-fractionated aerosol particles in Japan

5 Kohei Sakata<sup>1\*</sup>, Aya Sakaguchi<sup>2</sup>, Yoshiaki Yamakawa<sup>3</sup>, Chihiro Miyamoto<sup>3</sup>, Minako Kurisu<sup>4</sup>, Yoshio Takahashi<sup>3</sup>

<sup>1</sup>Earth System Division, National Institute for Environmental Studies, 16-2 Onogawa, Tsukuba, Ibaraki 305-8506, Japan

<sup>2</sup>~~Faculty~~<sup>2</sup>Institute of Pure and Applied Science, University of Tsukuba, 1-1-1 Tennodai, Tsukuba, Ibaraki 305-~~8574~~8577, Japan

<sup>3</sup>Graduate School of Science, the University of Tokyo, 7-3-1 Hongo, Bunkyo-ku, Tokyo, 113-0033, Japan

<sup>4</sup>Research Institute for Marine Resources Utilization, Japan Agency for Marine-Earth Science and Technology, 2-15

10 Natsuhshima-cho, Yokosuka, Kanagawa 237-0061, Japan

*Correspondence to:* Kohei Sakata ([sakata.kohei@nies.go.jp](mailto:sakata.kohei@nies.go.jp))

## Abstract.

15 ~~Atmospheric deposition of iron (Fe) in aerosol particles is enhanced primary production on the ocean surface, resulting in promoting the uptake of carbon dioxide into the surface seawater. Atmospheric~~The atmospheric deposition of iron (Fe) promotes primary production in the surface ocean, ~~resulting~~which results in ~~the~~ enhanced uptake of carbon dioxide into surface seawater. ~~Since~~Given that microorganisms in seawater utilize dissolved Fe (d-Fe) as a nutrient, the bioavailability of Fe in aerosol particles depends on its solubility. However, ~~the~~ factors controlling fractional Fe solubility ( $Fe_{sol}\%$ ) in aerosol particles

20 have not been fully understood. This study performed annual observations of  ~~$Fe_{sol}\%$~~ the total and dissolved metal concentrations in size-fractionated (seven fractions) aerosol particles at Higashi-Hiroshima, Japan. ~~In particular, the~~The feasibility of the molar concentration ratio of d-Fe relative to dissolved Al ( $[d-Fe]/[d-Al]$ ) as an indicator of ~~the~~ sources of d-Fe in aerosol particles ~~was investigated~~ because this ratio is likely dependent on the emission sources of Fe (e.g., mineral dust, fly ash, and anthropogenic Fe oxides) and their dissolution processes (proton-~~promoted~~ and ligand-promoted dissolutions). Approximately

25 70 % of ~~the~~ total Fe ~~and dissolved Fe was~~in total suspended particulate (TSP) were present in coarse ~~and fine~~ aerosol particles, ~~respectively, and the~~whereas about 70% of d-Fe in TSP were mainly found in fine aerosol particles. The average  $Fe_{sol}\%$  in fine aerosol particles ( $11.4 \pm 6.977.0$  %) was higher than that of coarse aerosol particles ( $2.19 \pm 2.27\%$ ). In addition, the average ratio of  $[d-Fe]/[d-Al]$  in coarse aerosol particles ( $0.408 \pm 0.168$ ) was lower than that in fine aerosol particles ( $1.15 \pm 0.80380$ ). The range of  $[d-Fe]/[d-Al]$  ratios in the coarse aerosol particles (0.121–0.927) was similar to that obtained by proton-promoted

30 ~~dissolutions~~dissolution of mineral dust (0.1–1.0), ~~indicating~~which indicates that ~~the~~ d-Fe in coarse aerosol particles ~~were~~was derived from mineral dust. The  $[d-Fe]/[d-Al]$  ratios of fine aerosol particles ranged from 0.386 to 4.67, and  $[d-Fe]/[d-Al]$  ratios greater than 1.550 cannot be explained by proton-~~promoted dissolution~~ and ligand-promoted ~~dissolution~~dissolutions ( $1.000 < [d-Fe]/[d-Al] < 1.550$ ). The  $[d-Fe]/[d-Al]$  ratio correlated with the enrichment factor of Fe in fine aerosol particles ( $r: 0.505$ ), ~~indicating~~which indicates that anthropogenic Fe with a high  $[d-Fe]/[d-Al]$  ratio was the source of d-Fe in fine aerosol particles.

35 The high  $[d-Fe]/[d-Al]$  ratio was attributed to anthropogenic Fe-oxides emitted from high-temperature combustions-~~(high-temp FeOx)~~. Finally, the fraction of high-temp FeOxanthropogenic Fe oxides to d-Fe in total suspended particulate (TSP) was calculated based on the  $[d-Fe]/[d-Al]$  ratio of aerosols and their emission source samples. As a result, the fraction of high-temp FeOxanthropogenic Fe oxides to d-Fe in TSP varied from 1.48 % to 80.7 %. ~~The~~A high fraction was ~~found~~observed in summer when air masses originated from industrial regions in Japan. By contrast, approximately 10 % of d-Fe in the TSP

40 samples collected in spring and during Asian dust events was derived from high-temp FeOxanthropogenic Fe oxides when air masses ~~were~~ frequently transported from East Asia to the Pacific Ocean. Thus, mineral dust ~~is~~was the dominant source of d-Fe in Asian outflow to the Pacific Ocean.

## 1. Introduction

Primary production in high-nutrient, low-chlorophyll regions, such as the North Pacific, Eastern Equatorial Pacific, and Southern Ocean, is limited by the depletion of dissolved Fe (d-Fe, Martin and Fitzwater, 1988; Boyd et al., 2007; Moore et al., 2013; Tagliabue et al., 2017). The atmospheric deposition of Fe activates primary productions in surface seawater, ~~enhancing which enhances~~ the oceanic uptake of atmospheric CO<sub>2</sub> (Martin, 1990; Martin et al., 1994; Falkowski et al., 2000; Jickells et al., 2005). In the last glacial–interglacial period, ~~the~~ atmospheric CO<sub>2</sub> concentration was inversely correlated with the supply of mineral dust to the Southern Ocean (Martínez-García et al., 2009, 2011, 2014). Thus, the fertilization of d-Fe in surface seawater via aerosol deposition is an important driver of the global climate system. Given that phytoplankton in surface seawater utilizes d-Fe as ~~nutrients~~ ~~nutrient~~, the bioavailability of Fe in aerosol particles depends on ~~their~~ ~~its~~ solubility (Moore et al., 2013). Iron in aerosols ~~is not highly~~ ~~has low solubility in~~ water-soluble, and the ~~solubility of~~ fractional Fe ~~solubility~~ ( $Fe_{sol}\% = \frac{\text{dissolved (d-Fe)}}{\text{total Fe}} \times 100$ ) in marine aerosols ranges from 0.1 % to 90 % (Sholkovitz et al., 2012; Mahowald et al., 2018). ~~Differences in~~ ~~Factors controlling~~ ~~Fe<sub>sol</sub>% include the differences in the~~ ~~Fe<sub>sol</sub>% among emission sources (e.g., mineral dust~~ ~~vs-versus~~ anthropogenic aerosol) and ~~the~~ atmospheric processes of Fe-bearing particles ~~are factors controlling~~ ~~Fe<sub>sol</sub>%~~ (Sedwick et al., 2007; Sholkovitz et al., 2009; Mahowald et al., 2018; Ito et al., 2019, 2021). ~~In fact,~~ ~~In addition,~~ ~~previous studies revealed that the factors have size dependences because~~ fine aerosol particles ~~have been found to~~ yield higher Fe<sub>sol</sub>% than coarse aerosol particles derived from either or both anthropogenic Fe and atmospheric processes, ~~as a result of size-fractionated samplings of marine aerosols~~ (Buck et al., 2010a; Chance et al., 2015; Sakata et al., 2018; Kurisu et al., 2021; Baker and Jickells, 2006, 2017; Baker et al., 2020; Gao et al., 2019). ~~However, the factors controlling~~ ~~Fe<sub>sol</sub>% in aerosol particles have not been fully understood.~~

~~The source~~ ~~Source~~ apportionment of ~~dissolved~~ ~~d-Fe~~ in aerosol particles has been conducted ~~based on the basis of~~ the correlation analysis of Fe<sub>sol</sub>% with the concentrations and enrichment factors (EFs) of coexisting elements. ~~For example,~~ ~~the~~ ~~The~~ EFs of ~~vanadium (V)~~ and ~~lead (Pb)~~ are used as tracer elements of heavy-oil and coal combustion processes, respectively (Sholkovitz et al., 2009; Conway et al., 2019; Hsieh et al., 2022). ~~Indeed,~~ ~~the~~ ~~The~~ correlations of Fe<sub>sol</sub>% with the EFs of V and Pb are useful for evaluating the presence of anthropogenic Fe. However, quantitative ~~evaluating~~ ~~evaluation of~~ the fraction of anthropogenic Fe in d-Fe in aerosol particles is difficult. Therefore, an indicator that can estimate the fraction of anthropogenic Fe in d-Fe in aerosols is required to evaluate quantitatively the Fe supply from aerosols to the ocean surface. The fraction of anthropogenic Fe ~~has~~ ~~was~~ recently ~~been~~ ~~estimated by~~ using the Fe isotope ratio ( $\delta^{56}\text{Fe}$ ) ~~because~~; anthropogenic Fe has a lower  $\delta^{56}\text{Fe}$  than mineral dust (Kurisu et al., 2016a and b, 2019, 2021; Conway et al., 2019). Although the  $\delta^{56}\text{Fe}$  of total Fe in marine aerosol particles has been reported by previous studies, data on the  $\delta^{56}\text{Fe}$  of d-Fe in marine aerosol particles are limited due to analytical difficulties, including high filter blanks (Conway et al., 2019; Kurisu et al., 2021). ~~Considering~~ ~~Given~~ that the ~~fractions~~ ~~fraction~~ of anthropogenic Fe in d-Fe depends on the Fe<sub>sol</sub>% of anthropogenic Fe and mineral dust, the contribution of ~~non-crustal~~ ~~anthropogenic~~ Fe ~~into the~~ total Fe is not always directly reflected ~~into~~ that of d-Fe. Therefore, ~~attaining~~ the

75 ~~ability~~capability to produce indicators for ~~the~~ source estimation of d-Fe in aerosol particles with low analytical difficulty is ideal.

The stoichiometry of the mineral dissolution of major elements (e.g., Si, Al, Fe, and Mg) has been investigated to understand the dissolution processes of minerals in the environment (Acker and Bricker, 1992; Brantley et al., 2008; Bibi et al., 2011; Bray et al., 2015). The stoichiometry of mineral dissolution is controlled by acid type, pH, and ionic strength, ~~as well~~  
80 ~~as and~~ the presence or absence of organic ligands (Brantley et al., 2008; Bray et al., 2015). Therefore, the ratios of dissolved concentrations of major elements vary depending on their dissolution processes from ~~the~~ minerals (Acker and Bricker, 1992; Brantley et al., 2008; Bibi et al., 2011; Bray et al., 2015). However, studies on Fe dissolution from aerosols have focused exclusively on Fe and ~~have paid little attention to neglected~~ other dissolved metals in aerosol particles. In general, although the stoichiometry of mineral dissolution is discussed based on the ratio of the dissolution rate of major elements versus that of Si  
85 (Acker and Bricker, 1992; Brantley et al., 2008; Bibi et al., 2011; Bray et al., 2015), the data on total and dissolved Si concentrations in aerosol particles are limited relative to those on Fe and Al concentrations (Jickells et al., 2016). ~~Discussing~~Discussion of the dissolution processes of mineral dust ~~by using Mg concentrations~~concentration is difficult because Mg in marine aerosol particles is usually derived from sea spray aerosol (~~SSA~~). Therefore, this study focused on the molar ratio of d-Fe to dissolved Fe to Al ( $[d-Fe]/[d-Al]$ ) ~~in aerosol particles as the an~~ indicator of the sources of d-Fe in aerosol  
90 particles because (i) previous studies have frequently determined d-Fe and d-Al concentrations in aerosol particles, and (ii) mineral dust is the dominant source of Fe and Al.

Iron-bearing particles derived from mineral dust and anthropogenic Fe have different chemical compositions and mineralogy. Mineral dust is mainly composed of crystalline aluminosilicates (Jeong and Achterberg, 2014; Jeong et al., 2014; Jeong, 2020). ~~Fly~~The fly ash emitted from anthropogenic high-temperature combustion processes can be categorized into two  
95 groups: non-magnetic and magnetic particles. Non-magnetic particles in fly ash consist of aluminosilicate glass (Furuya et al., 1987; Rivera et al., 2015). ~~The dominant Fe species in this~~This fraction is dominated by poorly ordered polymerized hydroxyl Fe(III) (Rivera et al., 2015). The magnetic fraction is composed of crystalline Fe oxides (e.g., hematite and magnetite) formed through the condensation of evaporated Fe during gas cooling (Kukier et al., 2003; Fomenko et al., 2019; Czech, 2022). ~~Both~~  
~~particle types~~Magnetic and non-magnetic particles have been found in ambient aerosol particles (Li et al., ~~2017~~2021; Zhu, Y.  
100 et al., 2020, 2022) ~~and have higher Fe<sub>oxi</sub>% than mineral dust (Kurisu et al., 2016a, 2019).~~ Therefore, ~~the~~ differences in the mineralogy and chemical composition ~~between of~~ mineral dust, ~~non-magnetic, and~~ non-magnetic particles likely possibly affect the  $[d-Fe]/[d-Al]$  ratio in aerosol particles. ~~For example, the~~The  $[d-Fe]/[d-Al]$  ratio of clay minerals ranges from 0.100 to 1.00 (Kodama and Schnitzer, 1973; Lowson et al., 2005; Bibi et al., 2011; Bray et al., 2015), whereas that of fly ash emitted from coal and municipal solid-waste incinerators (MSWIs) is less than 0.4100 (Seidel and Zimmels, 1998; Kim  
105 et al., 2003; Huang et al., 2007). In addition, the  $[d-Fe]/[d-Al]$  ratio of ~~the~~ aggregates of Fe oxide nanoparticles derived from anthropogenic emissions is expected to be higher than that of mineral dust and fly ash because Fe oxide nanoparticles have contain minimal amounts of coexisting elements (Kukier et al., 2003; Fomenko et al., 2019). ~~The~~If the  $[d-Fe]/[d-Al]$  ratio of mineral dust and anthropogenic Fe is generalized, the fractions of mineral dust and anthropogenic Fe in d-Fe in aerosol

particles can be estimated based on the basis of the  $[\text{d-Fe}]/[\text{d-Al}]$  ratio if the  $[\text{d-Fe}]/[\text{d-Al}]$  ratio of mineral dust and anthropogenic Fe is generalized.

In 2013, the annual observation of Fe, Al, and other trace ~~metals~~ metal concentrations and their fractional solubilities in size-fractionated aerosol particles (seven fractions) was conducted in Higashi-Hiroshima, Hiroshima, Japan. ~~Our previous study identified that fine aerosol particles collected (Fig. 1). Air masses at the sampling site contained in summer were mainly derived from the domestic region of Japan, whereas air masses passing over East Asia arrived at the site in winter and spring (Fig. S1). Our sample set included samples affected by Asian dust and serious haze events associated with anthropogenic Fe with a negative  $\delta^{56}\text{Fe}$  (Kurisu et al. 2016a). Therefore, the sampling site is useful~~ emissions, which allowed us to obtain aerosol samples with considerable differences depending on the size dependence and seasonal variation expected for evaluating the availability of the  $[\text{Fe chemistry and d-Fe}]/[\text{d-Al}]$  ratio as an indicator of the fractions of mineral dust and anthropogenic Fe in d-Fe in aerosol particles. In addition, the ground sources. Ground-based long-term observations of  $\text{Fe}_{\text{sol}}\%$  are important for complementing to complement the observed data on  $\text{Fe}_{\text{sol}}\%$  in marine aerosols because (i) mineral dust and anthropogenic Fe (excluding ship emissions) are emitted in continental regions, and (ii) the representativeness of the  $\text{Fe}_{\text{sol}}\%$  data obtained by ship-board observation is often problematic due to the difficulties in the long-term observation of marine aerosol particles at fixed stations (Mahowald et al., 2018). The ground based observation of  $\text{Fe}_{\text{sol}}\%$  in aerosol particles is a strategy for obtaining long term data on  $\text{Fe}_{\text{sol}}\%$  because mineral dust and anthropogenic Fe (excluding ship emissions) are emitted in continental regions. In addition, Fe bearing particles In addition, mineral dust and anthropogenic Fe internally mixed with sulfate, nitrate, and organics are frequently found in the continental atmosphere, indicating which indicates that the chemical aging of Fe-bearing particles begins during transport in continental regions. In the chemical aging of Fe bearing particles during transport from East Asia to the Pacific Ocean, Previous studies reported that atmospheric processing after passing over Japan has a small effect on the  $\text{Fe}_{\text{sol}}\%$  of marine aerosol particles in the case of Fe-bearing particles during their transport from East Asia to the Pacific Ocean (Buck et al., 2013; Sakata et al., 2022). Given that Japan is located at the rim of East Asia (or the entrance of the North Pacific Ocean), and thus, it can collect/accumulate mineral dust and anthropogenic Fe aged during their transport from East Asia to Japan. Therefore, #Japan can be an important observation site for the characterization of aerosols transported to the North Pacific Ocean. This study aims/aimed to evaluate the availability of the source identification of d-Fe in aerosol particles based on  $[\text{d-Fe}]/[\text{d-Al}]$  ratios and to understand/gain insights into the seasonal variability of the fraction/fractions of mineral dust and anthropogenic Fe in d-Fe in aerosols.

## 2. Method

### 2.1. Aerosol sampling

Aerosol sampling was performed at Higashi-Hiroshima, Hiroshima, Japan (Fig. 1;  $34.40^\circ\text{N}$ ,  $132.71^\circ\text{E}$ ). Size-fractionated aerosol particles were collected ~~by~~ using a high-volume air sampler (MODEL 123-SL, Kimoto, Japan) with a ~~sierra~~ Sierra-type

cascade impactor (TE-236, Tisch Environmental Inc., USA) installed on a roof 10 m above ground level. The cascade impactor had seven stages, and the aerodynamic diameters of the aerosol particles collected in each stage from ~~stages~~Stage 1 to ~~Stage~~ 7 followed the order of  $>10.2$ ,  $4.2\text{--}10.2$ ,  $2.1\text{--}4.2$ ,  $1.3\text{--}2.1$ ,  $0.69\text{--}1.3$ ,  $0.39\text{--}0.69$ , and  $<0.39$   $\mu\text{m}$ . ~~Coarse~~The coarse aerosol particles were coarser than  $1.3$   $\mu\text{m}$  (~~stages~~Stages 1 to ~~4~~), whereas ~~the~~ fine aerosol particles were finer than  $1.3$   $\mu\text{m}$  (~~stages~~Stages 5 to ~~7~~). Aerosol particles were collected onto cellulose filters (~~stages~~Stages 1 to ~~6~~: TE-230WH, Tisch Environmental Inc., USA, and ~~S-Stage~~ 7: Whatman 41,  $8 \times 10$  ~~inches~~ $\text{in}^2$ , GE Healthcare, USA). Aerosol samplings during non-dust events were conducted every month from December 2012 to December 2013 (Table S1). The flow rate of the air sampler was fixed at  $0.566$   $\text{m}^3/\text{min}^{-1}$ . The typical sampling period was 2 weeks. However, if the sampling flow rate decreased due to ~~the~~clogging of the ~~stage~~Stage 7 filter, aerosol sampling was immediately stopped. Aerosol samplings were also performed during two dust events associated with haze and Asian dust ~~in~~on January 31, 2013 to February 1, 2013 and ~~on~~March 4, 2013 to March 9, 2013, respectively. Aerosol mass concentrations in China exceeded  $600$   $\mu\text{g m}^{-3}$  at the end of January 2013 (Tian et al., 2014; Wang et al., 2014), and their transported particles can be collected during the haze event. The sampling periods for the ~~polluted~~haze and Asian dust events were 1 and 5 days, respectively, ~~and~~. The sampling periods for haze and Asian dust events were decided based on the basis of a chemical weather forecasting system, which predicted the mass concentrations of Asian dust and sulfate aerosols (Uno et al., 2004). Serious haze events occurred in East Asia at the end of January when aerosol mass concentrations exceeded  $600$   $\mu\text{g}/\text{m}^3$  (Tian et al., 2014; Wang et al., 2014). Therefore, the haze sample was influenced by the serious air pollution event in East Asia. The backwardBackward trajectories at the altitude of  $100$  m were calculated ~~by~~ using the Hybrid Single-Particle Lagrangian-Integrated Trajectory model (Stein et al., 2015). Global Data Assimilation System (GDAS 0.5 degree archive) was used to collect ~~the meteorology~~meteorological data. The total run time was 72 h, and the backward trajectory was calculated every 6 h. Figs. Backward-S1 and S2 show the backward trajectories for non-dust and dust events ~~are shown in Figs. S1 and S2~~, respectively.

## 2.2. Major ion concentrations

Aerosol particles on approximately one-fourth of the filter strips were used for the extraction of major ions ( $\text{Na}^+$ ,  $\text{NH}_4^+$ ,  $\text{K}^+$ ,  $\text{Mg}^{2+}$ ,  $\text{Ca}^{2+}$ ,  $\text{Cl}^-$ ,  $\text{NO}_3^-$ , and  $\text{SO}_4^{2-}$ ) ~~by~~ using  $5$  mL ~~of~~ ultrapure water (MQ, Merck Millipore, USA) in polypropylene vials with ultrasonication for 30 min. Suspended particles in the extract were removed ~~by~~ using a hydrophilic polytetrafluoroethylene (PTFE) filter ( $\phi$ :  $0.20$   $\mu\text{m}$ , DISMIC, ADVANTEC, Tokyo Roshi Kaisha, Ltd., Japan). All materials used for the extraction of major ions were rinsed thrice with MQultrapure water ~~three times~~ before use.

Major ion concentrations were determined through ion chromatography (ICS-1100, Dionex Japan, Japan). The guard columns for cations and anions were Dionex Ion Pack CG12A and AG22, respectively. The separation columns for cations and anions were Dionex CS12A and AS22, respectively. The eluents for cations and anions were methanesulfonic acids and ~~the~~ mixed solution of  $4.5$   $\text{mmol}/\text{L}^{-1}$   $\text{Na}_2\text{CO}_3$  and  $1.4$   $\text{mmol}/\text{L}^{-1}$   $\text{NaHCO}_3$ , respectively. The ~~detail~~detailed procedure of ion chromatography was described ~~by~~in the work of Sakata et al. (2014).

Non-sea-salt (nss)  $K^+$ ,  $Mg^{2+}$ ,  $Ca^{2+}$ , and  $SO_4^{2-}$  concentrations were estimated as follows:

$$[nss-X]_{\text{aerosol}} = [\text{Total-X}]_{\text{aerosol}} - [Na]_{\text{aerosol}} \times ([X]/[Na^+])_{\text{seawater}}, \text{ (Eq. 1)}$$

where X is the molar concentration of either  $K^+$ ,  $Mg^{2+}$ ,  $Ca^{2+}$ , or  $SO_4^{2-}$ . ~~All the quantitative data of the major ions in size-fractionated aerosol particles are shown in Table S2.~~ The molar ratios of  $[K^+]/[Na^+]$ ,  $[Mg^{2+}]/[Na^+]$ ,  $[Ca^{2+}]/[Na^+]$ , and  $[SO_4^{2-}]/[Na^+]$  were 0.0213, 0.113, 0.0213, and 0.0596, respectively (Nozaki, 2001).

### 180 2.3. Estimation of aerosol pH

The aerosol pH of fine aerosol particles was estimated ~~by~~ using the thermodynamic ~~model~~ E-AIM Model IV (Clegg et al., 1998; Friese and Ebel, 2010). The calculation parameters for the model were ~~temperature, relative humidity,~~  $[H^+]$ ,  $[NH_4^+]$ ,  $[Na^+]$ ,  $[Cl^-]$ ,  $[NO_3^-]$ , ~~and~~  $[SO_4^{2-}]$ , ~~temperature, and relative humidity (RH)~~. Ammonia gas concentration was not measured during the sampling campaign. Therefore, aerosol pH was calculated through a reverse mode that tended to overestimate aerosol acidity (Song and Osada, 2020). Previous studies have reported that nonvolatile cations (e.g.,  $Mg^{2+}$  and  $Ca^{2+}$ ) affect the calculation results of aerosol pH (Guo et al., 2018; Pye et al., 2020).  $[Na^+]$  was used as a representative of nonvolatile cations ( $= [Na^+] + [K^+] + 2 \times [Mg^{2+}] + 2 \times [Ca^{2+}]$ ) to estimate aerosol pH because the E-AIM model IV cannot incorporate the concentrations of nonvolatile cations other than  $Na^+$  (Tao and Murphy, 2019a). ~~The~~  $[H^+]$  concentration in aerosol particles was estimated on the basis of ~~the~~ charge balance. Several samples had negative  $[H^+]$  concentrations and were thus excluded from the estimation of aerosol pH. ~~Aerosol pH was calculated by~~ In addition, E-AIM model IV cannot calculate aerosol pH when the RH is below 60 %. The average RH during each sampling period was higher than 60 %, except for those of aerosol samples collected in April and May 2013. The aerosol pH collected in April and May was calculated under the assumption of 60 % RH because the average RHs of the samples for these months were 59.4 % and 59.5 %, respectively. Aerosol pH was calculated using the following equation:

$$195 \quad \text{Aerosol pH} = -\log_{10}(m_{H^+} \times \gamma_{H^+}), \text{ (Eq. 2)}$$

where  $m_{H^+}$  and  $\gamma_{H^+}$  are the molar fraction and activity coefficient of  $H^+$ , respectively.

### 2.4. Trace metal concentrations

200 ~~The target trace metals in this study were Al, Ti, V, Mn, Fe, Co, Ni, Cu, Zn, Cd, Sb, and Pb.~~ Approximately one-fourth of the filter strips ~~was~~ used for acid digestion to determine the total trace metal concentrations. Each filter piece was digested with a mixed acid solution of  $15.2 \text{ mol/L L}^{-1}$   $HNO_3$ ,  $9.3 \text{ mol/L L}^{-1}$   $HCl$ , and  $20 \text{ mol/L L}^{-1}$   $HF$  in a  $7 \text{ mL}$  ~~of~~ perfluoroalkoxyalkane vial heated at  $120 \text{ }^\circ\text{C}$  for 12 h (all mineral acids were procured from TAMAPURE AA-100, Tama Chemicals Co., Ltd., Japan). Subsequently, the mixed acid was evaporated to dryness. The dried residue was dissolved in  $5$  205  $\text{mL}$  ~~of~~  $0.15 \text{ mol/L L}^{-1}$   $HNO_3$  heated at  $120 \text{ }^\circ\text{C}$  for 3 h. The solution was filtered through a hydrophilic PTFE filter ( $\phi$ :  $0.20 \text{ }\mu\text{m}$ , Dismic<sup>®</sup>, 25HP020AN, Advantec, Japan) to prepare the analytical solution. Soluble metals in aerosol particles were extracted ~~by~~ using  $5 \text{ mL}$  ~~of~~ MQuiltrapure water with ultrasonication for 30 min. Then, the extracted solution was filtrated with a

hydrophilic syringe PTFE filter. The filtrated solution was acidified to prepare a 0.15 mol/L HNO<sub>3</sub> solution by ~~adding the~~  
210 ~~addition of~~ 15.3 mol/L HNO<sub>3</sub>. The filtrated solutions for total and dissolved metal concentration analyses were diluted with  
0.15 mol/L HNO<sub>3</sub> by factors of 10–1000.

The total and dissolved metal concentrations of the sample solution were determined via inductively coupled plasma  
mass spectrometry (ICP–MS, Agilent 7700, Agilent, Japan). The sample introduction system consisted of a borosilicate  
nebulizer (MicroMist, Agilent, Japan) and a quartz Scott double-pass spray chamber. The elements in the sample solution were  
215 ionized by ~~an~~ argon plasma (RF power: 1500 W, Ar flow for ~~plasma carrier gas~~: 1.0 L/min<sup>-1</sup>). The ions were introduced into  
the detection system by passing ~~them~~ through ~~Nickel~~ sampling and skimmer cones. The ion beam was focused ~~by using with~~  
x-type ion lenses. ~~The HeHelium~~ collision mode was ~~employed used~~ to reduce interference from oxides (e.g., <sup>40</sup>Ar<sup>16</sup>O<sup>+</sup> for  
<sup>56</sup>Fe). Helium gas was injected into a dynamic reaction cell at a rate of 3.6 mL/min<sup>-1</sup>. Then, mass selection was performed ~~by~~  
~~using on~~ a quadrupole system. Target metal concentrations were measured in pulse (ion-counting) mode. The sensitivity drift  
during ~~the~~ measurements was corrected ~~by~~ using the internal standard of 1 ng/g of In. ~~All quantitative data on total and~~  
220 ~~dissolved Fe and Al concentrations and their fractional solubilities are shown in Table S3. The total and dissolved metal~~  
~~concentrations of other target elements are shown in Tables S4 and S5, respectively.~~<sup>-1</sup> indium.

## 2.5. Estimation of EF of Fe and Fe<sub>sol</sub>%

The total and dissolved metal concentrations in TSP were calculated by the summation of the target metal concentrations  
225 in all sampling stages. Crustal and non-crustal Fe concentrations and the EF of target metals normalized by the average  
continental crust were calculated by using the following equations:

$$\text{Crustal Fe} = \text{Al}_{\text{crust}} \times (\text{Fe}/\text{Al})_{\text{aerosol}}, \text{ (Eq. 3)}$$

$$\text{Non-crustal Fe} = \text{Total Fe} - \text{crustal Fe}, \text{ (Eq. 4)}$$

$$\text{EF} = (\text{M}/\text{Al})_{\text{aerosol}}/(\text{M}/\text{Al})_{\text{crust}}, \text{ (Eq. 5)}$$

230 where M is the target metal. Iron and Al concentrations in the average continental crust (Fe/Al: 0.684) were acquired by  
referring to Taylor (1964). Given the variability of the Fe/Al ratio in crustal materials, significant enrichment of the Fe derived  
from anthropogenic emissions is usually recognized at EF values higher than 10.0. The EF equation suggests that about 90 %  
of Fe is derived from anthropogenic sources when the EF is 10.0. Given that the emission amount of crustal Fe is an order of  
magnitude higher than that of anthropogenic Fe, the EF for Fe in aerosol particles is usually below 10.0, except for aerosol  
235 samples collected near steel plants and in urban areas. Therefore, classification of Fe as anthropogenic Fe by the criterion EF  
> 10.0 substantially simplifies the origin of Fe in aerosol particles. If the variation of Fe/Al ratio in natural-source aerosol is  
limited in a narrow range, aerosols with EF > 2.00 can still be evaluated as aerosol samples containing anthropogenic Fe  
component to a certain degree. The small variability of the Fe/Al ratio in desert soil in East Asia was confirmed (average ± 1σ  
standard deviation (ave.±1σ): 0.555 ± 0.170, range: 0.294–1.05, Nishikawa et al., 2013; Ding et al., 2001; Cao et al., 2008;  
240 Liu, X. et al., 2022 and references therein). The Fe/Al ratio in mineral dust exhibits a small variability, and thus,



enrichment of anthropogenic Fe is recognized when the EF of Fe is higher than 2.00 ( $Fe/Al > 1.37$ ). The  $Fe_{sol}\%$  in aerosol samples was calculated by using the following equation:

$$\text{Fractional solubility (\%)} = (\text{Dissolved Md-Fe} / \text{total M}) \times 100. \text{ (Eq. 6)}$$

245

### 3. Results and Discussion

#### 3.1. Major ion concentrations

##### 3.1.1. Cations

Sodium ion,  $Mg^{2+}$ , and  $Ca^{2+}$  were mainly distributed in coarse aerosol particles, accounting for 88.3 %, 84.8 %, and 250 79.3 % of the ions in TSP, respectively (Figs. 2a–2c). Sodium ion in aerosol particles was mainly associated with sea spray aerosol (SSA). Magnesium ion was mainly derived from SSA considering that nss  $Mg^{2+}$  accounted for  $26.2 \pm 22.4$  % of the total  $Mg^{2+}$ . By contrast, almost all  $Ca^{2+}$  ( $90.8 \pm 9.45$  %) was present in the form of nss  $Ca^{2+}$ . Calcium ion concentration was higher in spring (March to May) than in other seasons and during Asian dust events (Fig. 2b). A large amount of Asian dust is transported from the Gobi or Taklamakan Deserts in spring (Uematsu et al., 1983; Sullivan et al., 2007a). Therefore, the high 255  $Ca^{2+}$  concentration in spring was attributed to Asian dust. Potassium ion and  $NH_4^+$  were mainly distributed in fine aerosol particles, which accounted for  $68.2 \pm 9.69$  % and  $83.0 \pm 3.49$  % of the ions in TSP, respectively (Figs. 2d and 2e). More than 90 % of  $K^+$  in fine aerosol particles (annual average:  $94.5 \pm 14.8$  %) was present in the form of nss  $K^+$ . The nss  $K^+$  in fine aerosol particles is mainly derived from either biomass burning or coal combustion (Echalar et al., 1995; Simoneit et al., 2002; Yu et al., 2018). The discussion on the size and seasonal variation of  $NH_4^+$  with  $NO_3^-$  and  $SO_4^{2-}$  is provided in the next section.

260

##### 3.1.2. Anions

Chloride ion dominated in coarse aerosol particles, which contributed  $79.5 \pm 14.1$  % of  $Cl^-$  in TSP (Fig. 2f). SSA is the dominant source of  $Cl^-$  in aerosol particles. However, the  $Cl^-/Na^+$  mass ratio of aerosol particles was not identical to that of seawater (Fig. S3a). Chloride ion concentration in coarse aerosol particles was depleted relative to the expected  $Cl^-$  265 concentration in non aged SSA ( $= Na^+_{aerosol} \times [Cl^-/Na^+]_{seawater}$ ), and the depletion ratio of  $Cl^-$  in coarse aerosol particles to  $Cl^-$  in non aged SSA was  $34.7\% \pm 28.2\%$ .  $Cl^-$  depletion was caused by the chemical reaction of NaCl with  $HNO_3$  and  $H_2SO_4$  as follows (Finlayson Pitts, 2003):



270 The frequent enrichment of  $Cl^-$  in fine aerosol particles relative to that in non aged SSA (Fig. S3a) and in contrast to that in coarse aerosol particles indicated that emission sources other than SSA contributed to  $Cl^-$  in fine aerosol particles.  $Cl^-$  enrichment was observed in aerosol samples collected in winter and spring when air masses mainly originated from East Asia (Fig. S1 and S3a). Previous studies have reported that anthropogenic emissions (e.g., coal combustion, industrial processes,

and MSWI) and biomass burning are the dominant sources of HCl and  $\text{Cl}^-$  in fine aerosol particles in East Asia (Fu et al., 2018; Liu et al., 2018). Indeed, the correlation of excess  $\text{Cl}^-$  concentration ( $=-1 \times \text{Cl}^-$  loss) with nss  $\text{K}^+$  is a tracer of biomass burning and coal combustion ( $r: 0.570$ ). In addition, pre-existing particles, including  $\text{CaCO}_3$  in mineral dust, act as the sink of Cl species (Sullivan et al., 2007b; Tobo et al., 2010). Therefore, the enrichment of  $\text{Cl}^-$  in fine aerosol particles was caused by the uptake of anthropogenic  $\text{Cl}^-$  by pre-existing particles.

Sulfate ions and  $\text{NH}_4^+$  were mainly distributed in fine aerosol particles (Figs. 2e and 2g) and accounted for  $75.8 \pm 11.1\%$  and  $88.8 \pm 7.68\%$  of the total anions and cations in fine aerosol particles, respectively. The average fraction of nss  $\text{SO}_4^{2-}$  to total  $\text{SO}_4^{2-}$  (nss- $\text{SO}_4^{2-}$ /total  $\text{SO}_4^{2-}$ ) in coarse and fine aerosol particles were  $70.1 \pm 23.1\%$  and  $99.3 \pm 1.44\%$ , respectively. Thus, nss  $\text{SO}_4^{2-}$  was dominant in coarse and fine aerosol particles. Ammonium ion concentration had a good correlation with but was higher than nss  $\text{SO}_4^{2-}$  concentration (Fig. S3b). This result indicated that ammonium salts other than  $(\text{NH}_4)_2\text{SO}_4$  and  $\text{NH}_4\text{HSO}_4$  were present in fine aerosol particles. Ammonium ion concentration was found to have an excellent correlation with  $2 \times [\text{nss } \text{SO}_4^{2-}] + [\text{NO}_3^-]$  in fine aerosol particles (Fig. S3c). The slope of the regression line was 0.965, indicating that  $(\text{NH}_4)_2\text{SO}_4$  and  $\text{NH}_4\text{NO}_3$  were the dominant major ion components in fine aerosol particles.

Nitrate ion had concentration peaks not only in fine aerosol particles but also in coarse aerosol particles (Fig. 2h). The average fractions of  $\text{NO}_3^-$  in coarse and fine aerosol particles in TSP were  $61.3 \pm 12.3\%$  and  $36.9 \pm 10.5\%$ , respectively. As previously mentioned,  $\text{NO}_3^-$  in coarse aerosol particles was derived from  $\text{Cl}^-$  depletion as described in R1. Assuming that  $\text{NO}_3^-$  caused the depletion of all Cl from SSA in coarse aerosol particles, SSA-associated  $\text{NO}_3^-$  accounted for only  $35.1 \pm 25.1\%$  of  $\text{NO}_3^-$  in coarse aerosol particles. Therefore,  $\text{NO}_3^-$  ions were mainly present in coarse aerosol particles other than SSA (non-SSA  $\text{NO}_3^-$ ). Previous studies have reported that mineral dust is the dominant driver of  $\text{NO}_3^-$  concentration in coarse aerosol particles (Karydis et al., 2016; Kakavas et al., 2021). In fact, the good correlation between nss  $\text{Ca}^{2+}$  and non-SSA  $\text{NO}_3^-$  ( $=$  total  $\text{NO}_3^-$   $-$  Cl depletion) found in our coarse aerosol particles (Fig. S3d) indicated that non-SSA  $\text{NO}_3^-$  was present in coarse aerosol particles in the form of  $\text{Ca}(\text{NO}_3)_2$ . However, our previous study identified gypsum ( $\text{CaSO}_4 \cdot 2\text{H}_2\text{O}$ ) rather than  $\text{Ca}(\text{NO}_3)_2$  as the dominant secondary Ca species in coarse aerosol particles collected in January, November, and the Asian dust event (Miyamoto et al., 2020). Recent studies have demonstrated that hygroscopic  $\text{Ca}(\text{NO}_3)_2$  on the surfaces of mineral dust reacted with  $(\text{NH}_4)_2\text{SO}_4$ , resulting in the formation of  $\text{NH}_4\text{NO}_3$  and  $\text{CaSO}_4 \cdot 2\text{H}_2\text{O}$  (Wu et al., 2019, 2020). Thus,  $\text{NO}_3^-$  taken up in the reaction with  $\text{CaCO}_3$  is considered to exist in the form of  $\text{NH}_4\text{NO}_3$  instead of  $\text{Ca}(\text{NO}_3)_2$ .

### **3.2.3.1. Total Fe and Al concentrations**

The total Fe and Al concentrations in the TSP collected during the non-dust event were 256–1561 and 170–1716  $\text{ng m}^{-3}$ , respectively (Figs. 3a2a and 3b2b). Coarse aerosol particles accounted for  $69.4 \pm 7.192\%$  and  $72.9 \pm 7.556\%$  of the total Fe and Al in TSP, respectively. The total Fe and Al concentrations were higher in spring (March to May) and Asian dust events than in other seasons (Figs. 2a and 2b). A higher  $\text{Ca}^{2+}$  concentration, as a marker of Asian dust, was also observed in spring than in other seasons (Fig. S3b, Supplemental Note). Therefore, the high Fe and Al concentrations in spring were due to the strong influence of Asian dust in spring (Figs. 3a and 3b). The total Fe and Al concentrations in the samples collected during

the Asian dust event were considerably higher than those in the samples collected during the non-dust event (Figs. 3a2a and 3b2b). The average EF of Fe in the TSP samples collected in from summer, to fall (June to October) was  $2.84 \pm 0.83$  when air masses mainly originated from Japan, was higher than (Fig. S6a). By contrast, the average EF of Fe in TSP samples collected in other seasons (the TSP derived from East Asia in winter and spring was  $1.57 \pm 0.35$  (Fig. S6a). Thus, the influences of anthropogenic emission on the total Fe in TSP are more significant in the air mass derived from Japan than that from East Asia (Figs. S1, S2, and S4a-S6a). The total Al concentrations sharply decreased from May to June, whereas the decrease in the total Fe concentrations did was not decrease as significantly as the total Al significant (Figs. 3a2a and 3b2b). This result indicated that the aerosol particles emitted in Japan contained non-crustal Fe. In addition, the total Fe concentration in the haze event was almost the same as that in the Asian dust event. However, whereas the total Al concentration in the haze event was lower than that in the Asian dust event. This result demonstrated that during haze events, the total Fe concentrations were significantly higher than total Al concentrations due to the influence of enhanced by the non-crustal Fe emitted from anthropogenic emissions.

The average EFs of Fe in coarse and fine aerosol particles were  $1.99 \pm 0.89$  and  $2.49 \pm 1.09$ , respectively (Fig. 3e Figs. 2c and S6a). Therefore, non-crustal Fe may be present in coarse and fine aerosol particles. Non-crustal Fe concentration were in coarse aerosol particles correlated with Cu, Zn, Sb, and Pb in road dust (Figs. 4a-d). The Sb ( $r > 0.500$ , Table S2). These elements in coarse aerosol particles are known as the-tracer elements of fragments fragment vehicle-related materials in road dust (brake dust: Cu and Sb, and tire wear: Zn, and road paint: Pb) (Adachi and Tainosho, 2004; Wählín et al., 2006; Iijima et al., 2007; Gietl et al., 2010; Sakata et al., 2014; Harrison et al., 2021). The correlation coefficient of non-crustal Fe with Cu as a tracer element of brake padpads was the highest among these tracer elements. It is known that ( $r: 0.747$ , Table S2). Fe is the most dominant metal in brake rings (up to 50 wt%), and its concentration is about an order of magnitude higher than that of Al in the-brake padpads. Therefore, the-brake padpads can increase the EF of Fe in aerosol particles. In fact, The EF of Fe in road dust ( $<40 \mu\text{m}$ ) collected from tunnels and roadsides around the sampling site were 3.41 and 6.04, respectively. Therefore, the-resuspensions of brake pad fragments in road dust could be considered as non-crustal Fe in coarse aerosol particles. This result is consistent with the finding of a previous model study because, which showed that road dust is was the dominant source of Cu and non-crustal Fe in  $\text{PM}_{10}$  in the Chugoku-Shikoku area (the locality around the sampling site) (Kajino et al., 2020).

In fine aerosol particles, non-crustal Fe concentrations were correlated with Zn, Sb, Cd, and Pb (Fig. 5a-e), which were emitted by from high-temperature combustions, including coal combustion, MSWI, and steel/iron industrial processes ( $r > 0.700$ , Table S3, Pacyna and Pacyna, 2001; Sakata et al., 2000; Sakata et al., 2014; Kajino et al., 2020). These high-temperature combustion processes emit nanoparticles of hematite and magnetite with a small number of coexisting elements, which can increase the EF of Fe in fine aerosol particles. Indeed, in this study, the The negative  $\delta^{56}\text{Fe}$  associated with hematite derived from high-temperature combustion processes was detected in aerosol samples collected at the same sampling site (Kurusu et al., 2016a). Therefore, the nanoparticles of hematite and magnetite are likely the dominant sources of non-crustal Fe in fine aerosol particles. In addition, in fine aerosol particles, the non-crustal Fe concentration was weakly correlated with V (Fig. 5d), which is a tracer element of heavy-oil combustion (Nriagu and Pacyna, 1988); however, the correlation factor between

non-crustal Fe and V was lower than those of Zn, Sb, Cd, and Pb (r: 0.601, Table S3). A previous model study predicted that V around the sampling site was derived from vessel emissions in the Seto Inland Sea (Kajino et al., 2020), which is located at the southern part of the sampling site (Figure Fig. 1, Kajino et al., 2020). Our results also showed that V concentrations in fine aerosol particles were higher from July to September, during which air masses ~~passpassed~~ through the Seto Inland Sea (Figs. 1 and S5a), than in other periods (Figs. 1 and S7a). At this ~~timepoint~~, the concentrations of Zn, Sb, and Pb did not increase (Fig. S5b ~~d~~Figs. S7b–S7d). Therefore, in addition to the high-temperature combustion processes mentioned above, heavy-oil combustion processes around the Seto Inland Sea ~~likely~~ were ~~the possible~~ emission sources of ~~the~~ non-crustal Fe in fine aerosol particles collected in summer.

350

### **3.3.3.2. Size distributions of d-Fe and d-Al concentration and their fractional solubility**

Dissolved Fe and Al The concentrations ~~in~~ of d-Fe and Al in the TSP collected during the non-dust event ranged from 11.4 ~~mgng~~  $\text{m}^{-3}$  to 65.0  $\text{ng m}^{-3}$  and from 8.30  $\text{ng m}^{-3}$  to 40.6  $\text{ng m}^{-3}$ , respectively (Figs. 6a3a and 6d3d). The  $\text{Fe}_{\text{sol}}\%$  and  $\text{Al}_{\text{sol}}\%$  of the TSP ranged from 2.00 % to 7.73 % and 1.46 % to 7.39 %, respectively (Figs. S4bS6b and S4e,S6c), which were within the typical range of  $\text{Fe}_{\text{sol}}\%$  in the TSP collected from East Asia and north-western Pacific Ocean (Buck et al., 2006, 2013; Takahashi et al., 2013; Sakata et al., 2022). Although approximately 70 % of the total Fe and Al in the TSP were present in coarse aerosol particles, high concentrations of d-Fe and d-Al were found in fine aerosol particles (Figs. 6a3a and 6d3d). The average d-Fe and d-Al concentrations of fine aerosol particles were  $27.3 \pm 17.4$  and  $14.3 \pm 10.9$   $\text{ng m}^{-3}$ , which accounted for  $72.0 \pm 8.87\%$  and  $53.1 \pm 9.90\%$ , respectively. Thus, d-Fe and d-Al concentrations yielded different size distributions from total Fe and Al concentrations. The reason for the enrichment  $9\%$  of d-Fe and d-Al in fine aerosol particles was higher  $\text{Fe}_{\text{sol}}\%$  and  $\text{Al}_{\text{sol}}\%$  in fine aerosol particles than coarse aerosol particles. The average  $\text{Fe}_{\text{sol}}\%$  in fine aerosol particles ( $11.4 \pm 6.97\%$ ) was about five times higher than that of coarse aerosol particles ( $2.19 \pm 2.27\%$ , Figs. 6b and 6e). In the case of Al, fine aerosol particles ( $8.82 \pm 6.48\%$ ) yielded twice as much  $\text{Al}_{\text{sol}}\%$  as coarse aerosol particles ( $3.25 \pm 3.41\%$ , Figs. 6e and 6f). the TSP, respectively. Enrichment of d-Fe and d-Al in size-fractionated fine aerosol ~~samples~~ particles has been reported not only in the urban atmosphere (Fang et al., 2017; Hsieh et al., 2022; Liu, L. et al., 2022) but also in the marine atmosphere (McDaniel et al., 2019; Baker et al., 2020; Sakata et al., 2022). These previous studies have reported that the higher amounts of d-Fe and d-Al in fine aerosol particles than coarse aerosol particles were caused by either or both (i) contamination of the anthropogenic aerosol with high  $\text{Fe}_{\text{sol}}\%$  and  $\text{Al}_{\text{sol}}\%$  and (ii) solubilization of Fe and Al in fine aerosol particles by atmospheric processes. ~~It should be noted that~~ The average  $\text{Fe}_{\text{sol}}\%$  in fine aerosol particles in this study ( $11.4 \pm 7.0\%$ ) was about five times higher than that of coarse aerosol particles ( $2.19 \pm 2.27\%$ , Figs. 3b and 3c). In the case of Al, fine aerosol particles ( $8.82 \pm 6.48\%$ ) yielded about twice as much as the  $\text{Al}_{\text{sol}}\%$  of coarse aerosol particles ( $3.25 \pm 3.41\%$ , Figs. 3e and 3f). These results indicated that the Fe in fine aerosol particles is more susceptible to dissolution in water by anthropogenic activities and chemical aging than Al. The  $\text{Fe}_{\text{sol}}\%$  and  $\text{Al}_{\text{sol}}\%$  in coarse aerosol particles were higher than those in desert dust soil (typical  $\text{Fe}_{\text{sol}}\%$  and  $\text{Al}_{\text{sol}}\%$ : 0.4–100 %). Therefore, the  $\text{Fe}_{\text{sol}}\%$  and  $\text{Al}_{\text{sol}}\%$  in coarse aerosol particles were increased by due to anthropogenic aerosol and/or atmospheric processes, but the effect was not as pronounced as ~~for~~ in fine aerosol particles.

375

### 3.4.3.3. Possible factor controlling $Fe_{sol}\%$ and $Al_{sol}\%$

#### 3.4.1.3.3.1. Coarse aerosol particles

Non-crustal Fe in coarse aerosol particles was derived from brake ~~bad~~ pads and tire wear debris in road dust: ~~as mentioned~~  
380 ~~above~~. If road dust is the dominant source of d-Fe in coarse aerosol particles, ~~then the~~ d-Fe concentration ~~is correlated~~ ~~correlates~~  
with non-crustal Fe concentration. However, ~~no~~ correlation ~~was found~~ between non-crustal Fe and d-Fe  
~~concentration~~ ~~concentrations~~ in coarse aerosol particles ~~was not found~~ ( $r: 0.352$ ), ~~indicating that~~. Thus, road dust was not the  
source of d-Fe in coarse aerosol particles. This result is consistent with ~~that of~~ previous studies ~~because in which the~~  $Fe_{sol}\%$  of  
~~debris of~~ brake pads and tire wear ~~is debris was~~ lower than 0.01% (Shupert et al., 2013; Halle et al., 2021).

385 The  $Fe_{sol}\%$  and  $Al_{sol}\%$  of coarse aerosol particles increased with the decrease in aerosol diameter (Fig. 6b, 6e, 6e Figs. 3b,  
3c, 3e, and 6f3f). Specific surface area is one of the factors controlling  $Fe_{sol}\%$  and  $Al_{sol}\%$  in aerosol particles (Baker and  
Jickells, 2006, 2017; McDaniel et al., 2019), and the chemical reactivity of aerosol particles ~~is increased~~ ~~increases~~  
~~increasing the increase~~ specific surface area (~~decreasing~~ ~~decrease in~~ aerosol diameter). Previous studies have reported that  
~~the~~ chemical aging of coarse aerosol particles by acidic species, including  $HNO_3$  and  $H_2SO_4$ , ~~were~~ solubilized Fe in aerosol  
390 particles (Takahashi et al., 2011; Zhu et al., 2022). The  $Fe_{sol}\%$  and  $Al_{sol}\%$  ~~in of~~ coarse aerosol particles correlated with ~~as the~~  
~~molar concentration ratios of nss-SO<sub>4</sub><sup>2-</sup> relative to the total Al and nss-SO<sub>4</sub><sup>2-</sup> or total Fe (Fig. 7a) 4a),  $[nss-SO_4^{2-}]/[total Fe]$ ,  
~~and~~  $[nss-SO_4^{2-}]/[total Al]$ . This result is consistent with previous findings ~~because showing that~~ aluminosilicates in aerosol  
particles react preferentially with  $H_2SO_4$  (Sullivan et al., 2007a 2007; Fitzgerald et al., 2015). Furthermore, our previous studies  
showed that ~~at the~~ relative abundance of ferrihydrite formed by hydrolysis of Fe in coarse aerosol particles ~~was~~ increased with  
395 ~~decreasing the decrease in~~ diameter (Takahashi et al., 2011; Sakata et al., 2012 2022). These results ~~indicated~~ ~~indicate~~ that  
atmospheric processes of coarse aerosol particles by  $H_2SO_4$  ~~promote~~ ~~promoted~~ the formation of d-Fe via proton-promoted  
dissolution or hydrolysis of Fe. By contrast, no good correlation ~~was found between of~~  $Fe_{sol}\%$  and  $Al_{sol}\%$  ~~and between with~~  
 $[NO_3^-]/[total Fe]$  and  $[NO_3^-]/[total Al]$  ~~was found~~ because  $HNO_3$  reacts mainly with Ca-rich particles (e.g.,  $CaCO_3$ ) in mineral  
dust, ~~as mentioned above~~ (Fig. 7b 4b, Karydis et al., 2016; Kakavas et al., 2021).~~

#### 3.4.2.3.3.2. Fine aerosol particles

400 Unlike ~~the~~ d-Fe in coarse aerosol particles, ~~the~~ d-Fe concentrations in fine aerosol particles correlated with non-crustal  
Fe concentrations (Fig. 8a 5a). Good correlations of d-Fe in fine aerosol particles with concentrations of V, Zn, Sb, and Pb as  
tracer elements for high-temperature combustions were also found (Fig. 8b 8e). ~~Among these tracer elements, the~~ Figs. 5b–5c).  
405 ~~The~~ correlation coefficient between d-Fe and Zn was the largest (Fig. 8e). ~~Since Zn~~ 5c). Zinc in fine aerosol particles ~~at from~~  
the sampling sites originated from various high-temperature combustions, including ~~MSW~~ ~~those in MSWIs~~, steel/iron  
industries, and coal power ~~plant~~ ~~plants~~ (Kajino et al., 2020). Therefore, ~~the non-crustal Fe emitted from~~ high-temperature  
combustion is one of the dominant sources of d-Fe in fine aerosol particles, ~~though it is not easy to identify~~ ~~although~~  
~~identification of~~ specific sources of ~~non-crustal~~ d-Fe around the sampling site ~~was difficult~~. This result is consistent with our

410 previous studies because study, which showed that negative  $\delta^{56}\text{Fe}$  associated with high-temperature combustions were/was detected in fine aerosol particles (Kurusu et al., 2016a).

It is known that fine aerosol particles usually yield lower aerosol pH compared to coarse aerosol particles. In addition to coarse aerosol particles, the input of non-crustal Fe with high  $\text{Fe}_{\text{sol}}\%$  in fine aerosol particles, aerosol acidification resulted in the high  $\text{Fe}_{\text{sol}}\%$  and  $\text{Al}_{\text{sol}}\%$  in fine aerosol particles (Pye/Fang et al., 2020). Therefore, as well as 2017; Sakata et al., 2022). Along with coarse aerosol particles, atmospheric processes also contribute to solubilizing Fe.  $\text{Fe}_{\text{sol}}\%$  and  $\text{Al}_{\text{sol}}\%$  in fine aerosol particles did not correlate with  $[\text{NO}_3^-]/[\text{total Fe}]$  and  $[\text{NO}_3^-]/[\text{total Al}]$  due to the preferential reaction of  $\text{HNO}_3$  with  $\text{Ca}^{2+}$  (Fig. 4d). The  $\text{Fe}_{\text{sol}}\%$  and  $\text{Al}_{\text{sol}}\%$  of fine aerosol particles correlated with  $[\text{nss-SO}_4^{2-}]/[\text{total Fe}]$  and  $[\text{nss-SO}_4^{2-}]/[\text{total Al}]$ , respectively (Fig. 4c). Moreover, these solubilities increased with the decrease in aerosol pH (Fig. 4e), which indicates that acidification of fine aerosol particles by  $\text{H}_2\text{SO}_4$  plays a significant role in Fe solubilization. These results are reasonable and supported by previous studies reporting that mineral dust and anthropogenic Fe in fine aerosol particles were weakly correlated with  $\text{nss-SO}_4^{2-}/\text{Fe}$  and  $\text{nss-SO}_4^{2-}/\text{Al}$ , respectively, but not with  $\text{NO}_3^-/\text{Fe}$  and  $\text{NO}_3^-/\text{Al}$  (Figs. 7c and 7d). In addition,  $\text{Fe}_{\text{sol}}\%$  and  $\text{Al}_{\text{sol}}\%$  tended to increase with the decrease in aerosol pH (Fig. 7e). These results implied that the  $\text{Fe}_{\text{sol}}\%$  and  $\text{Al}_{\text{sol}}\%$  of fine aerosol particles increased via aerosol acidification, which occurred through the chemical reaction of Fe and Al bearing particles with  $\text{SO}_2$  and  $\text{H}_2\text{SO}_4$ . The correlation factor between  $\text{Al}_{\text{sol}}\%$  and  $\text{nss-SO}_4^{2-}/\text{Al}$  was higher than that between  $\text{Fe}_{\text{sol}}\%$  and  $\text{nss-SO}_4^{2-}/\text{Fe}$  (Figs. 7c and 7d). In addition, the correlation factor of the  $\text{Fe}_{\text{sol}}\%$  and  $\text{nss-SO}_4^{2-}/\text{Fe}$  sulfate promoted the dissolution of fine aerosol particles was lower than that of coarse aerosol particles (Figs. 7a and 7c). Given that Al in fine aerosol particles was derived from aluminosilicates,  $\text{Al}_{\text{sol}}\%$  was mainly controlled by the acidification of mineral dust. These results are reasonable because previous studies have reported that in fine aerosol particles, mineral dust was covered with sulfates-Fe (Sullivan et al., 2007a; 2007; Fitzgerald et al., 2015; Li et al., 2017, Zhu, Y. et al., 2020, 2022). By contrast/However, compared with the correlation factor of  $\text{Fe}_{\text{sol}}\%$  with  $[\text{nss-SO}_4^{2-}]/[\text{total Fe}]$ , coarse aerosol particles yielded a higher correlation factor than fine aerosol particles (Figs. 4a and 4c). Similar results have been reported by previous studies on  $\text{Fe}_{\text{sol}}\%$  in China, which indicated the presence of anthropogenic Fe with high  $\text{Fe}_{\text{sol}}\%$  as one of the reasons for the low value of the correlation factor (Zhang et al., 2022, 2023). Therefore, the low correlation between the  $\text{Fe}_{\text{sol}}\%$  and  $[\text{nss-SO}_4^{2-}]/[\text{total Fe}]$  of fine aerosol particles implied that the acidification of mineral dust was not the sole factor controlling  $\text{Fe}_{\text{sol}}\%$ .

435

#### 4. The Establishment of source estimation method for d-Fe using the [d-Fe]/[d-Al] ratio

##### 3.5.4.1. [d-Fe]/[d-Al] ratio in coarse aerosol particles and mineral dust

Thus, Correlation analysis between non-crustal Fe and d-Fe concentrations revealed that non-crustal Fe contributed to the source of d-Fe in fine aerosol particles but not in coarse aerosol particles. Correlation analysis is a simple method used to evaluate emission sources of d-Fe in aerosol particles, but, However, quantitative estimation estimations of the fraction of non-crustal Fe to d-Fe in aerosol particles present a challenge. Therefore, a quantitative indicator is preferable for the assessment of the relative abundance of non-crustal Fe to d-Fe in aerosol particles is difficult. Therefore, it is preferable to have a quantitative indicator to assess the relative abundance of non-crustal Fe to d-Fe. This study challenged/investigated the

440

evaluation of the relative abundance fraction of non-crustal Fe to d-Fe using the [d-Fe]/[d-Al] ratio. One of the reasons is that  
445 ~~that the [d-Fe]/[d-Al] ratio in mineral dust differs from that in non-crustal sources, as will be discussed below (Fig. 9a). In fact,~~  
~~the [d-Fe]/[d-Al] ratio in fine aerosol particles (average:  $1.15 \pm 0.803$ ) was different from that in coarse aerosol particles (Fig.~~  
~~9b, average:  $0.408 \pm 0.168$ ).~~

Evaluating the relative abundance of non-crustal Fe to d-Fe in aerosol particles, it is necessary to generalize the [d-Fe]/[d-  
Al] ratios of crustal and non-crustal Fe. Therefore, we performed data compiles of the [d-Fe]/[d-Al] ratio in mineral dust and  
450 ~~non-crustal Fe sources (6a).~~ In addition, the [d-Fe]/[d-Al] ratio may vary depending on the extraction method ~~as well as the~~  
~~chemical weathering and aging process in the atmosphere (Sholkovitz et al., 2012; Clough et al., 2019).~~ Therefore, the data of  
~~[d-Fe]/[d-Al] were compiled considering not only the differences in the emission sources of Fe in aerosols but also the~~  
~~differences in the dissolution processes (i.e. aerosol particles (Fig. 6a, e.g., proton-promoted vs. versus ligand-promoted~~  
~~dissolutions).~~ The ~~results are summarized in Fig. 9a.~~ [d-Fe]/[d-Al] ratio in fine aerosol particles (ave.  $\pm 1\sigma$ :  $1.15 \pm 0.80$ ) differed  
455 ~~from that in coarse aerosol particles (Fig. 6b, ave.  $\pm 1\sigma$ :  $0.408 \pm 0.168$ ).~~ With the evaluation of the fraction of non-crustal Fe to  
d-Fe in aerosol particles, the [d-Fe]/[d-Al] ratios of crustal and non-crustal Fe can be generalized.

In the present study, we focused on biotite Biotite, illite, and Fe-rich chlorite ~~as they are considered~~ representative mineral  
species of aluminosilicates in aerosol particles because ~~these aluminosilicates were they are~~ detected in aerosol particles  
collected in East Asia (Takahashi et al., 2011; Kurisu et al., 2016a; Sakata et al., 2022). When Fe and Al in these  
460 aluminosilicates were ~~leached dissolved~~ by proton-promoted dissolution (pH 1.0–7.0) under oxic conditions, the [d-Fe]/[d-Al]  
ratios of biotite, illite, and Fe-rich chlorite ~~was were within~~ 0.427–0.930 (average: ave.  $\pm 1\sigma$ :  $0.776 \pm 0.152$ ), 0.156–0.689  
(average: ave.  $\pm 1\sigma$ :  $0.404 \pm 0.189$ ), and 0.142–1.03 (average: ave.  $\pm 1\sigma$ :  $0.699 \pm 0.303$ ), respectively (Fig. ~~9a~~6a; Kodama and  
Schnitzer, 1973; Lawson et al., 2005; Bibi et al., 2015; Bray et al., 2015). In addition, the average [d-Fe]/[d-Al] ratios of Asian  
dust, Saharan dust, and Arizona test dusts obtained by proton-promoted dissolution were  $0.238 \pm 0.201$ ,  $0.163 \pm 0.157$ , and  
465  $0.230 \pm 0.009$ , respectively (Fig. 6a, Desboeufs et al., 2001; Duvall et al., 2008; Shi et al., 2011). The [d-Fe]/[d-Al] ratio ~~tended~~  
~~to decrease decreased~~ with the increase in pH due to either or both the preferential retention of Fe in the mineral phase and  
precipitation of secondary ferrihydrite under near-neutral conditions (Fig. ~~S6~~S8, Kodama and Schnitzer, 1973; Desboeufs et  
al., 2001; Lawson et al., 2005; Bray et al., 2015). ~~In addition, the average [d-Fe]/[d-Al] ratios of Asian dust, Saharan dust, and~~  
~~Arizona test dust obtained by proton promoted dissolution were  $0.238 \pm 0.201$ ,  $0.163 \pm 0.157$ , and  $0.230 \pm 0.00926$ ,~~  
470 ~~respectively (Fig. 8a, Desboeufs et al., 2001; Duvall et al., 2008; Shi et al., 2011).~~ The [d-Fe]/[d-Al] ratio is also decreased  
with increasing pH (Fig. S6, Desboeufs, et al., 2001). Thus, the [d-Fe]/[d-Al] ratio obtained from the proton-promoted  
dissolution of the mineral dust was between 0.4100 and 1.000.

Organic ligands promote the dissolution of Fe from the mineral phase through the direct complexation of organic ligands  
with Fe at the mineral surface and ~~the reduction in~~of the saturation index of inorganic Fe in aqueous phase due to the formation  
475 of organic complexes of Fe in solution (Chen and Grassian, 2013; Paris and Desboeufs, 2013; Wang et al., 2017). The [d-  
Fe]/[d-Al] ratios of biotite and Fe-rich chlorite associated with ligand-promoted dissolution were 0.795–3.83

(~~average:ave.±1σ: 1.20 ± 0.66066~~) and 1.19–1.37 (~~average:ave.±1σ: 1.31 ± 0.062906~~), respectively (Kodama and Schnitzer, 1973; Bray et al., 2015). A previous study ~~foundshowed~~ that the [d-Fe]/[d-Al] ratios of coarse aerosol particles extracted by 20 mmol/L of oxalate at pH 4.7 (~~1.31 ± 0.41842~~) were higher than that of ~~MQu~~ultrapure water extraction ( $0.354 \pm 0.714$ ) (Coarse aerosol (Proton) and Coarse aerosol (Ligand/Ligand) in Fig. 9a6a, Kurisu et al., 2019). Thus, the [d-Fe]/[d-Al] ratio associated with ligand-promoted dissolution was higher than that associated with proton-promoted dissolution (Fig. 8a6a). The higher stability constant ( $\log K$ ) of Fe<sup>3+</sup> than that of Al<sup>3+</sup> with organic ligands (e.g.,  $\log K$  of AlC<sub>2</sub>O<sub>4</sub><sup>+</sup>: 7.73,  $\log K$  of FeC<sub>2</sub>O<sub>4</sub><sup>+</sup>: 9.15) ~~is a reason forcaused~~ the preferential dissolution of Fe over Al ~~by organic ligands, increasing from mineral dust, which increased~~ the [d-Fe]/[d-Al] ratio.

The [d-Fe]/[d-Al] ratio of coarse aerosol particles (~~collected by this study (n = 60, average: 0.121–0.927)~~) was within ~~at~~the range of ~~the~~[d-Fe]/[d-Al] ratios of mineral dust that underwent proton-promoted dissolutions (Fig. 9b). ~~In addition, the [d-Fe]/[d-Al] ratio of coarse aerosol particles, and it~~ increased with the increase in Fe<sub>sol</sub>% (Fig. 9b6b, r: 0.552). ~~Coarse aerosol particles with high As previously mentioned, [d-Fe]/[d-Al] and Fe<sub>sol</sub>% yielded high nss-SO<sub>4</sub><sup>2-</sup>/total Fe (Fig. 7a), indicating that coarse aerosol particles with high Fe<sub>sol</sub>% underwent acidic conditions. This result obtained by proton-promoted dissolution of mineral dust increased with the decrease in pH, which is consistent with a relationship of the [d-Fe]/[d-Al] ratio with dissolution pH correlation between Fe<sub>sol</sub>% and [nss-SO<sub>4</sub><sup>2-</sup>]/[total Fe] in coarse aerosol particles (Fig. 4a).~~ Therefore, the proton-promoted dissolution of mineral dust is the dominant source of d-Fe in coarse aerosol particles. ~~On the other hand~~By contrast, no coarse aerosol particles had [d-Fe]/[d-Al] ratios higher than 1.0 (Fig. 9b). ~~Therefore, 6b), which indicates that~~ the effect of organic ligands on the solubilization of Fe and Al in coarse aerosol particles was ~~not significant~~insignificant. In addition, ~~the~~ non-crystal Fe derived from road dust was not ~~factorsa factor~~controlling the [d-Fe]/[d-Al] ratio in coarse aerosol particles due to ~~no~~the lack of correlation between the [d-Fe]/[d-Al] ratio and EF of Fe. This result is reasonable because the ~~Fe<sub>sol</sub>% of brake pads and tire wear debris arewas~~ less than 0.01% (Shupert et al., 2013; Halle et al., 2021).

### 3.6.4.2. The [d-Fe]/[d-Al] ratio in fine aerosol particles and their emissions

The average [d-Fe]/[d-Al] ratio of fine aerosol particles (n = 45, ~~average:ave.±1σ: 1.15 ± 0.80380~~, range: 0.386–4.67) was higher than ~~thatthose~~ of coarse aerosol particles and mineral dust (Figs. 9a6a and 9b). ~~In particular, the 6b). The~~ [d-Fe]/[d-Al] ratios of several fine aerosol particles exceeded 1.5, which was beyond the range of the ratio of mineral dust that underwent ligand-promoted dissolutions (Fig. 9a6a and 9b). ~~Considering a 6b). Given the~~ good correlation between the [d-Fe]/[d-Al] ratio and EF of Fe (r: 0.505), the [d-Fe]/[d-Al] ratio higher than 1.5 was attributed to non-crystal Fe (Fig. 9e). ~~Non 6c). The non-~~ crystal Fe in fine aerosol particles was derived from fly ash ~~ofproduced by~~ high-temperature combustions, including steel/iron industrial processes, MSWI, and coal and fuel oil combustion. Fly ash contains two types of particles, namely, magnetic and non-magnetic particles (Kukier et al., 2003; Fomenko et al., 2021). ~~Since Fe and coexisted Given the different elemental concentrations compositions and Fe species are different of~~ between magnetic and non-magnetic particles, the ~~impactinfluences~~ of these particles on the [d-Fe]/[d-Al] ratio and Fe<sub>sol</sub>% in fine aerosol particles were evaluated separately.



### 3.6.1.4.2.1. [d-Fe]/[d-Al] ratio of non-crystal Fe: magnetic particles

515 ~~Mass~~The mass fraction of magnetic particles ~~was only~~accounts for a ~~few percent to~~small percentage of the total fly ash mass (Hansen et al., 1981), but up to 90 % ~~of~~Fe in fly ash ~~is~~was present as magnetic particles (Kukier et al., 2003). Iron species of magnetic particles in fly ash are mainly composed of ~~iron oxide~~Fe oxides, including hematite and magnetite. ~~From~~The iron concentration in magnetic particles ~~was reaches~~ up to 60– %–70 %, whereas ~~that of~~ Al ~~concentration in magnetic particles is~~ typically ~~amounts to~~ up to 10 % (Kukier et al., 2003; Fomenko et al., 2021). This result indicated that Fe in magnetic particles in fly ash can ~~be increased~~increase the EF of fine aerosol particles.

Previous studies have reported that d-Fe in fine aerosol particles yielded negative ~~Fe isotope ratio ( $\delta\delta^{56}\text{Fe} < 0\%$ ),~~ (Kurusu et al., 2016a, 2019)), and a recent ~~study show~~research showed negative  $\delta^{56}\text{Fe}$  in magnetic particles in PM<sub>2.5</sub> (Zuo et al., 2021).

520 The magnetic particles in fine fractions (<1.0  $\mu\text{m}$ ) are considered ~~to be~~formed by either or both ~~the~~ fragmentation of large particles and condensation of vaporized Fe. ~~In particular, The~~ Fe-oxides ~~partieles~~formed by condensation of vaporized Fe (hereafter high-temp-FeOx) is ~~recognized as~~ one of the important sources of d-Fe in fine aerosol particles because the high-temp-FeOx yield negative ~~Fe isotope ratio caused~~ $\delta^{56}\text{Fe}$ , which is formed by kinetic Fe isotope fractionation during vaporization ~~process~~(Kurusu et al., ~~2016~~2016a, 2019). ~~In addition, The high-temp-FeOx can increase~~ the [d-Fe]/[d-Al] ratio ~~in of fine aerosol~~

525 ~~particles because the [d-Fe]/[d-Al] ratio of~~ fine aerosol particles with low  $\delta^{56}\text{Fe}$  (~~←~~←-1.0‰) collected near a steel plant was higher than 1.5 when extracted with proton-~~promoted~~ (MQ (ultrapure water) and ligand-promoted (20 mmol/L oxalic acid at pH 4.7) dissolutions (*Anthropogenic Fe in fine aerosols (Proton) and Anthropogenic Fe in fine aerosols (Ligand)* in Fig. 6a; Kurusu et al., 2019). ~~Thus, high temp FeOx can increase the [d-Fe]/[d-Al] ratio of fine aerosol particles.~~ However, ~~Fe<sub>sol</sub>% of~~ the ~~Fe<sub>sol</sub>% in~~ magnetic particles in coal fly ash was less than 0.4±100 % in weakly acidic solutions (Kukier et al., 2003), which 530 was ~~much~~considerably lower than ~~the~~ Fe<sub>sol</sub>% in fine aerosol particles (11.4 ± 6.977.0 %). As previously mentioned, the Fe<sub>sol</sub>% ~~of in~~ fine aerosol particles ~~in fine aerosol particles increased with the~~ increase ~~with the increasing in~~ [nss-SO<sub>4</sub><sup>2-</sup>]/[total Fe] and with ~~the decrease in~~ aerosol pH (Fig. ~~7e~~Figs. 4c and ~~7e~~4e, respectively). In addition, ~~aerosol pH with a~~ high Fe<sub>sol</sub>% (>10 %), ~~the aerosol pH~~ was ~~basically~~lower than 4.3.0, which was consistent with previous observations (Tao and Murphy, 2019b). Therefore, aerosol acidification is also ~~the~~a dominant factor ~~controlling that controls~~ Fe<sub>sol</sub>% in fine aerosol particles.

535 ~~Ligand promoted process may have partly enhanced Fe dissolution in mineral dust in As for~~ fine aerosol particles with [d-Fe]/[d-Al] ~~ratios between 1.00 and 1.50, the effect of 1.0 to 1.5~~ligand-promoted dissolution of mineral particles should be ~~considered~~ (Fig. ~~9b~~6b). If ligand-promoted dissolution of mineral dust ~~in fine aerosol particles is~~ the dominant source of d-Fe in fine aerosol particles, a ~~good~~the correlation between ~~the~~ [d-Fe]/[d-Al] ratio and EF of Fe should not be observed because ~~the~~ EF of mineral dust ~~is~~should be about 1.000. Therefore, ~~we conclude~~the high [d-Fe]/[d-Al] ratio in fine aerosol particles 540 ~~was~~ attributed to the presence of high-temp-FeOx rather than ligand-promoted dissolution of mineral dust.

### 3.6.2.4.2.2. The [d-Fe]/[d-Al] ratio of non-crystal Fe: non-magnetic fraction of fly ash

Non-magnetic particles are mainly composed of amorphous aluminosilicate glasses. ~~The amorphous aluminosilicates, which are considered to be formed by the melting of crystalline aluminosilicate or chemical reactions of melted Al<sub>2</sub>O<sub>3</sub> and SiO<sub>2</sub> (Zhang et al., 2007). The~~ Although previous studies did not perform the separation of magnetic and non-magnetic particles, ~~the~~ average [d-Fe]/[d-Al] ratio of coal and MSWI fly ash under acidic and circumneutral conditions was  $0.104 \pm 0.075$  (Fig. 9a6a, Seidel and Zimmels, 1998; Praharaj et al., 2002; Kim et al., 2003; Huang et al., 2007; Chang et al., 2009; Gitari et al., 2009; Komonweeraket et al., 2015). ~~These studies determined d-Fe and d-Al concentrations in fly ash without a separation between magnetic and non-magnetic particles. Considering~~ Given the high [d-Fe]/[d-Al] ratio in the magnetic particles, ~~it is expected that mentioned above,~~ the [d-Fe]/[d-Al] ratio of non-magnetic particles ~~is~~ should be less than 0.1. ~~However, no (Fig. 6a). Such a low [d-Fe]/[d-Al] ratio has not been detected in fine aerosol particles had, which indicates that non-magnetic aluminosilicate glass in fly ash is not a~~ dominant source of d-Fe/[d-Al] ratio less than 0.1 (Fig. 9b). In addition, non-magnetic aluminosilicates of coal combustions and MSWI could not increase the EF of Fe in fine aerosol particles because (Fig. 6b). Furthermore, the EF of Fe in non-magnetic aluminosilicate glass emitted from MSWI and coal fly ash is almost 1, which cannot explain the correlation between EF and Fe<sub>sol</sub>% for these ashes was almost 1 particles (Sakata et al., 2022; Li et al., 2022). Therefore, ~~the~~ non-magnetic aluminosilicates ~~aluminosilicate glass~~ derived from coal combustion and MSWI were unlikely ~~theis possibly not a~~ dominant source of aerosol particles with high Fe<sub>sol</sub>% and [d-Fe]/[d-Al] ratios ~~ratio in fine aerosol particles.~~

In the case of heavy-oil combustion, Fe<sub>sol</sub>% in oil fly ash can reach 80% under circumneutral pH conditions ~~because of~~ due to the presence of water-soluble Fe(III)-sulfate (Schroth et al., 2009; Oakes et al., 2012). ~~Despite~~ In addition, the fly ash emitted from heavy-oil combustions may be a source of d-Fe in fine aerosol particles collected in summer. Despite the limited data, the [d-Fe]/[d-Al] ratios of oil fly ash ~~were~~ reached 0.403, 1.07, and 7.00 at pH 5.7, 4.7, and -0.3, respectively (Akita et al., 1995; Desboeufs et al., 2001). ~~Assuming~~ With the assumption of a linear relationship between the ~~dissolution pH of heavy oil fly ash and the~~ [d-Fe]/[d-Al] ratio of heavy-oil fly ash, the expected [d-Fe]/[d-Al] ratio of heavy-oil ash was approximately 4.0 at the average aerosol pH in fine aerosol particles collected in summer (average:  $2.11 \pm 0.45$ ). However, ~~it is difficult to explain heavy oil fly ash was not the reason for the correlation between the [d-Fe]/[d-Al] ratio and EF of Fe in source of fine aerosol particles with high EF of Fe and [d-Fe]/[d-Al] ratio~~ because the EF of Fe in heavy-oil fly ash was almost 1.0 as well as non-magnetic aluminosilicates of coal and MSWI (Sakata et al., 2017). ~~Therefore, it is considered that the contribution of fly ash emitted from heavy-oil combustion is not large.~~

### 3.7.4.3. Fractions of crustal Fe and high-temp-FeOx in d-Fe and their Fe<sub>sol</sub>%

#### 3.7.4.3.1. Estimation method for the fractions of crustal and high-temp-FeOx and their Fe<sub>sol</sub>%

The fractions of ~~mineral dust and non~~ d-Fe derived from crustal Fe and high-temp-FeOx in d-Fe in fine aerosol particles were estimated based on the [d-Fe]/[d-Al] ratio of fine aerosol particles. ~~The [d-Fe]/[d-Al] ratios of crustal Fe and non-crustal Fe were set to values generalized from the results obtained in this study. The average [d-Fe]/[d-Al] ratio of coarse aerosol particles was 0.408, which was within the range of the ratios of aluminosilicates and loess samples in the references (Fig. 9a~~

and 9b). In the case of non-crystal Fe, we only focused on high-temp FeOx because the fine aerosol particles did not exhibit the low [d-Fe]/[d-Al] ratio attributed to non-magnetic aluminosilicates of coal combustions and MSWI ([d-Fe]/[d-Al] < 0.1, Fig. 9a). However, the [d-Fe]/[d-Al] ratio of high-temp FeOx has not been reported. Therefore, two [d-Fe]/[d-Al] ratios of pyrogenic FeOx were used in the calculation: the non-crystal [d-Fe]/[d-Al] ratio of 4.67, which was the highest [d-Fe]/[d-Al] ratio of fine aerosol particles. Another is the average [d-Fe]/[d-Al] ratio of 2.08 of fine aerosol particles with [d-Fe]/[d-Al] ratios higher than 1.5.

In consideration of the binary mixing of d-Fe in crystal d-Fe and high-temp FeOx (crystal d-Fe and high-temp FeOx d-Fe), the fraction of high-temp FeOx d-Fe in d-Fe were estimated by using the following equations:

$$f_{\text{crystal-dFe}} + f_{\text{high-temp-FeOx-dFe}} = 1, \text{ (Eq. 7)}$$

$$[\text{d-Fe}]/[\text{d-Al}]_{\text{aerosol}} = ([\text{d-Fe}]/[\text{d-Al}])_{\text{crystal}} \times f_{\text{crystal-dFe}} + ([\text{d-Fe}]/[\text{d-Al}])_{\text{non-crystal}} \times f_{\text{high-temp-FeOx-dFe}}, \text{ (Eq. 8)}$$

where  $f_{\text{crystal-Fe}}$  and  $f_{\text{high-temp-FeOx-dFe}}$  are. Hereafter, the fractions of d-Fe derived from crystal Fe and high-temp-FeOx are denoted as  $F_{\text{crust}}$  and  $F_{\text{anthro}}$ , respectively.  $([\text{d-Fe}]/[\text{d-Al}])_{\text{aerosol}}$ ,  $([\text{d-Fe}]/[\text{d-Al}])_{\text{crystal-Fe}}$ , and  $([\text{d-Fe}]/[\text{d-Al}])_{\text{high-temp-FeOx-dFe}}$  are the molar [d-Fe]/[d-Al] ratios of aerosol particles, crystal Fe, and high-temp FeOx, respectively. In addition, the  $f_{\text{high-temp-FeOx-dFe}}$  of TSP (= coarse + fine aerosol particles) was estimated by using the [d-Fe]/[d-Al] ratio of TSP. For the comparison of the  $f_{\text{high-temp-FeOx-dFe}}$  of TSP, the relative abundance of non-crystal d-Fe in fine aerosol particles to that of d-Fe in TSP samples ( $f_{\text{high-temp-FeOx-dFe-fine/TSP}}$ ) was calculated by using the following equation. In consideration of the binary mixing of d-Fe derived from mineral dust and high-temp-FeOx, the  $F_{\text{anthro}}$  in fine aerosol particles and  $F_{\text{anthro}}$  in TSP ( $F_{\text{anthro-TSP}}$ ) were estimated with the following equations:

$$(f_{\text{high-temp-FeOx-dFe/TSP}}) = \Sigma(f_{\text{high-temp-FeOx-dFe}} \times [\text{d-Fe}]_{\text{fine}}) / [\text{d-Fe}]_{\text{TSP}}, \text{ (Eq. 9)}$$

where  $\Sigma(f_{\text{high-temp-FeOx-dFe}} \times [\text{d-Fe}]_{\text{fine}})$  is the summation of non-crystal d-Fe concentration in fine aerosol particles (<1.3 μm). The  $f_{\text{high-temp-FeOx-dFe/TSP}}$  calculated by using Equation 9 was almost identical to the  $f_{\text{non-crystal-Fe}}$  of TSP calculated by using Equations 7 and 8 (Fig. S7). This result provided evidence that the coarse aerosol particles contained low amounts of non-crystal d-Fe that increased the [d-Fe]/[d-Al] ratio of TSP.

### 3.7.2. The fraction of high-temp FeOx to d-Fe

The calculation showed that the  $F_{\text{crust}} + F_{\text{anthro}} = 1$ , (Eq. 7)

$$[\text{d-Fe}]/[\text{d-Al}]_{\text{aerosol}} = ([\text{d-Fe}]/[\text{d-Al}])_{\text{crust}} \times F_{\text{crust}} + ([\text{d-Fe}]/[\text{d-Al}])_{\text{anthro}} \times F_{\text{anthro}}, \text{ (Eq. 8)}$$

where  $([\text{d-Fe}]/[\text{d-Al}])_{\text{aerosol}}$  is the [d-Fe]/[d-Al] ratio in aerosol particles. The  $([\text{d-Fe}]/[\text{d-Al}])_{\text{crust}}$  and  $([\text{d-Fe}]/[\text{d-Al}])_{\text{anthro}}$  are the representative values of [d-Fe]/[d-Al] ratios of mineral dust and anthropogenic Fe, respectively. Here, the  $([\text{d-Fe}]/[\text{d-Al}])_{\text{crust}}$  and  $([\text{d-Fe}]/[\text{d-Al}])_{\text{anthro}}$  were defined based on our observational results. The average [d-Fe]/[d-Al] ratio in coarse aerosol particles (0.408) was used as a representative  $([\text{d-Fe}]/[\text{d-Al}])_{\text{crust}}$ , and its value was within the range of proton-promoted dissolution of mineral dust (Figs. 6a and 6b). Given that the  $([\text{d-Fe}]/[\text{d-Al}])_{\text{anthro}}$  has not been reported by previous studies, its two types were used in the calculation. The  $([\text{d-Fe}]/[\text{d-Al}])_{\text{anthro}}$  was 4.67, which was the highest value observed in fine aerosol particles. Another  $([\text{d-Fe}]/[\text{d-Al}])_{\text{anthro}}$  was the average [d-Fe]/[d-Al] ratio of fine aerosol particles with [d-Fe]/[d-Al] ratios

higher than 1.5. At this time, the  $([d\text{-Fe}]/[d\text{-Al}])_{\text{anthro}}$  was 2.08. When the average  $[d\text{-Fe}]/[d\text{-Al}]$  was used for the calculation, the  $F_{\text{anthro}}$  was higher than the value calculated by the highest  $([d\text{-Fe}]/[d\text{-Al}])_{\text{anthro}}$  (Figs. S9a and S9b).  $F_{\text{anthro}}$  was calculated using the average  $([d\text{-Fe}]/[d\text{-Al}])_{\text{anthro}}$  to avoid underestimation.

615 Finally, the  $\text{Fe}_{\text{sol}}\%$  of crustal and high-temp-FeOx (crustal- $\text{Fe}_{\text{sol}}\%$  and anthro- $\text{Fe}_{\text{sol}}\%$ ) in fine aerosol particles were estimated through the following equations:

$$\text{Crustal-Fe}_{\text{sol}}\% = [(d\text{-Fe} \times F_{\text{crustal}})/\text{crustal Fe}] \times 100, \text{ (Eq. 9)}$$

$$\text{Anthro-Fe}_{\text{sol}}\% = [(d\text{-Fe} \times F_{\text{anthro}})/\text{non-crustal Fe}] \times 100. \text{ (Eq. 10)}$$

Crustal and non-crustal Fe concentrations were calculated using Eqs. 3 and 4, respectively.

#### 620 **4.3.2. Size dependence and seasonal variation of $F_{\text{anthro}}$**

The annual average of the fractions of non crustal Fe in d-Fe in  $F_{\text{anthro-TSP}}$  was  $19.9 \pm 19.2\%$  (Fig. 4a7a, range: 1.48–80.7%). The fraction of non-crustal Fe calculated with the  $[d\text{-Fe}]/[d\text{-Al}]$  ratio of 4.67 was lower than that calculated. The  $F_{\text{anthro-TSP}}$  was higher in summer–fall with the  $[d\text{-Fe}]/[d\text{-Al}]$  ratio of 2.08 (Figs. S8a and S8b). High non-crustal Fe fractions were observed in summer and fall influence of Japanese air mass (average:  $29.4 \pm 25.8\%$ , range: 9.41–80.7%) when the air mass originated from the domestic region (Fig. S1). By contrast, non-crustal Fe (than in winter–spring with the influence of Asian outflow (Fig. 7a, average:  $13.5 \pm 10.6\%$ , range: 1.48–34.4%) in winter and spring, when air masses originated from East Asia, was lower than that%). The high  $F_{\text{anthro-TSP}}$  in summer and was attributed to the high EF of Fe and  $[d\text{-Fe}]/[d\text{-Al}]$  ratio in the season. From the viewpoint of size dependence of  $F_{\text{anthro}}$ , the largest  $F_{\text{anthro}}$  in summer–fall. A satellite based observation reported that and winter–spring was found in the finest and 0.39–0.69  $\mu\text{m}$  fractions, respectively (Fig. 7b). These results are consistent with the source apportionment of Fe using  $\delta^{56}\text{Fe}$  at the same sampling site because (i) the contribution of anthropogenic Fe to d-Fe in fine aerosol particles was more significant in summer than in spring due to the low  $\delta^{56}\text{Fe}$ , and (ii) the lowest  $\delta^{56}\text{Fe}$  was found in the finest and 0.39–0.69  $\mu\text{m}$  fractions in summer and spring, respectively. Thus, the source estimation of Fe using  $[d\text{-Fe}]/[d\text{-Al}]$  is consistent with that which uses  $\delta^{56}\text{Fe}$ .

635 Given the Fe supply to the Pacific Ocean, spring is the most important season throughout the year because approximately half of aerosol transport events from East Asia to the Pacific Ocean occurred in spring between 2007 and 2016 occurred in spring, and that dust they were mainly associated with mineral dust events mainly occurred in spring (Zhu, Q., 2020). In addition, atmospheric Fe is supplied to the surface ocean by an episodic dust event that accounts for approximately 30–90% of annual Fe depositions within 5% of the days of a year (Mahowald et al., 2009). In consideration of these phenomena facts with the estimation results of  $F_{\text{anthro-TSP}}$  and  $F_{\text{crust-TSP}}$ , mineral dust was the dominant source of d-Fe in aerosol particles deposited in the North Pacific Ocean. (Fig. 7a). Nevertheless, the contribution of high-temp-FeOx, as a source of d-Fe in surface seawater during dust events, cannot be negligible disregarded because the average fraction of non-crustal Fe during spring and dust events was  $10.2 \pm 7.586\%$ .

On the basis of the fractions of crustal and non-crustal Fe, the  $Fe_{sol}$ % of crustal and non-crustal Fe in fine aerosol particles were estimated by using following equations:

645 **4.3.3. Crustal- $Fe_{sol}$ % =  $[(d\text{-}Fe \times f_{\text{crustal-d}Fe}) / \text{crustal Fe}] \times 100$ , (Eq. 10) and anthro- $Fe_{sol}$ %**

$\text{High-temp-}FeOx\text{-}Fe_{sol}\% = [(d\text{-}Fe \times f_{\text{high-temp-}FeOx\text{-}dFe}) / \text{non-crustal Fe}] \times 100$ . (Eq. 11)

Crustal and non-crustal Fe concentrations were calculated by using Equations 3 and 4, respectively. The annual average crustal- $Fe_{sol}$ % and non-crustal  $Fe_{sol}$ % of fine aerosol particles were (ave.  $\pm 1\sigma$ : 14.1 % (0–43.7 %) and 9.35 % (0.501–46.2 %), respectively (Figs. 8c and 8d). The average crustal  $Fe_{sol}$ % of TSP was  $6.52 \pm 3.05$  % ( $[d\text{-}Fe] / [d\text{-}Al]$ : 2.08) because insoluble Fe in mineral dust was mainly distributed in coarse aerosol particles. When the  $[d\text{-}Fe] / [d\text{-}Al]$  ratio was set to 4.67, the crustal- $Fe_{sol}$ % and non-crustal  $Fe_{sol}$ % of fine aerosol particles were 20.2 % (0.0285–65.1 %) and 4.62 % (0.209–35.9 %), respectively (Figs. S8c and S8d). The  $\pm 9.3$  % was higher value of crustal than the anthro- $Fe_{sol}$ % (ave.  $\pm 1\sigma$ :  $9.35 \pm 10.29$  %) when the  $[d\text{-}Fe] / [d\text{-}Al]$  ratio was set to 4.67 than that when the  $[d\text{-}Fe] / [d\text{-}Al]$  ratio was set to 2.08 was due to the large contribution of crustal Fe to d-Fe. Thus, when focusing focus was on fine aerosol particles (Figs. 7c and 7d), mineral dust showed higher  $Fe_{sol}$ % than high-temp FeOx. One reason is that high-temp FeOx was derived from local. This result is inconsistent with the finding of previous studies where the  $Fe_{sol}$ % of anthropogenic emissions and may not have undergone considerable chemical aging. Another possible reason Fe derived from high-temperature combustion was higher than that of mineral dust (Sedwick et al., 2007; Sholkovitz et al., 2009). One of the reasons is that the Fe oxide nanoparticles were poorly solubilized at the aerosol pH of the samples obtained in this study. Marcotte et al. 1.7 and 4.3, (2020) showed that the  $Fe_{sol}$ % of submicron Fe-oxides (<1.5 %) was lower than those of submicron illite and kaolinite (about Marcotte et al. 2020). As previously mentioned, fine aerosol particles with high  $Fe_{sol}$ % (>10 %) experienced highly acidic conditions (pH < 3.0). Therefore, %. Similar results have been obtained from the high  $Fe_{sol}$ % shown by mineral dust in non-crustal Fe in fine aerosol particles is consistent with the results of laboratory experiments (Marcotte et al. 2020). The  $Fe_{sol}$ % of fine aerosol particles on Fe dissolution from aluminosilicates and Fe-oxides at pH 2.0 (particle diameter < 100  $\mu\text{m}$ , Journet et al., 2008). According to the results of this study, the aerosol pH of fine aerosol particles with high  $Fe_{sol}$ % (>10 %) was lower than 3.0, but almost no fine aerosol samples whose aerosol pH was lower than 1.7 was observed (Fig. 4e). Therefore, even if the Fe-oxides were derived from high-temperature combustion, the significant increase in their anthro- $Fe_{sol}$ % was unlikely without sufficient acidification. Another reason is that mineral dust with a low  $Fe_{sol}$ % was mainly present in coarse aerosol particles. The annual average of crustal- $Fe_{sol}$ % in TSP was  $6.52 \pm 3.05$  %, which was lower than that of anthro- $Fe_{sol}$ %.

670 The crustal- $Fe_{sol}$ % of fine aerosol particles in the 0.39–0.69 and 0.69–1.3  $\mu\text{m}$  fractions were higher than that in the finest fraction throughout the year (Fig. 6e), indicating 7c), which indicates that mineral dust in the 0.39–0.69 and 0.69–1.3  $\mu\text{m}$  fractions was more aged than that in the finest fraction. Single-particle analyses of aerosol particles in East Asia showed that the abundance of the. This result is reasonable because internally mixed particles of Fe and sulfate were found in the fine aerosol particles, whose number fraction relative to the total number of Fe-bearing particles with sulfate was became the

highest/largest at approximately 0.7  $\mu\text{m}$  of aerosol diameter around 700 nm rather than finer than 400 nm (Sullivan et al., 2007a, 2007; Li et al., 2017; Zhu, Y. et al., 2020, 2022). In addition,  $\text{Fe}_{\text{sol}}\%$  The uptake of Fe-bearing particles into cloud water promotes internal mixing with sulfate (Li et al., 2017; Liu et al., 2018; Lin et al., 2019). However, the sufficient dissolution of Fe in fine aerosol particles at the pH condition of mineral dust/cloud water is unlikely (global average pH: 5.2, Shah et al., 2020), as observed in the 0.39–0.69 and 0.69–1.3  $\mu\text{m}$  fractions collected in the Pacific Ocean were higher than that in coarse relationship between aerosol particles due to chemical aging via condensation–evaporation/pH and  $\text{Fe}_{\text{sol}}\%$  (Fig. 4e). The aerosol pH decreased rapidly with the phase transition from cloud water to the aerosol concentration of protons in a tiny amount of aerosol liquid water content. Furthermore, the uptake coefficient of  $\text{SO}_2$  by aluminosilicates increases as they experience cloud processes, which is expected to further promotion of aerosol acidifications (Wang et al., 2019). Considering these facts,  $\text{Fe}_{\text{sol}}\%$  in fine aerosol particles was enhanced by the aerosol–cloud water cycle during transport (Sakata et al., 2022). Therefore, the chemical aging of mineral dust in fine aerosol particles plays an important role in the supply of Fe to the ocean surface.

#### 4.5. Implication for marine aerosol particles

The availability of the  $[\text{d-Fe}]/[\text{d-Al}]$  ratio for evaluating the emission source/evaluation of  $\text{d-Fe}$   $F_{\text{crust}}$  and  $F_{\text{anthro}}$  in marine aerosol particles was investigated by using the observational results of previous studies (Buck et al., 2006, 2010b; Shelley et al., 2018; Baker et al., 2020; Sakata et al., 2022). In general, soluble metals in aerosol particles were extracted by using MQ with ultrapure water through instantaneous or batch leaching, and only Baker et al. (2020) employed used ammonium acetate solution with a pH of 4.7. The  $[\text{d-Fe}]/[\text{d-Al}]$  ratio of the marine aerosol samples collected in the Pacific and Atlantic Oceans were rarely higher than 1.0 (Fig. 11a, Figs. 8a and 11b, 8b). The fractions of non-crustal  $\text{d-Fe}$  in  $F_{\text{anthro}}$  of TSP collected from the Atlantic and Pacific Oceans were 9.58 % and 13.4 %, respectively (Fig. 11e, 8c). In the Pacific Ocean, the contribution of non-crustal  $\text{d-Fe}$  tends to be  $F_{\text{anthro}}$  was higher in the region east of 170 °E because anthropogenic Fe in fine aerosol particles is/was transported farther than that in coarse mineral dust particles (Fig. 12a, 9a, Mahowald et al., 2018). By contrast, the large fraction of anthropogenic Fe  $F_{\text{anthro}}$  in the Atlantic was found/detected around the coastal areas/areas in North America and Europe (Fig. 12b, 9b). This result was consistent with the estimation of the non-crustal Fe fraction  $F_{\text{anthro}}$  based on  $\delta^{56}\text{Fe}$ , which indicated that more than half of the  $\text{d-Fe}$  in Fe around the coastal regions was derived from anthropogenic Fe with a negative  $\delta^{56}\text{Fe}$  (Conway et al., 2019). However, the fraction  $F_{\text{anthro}}$  of non-crustal Fe in TSP with negative  $\delta^{56}\text{Fe}$  values, which were estimated on the basis of the  $[\text{d-Fe}]/[\text{d-Al}]$  ratio, was  $12.4 \pm 2.9$  % (Fig. 8c). Thus, the  $F_{\text{anthro}}$  estimated by the  $[\text{d-Fe}]/[\text{d-Al}]$  ratio was only  $12.4 \pm 2.92$  % (Fig. 11e). Thus, a discrepancy existed between the results of  $\text{d-Fe}$  emission source estimates based on Fe isotopic ratios and those based on  $[\text{d-Fe}]/[\text{d-Al}]$ , differed from that estimated by  $\delta^{56}\text{Fe}$ . One of the reasons is/for this discrepancy is/was the limited data on/of the  $[\text{d-Fe}]/[\text{d-Al}]$  and  $\delta^{56}\text{Fe}$  ratios off/for emission source samples, in particular/specifically anthropogenic emissions. The  $[\text{d-Fe}]/[\text{d-Al}]$  ratio and  $\delta^{56}\text{Fe}$  of high-temp-FeOx were estimated based on the basis-of-the measurement values of aerosol particles. The due to the lack of reliable reference materials for high-temp-FeOx. By contrast, the  $[\text{d-Fe}]/[\text{d-Al}]$

ratios of mineral dust and non-magnetic aluminosilicates of coal combustion and MSWI had a small effect on the uncertainty of  $F_{\text{anthro}}$  estimation due to the ~~non-crustal Fe fraction estimates because measured presence of reference values were available.~~ Therefore, further studies involving the accumulated data on the [d-Fe]/[d-Al] ratio and  $\delta^{56}\text{Fe}$  of high-temp-FeOx collected from various industrial sites are required. Currently, the accurate  $\delta^{56}\text{Fe}$  and [d-Fe]/[d-Al] ratio of high-temp-FeOx may be obtained through the separation of magnetic particles, as performed by Zuo et al. (2022). The accumulated data on the previously reported values of [d-Fe]/[d-Al] ratio can be used and are expected to provide ~~insight~~ insights into the time-series variation in the contribution of anthropogenic Fe to aerosols in marine aerosols.

Figure 11b8b shows a scatter plot of the [d-Fe]/[d-Al] ratios and  $\text{Fe}_{\text{sol}}\%$  of size-fractionated aerosol particles collected from the Atlantic and Pacific Oceans (Baker et al., 2020; Sakata et al., 2022). The average [d-Fe]/[d-Al] ratios of coarse and fine aerosol particles collected offshore of the Sahara Desert were  $0.216 \pm 0.163$  and  $0.155 \pm 0.0549055$ , respectively. These values were similar to the [d-Fe]/[d-Al] ratio of Saharan dust ( $0.108 \pm 0.0609$ ), indicating 061), which indicates that the d-Fe in these size-fractionated aerosol samples originated from Saharan dust. Iron in the size-fractionated aerosol particles collected in the western Pacific Ocean was also derived from mineral dust regardless of aerosol diameter because the EF of Fe in all size fractions was almost 1.00 (Sakata et al., 2022). The average [d-Fe]/[d-Al] ratio of coarse aerosol particles collected above the Pacific Ocean ( $0.378 \pm 0.104$ ) was slightly higher than the average [d-Fe]/[d-Al] ratio of Asian dust ( $0.238 \pm 0.201$ ) but was similar to the ratio that of coarse aerosol particles collected in this study ( $0.408 \pm 0.168$ ). Therefore, the d-Fe in these samples was derived from the hydrolysis or proton-promoted dissolution of mineral dust. Although the Fe in coarse aerosol particles collected in the Atlantic and Pacific Oceans was derived from mineral dust, the [d-Fe]/[d-Al] ratios of the coarse and fine aerosol particles above the Atlantic Ocean ~~was were~~ lower than that of coarse aerosol particles collected in the Pacific Ocean. The differences in the mineralogical compositions of mineral dust in the hinterlands account for the differences in the ratios of the aerosol particles collected in the Atlantic and Pacific Oceans. Therefore, ~~measuring~~ measurement of the [d-Fe]/[d-Al] ratio of soil samples around the sampling site is important to determine the representative [d-Fe]/[d-Al] ratio of mineral particles in aerosol particles.

The high  $\text{Fe}_{\text{sol}}\%$  ( $>10\%$ ) of fine aerosol particles in the Pacific was attributed to ferric organic complexes of humic-like substances (Fe(III)-HULIS, Sakata et al. 2022). The [d-Fe]/[d-Al] ratio of fine aerosol particles containing Fe(III)-HULIS ~~is was~~ expected to be between 1.0 and 1.5 due to ligand-promoted dissolution. However, the ~~obtained~~ [d-Fe]/[d-Al] ratio of ~~of fine aerosol for these~~ particles containing Fe(III)-HULIS was  $0.440 \pm 0.117$  (range: 0.255–0.567), which was consistent with the ratio of Asian dust that underwent proton-promoted dissolution. A previous study reported that the  $\text{Fe}_{\text{sol}}\%$  of these samples ~~was enhanced by the~~ aerosol acidification of aluminosilicates ~~enhanced the  $\text{Fe}_{\text{sol}}\%$  of samples~~; Fe(III)-HULIS then formed via complexation reactions in cloud water (Sakata et al., 2022). ~~Thus, the~~ The [d-Fe]/[d-Al] ratio may not change even if the Fe species was altered by atmospheric processes after Fe solubilization. However, ~~this point needs~~ further investigation. ~~The of this point is required. Moreover, to evaluate source and dissolution processes using the [d-Fe]/[d-Al] ratio, we preferred the~~ determination of the [d-Fe]/[d-Al] ratio via ~~MQ~~ Ultrapure water extraction without organic ligands (e.g., oxalate and acetate) ~~is preferred for investigating the contribution of ligand promoted dissolution to  $\text{Fe}_{\text{sol}}\%$  enhancement~~ because the ratio is altered

if the extracted solution contains organic ligands (e.g., coarse aerosol ~~{(P)}-vs.~~ versus coarse aerosol ~~{(L)}~~, Fig. 9a).  
745 ~~However,6a).~~ The data on the [d-Fe]/[d-Al] ratio of size-fractionated marine aerosol particles under the effect of high-temp-  
FeOx ~~up to this point~~ have not ~~yet~~ been published ~~at this time.~~ Therefore, further studies on the [d-Fe]/[d-Al] ratio of marine  
aerosol particles influenced by high-temp-FeOx are required. If future studies detect high [d-Fe]/[d-Al] ratios in marine aerosol  
samples that are strongly affected by high-temp-FeOx, then the [d-Fe]/[d-Al] ratio will be a powerful tool for  
estimatingestimation of the fraction of crustal and non-crustal Fe in d-Fe in marine aerosol particles.

750

## 5.6. Conclusion

Annual observations ~~were conducted onof the~~ total and dissolved d-Fe and Al concentrations in size-fractionated aerosol  
particles. ~~Total were conducted at the eastern end of East Asia. The total~~ Fe and Al concentrations were mainly distributed in  
coarse aerosol particles, whereas d-Fe and d-Al concentrations dominated ~~in~~ fine aerosol particles. ~~ConsideringGiven~~  
755 higher d-Fe concentration and longer residence time of fine aerosol particles than ~~those of~~ coarse aerosol particles, the  
atmospheric deposition of fine aerosol particles was the dominant source of d-Fe in the surface ocean. ~~Since theThe~~ [d-Fe]/[d-  
Al] ratio of coarse aerosol particles ( $0.408 \pm 0.168$ ) was lower than that of fine aerosol particles ( $1.15 \pm 0.803$ ), ~~80~~. Thus, the  
sources of d-Fe differed between coarse and fine aerosol particles. The [d-Fe]/[d-Al] ratio of coarse aerosol particles was  
similar to that observed ~~offor~~ Fe dissolved via proton-promoted dissolution. ~~Indeed,The~~  $F_{\text{sol}}\%$  increased as the surfaces of  
760 coarse particles became hygroscopic through the reaction with sulfuric acid. This effect intensified with the reduction in  
particle size. The fine aerosol particles presented a wide range of [d-Fe]/[d-Al] ratios (0.386–4.67). The correlation of the [d-  
Fe]/[d-Al] ratio of the fine aerosol particles with the EF of Fe indicated that the high [d-Fe]/[d-Al] ratios ( $>1.5$ ) ~~couldcan~~ be  
attributed to non-crustal Fe. High-temp FeOx in magnetic particles ~~waswere~~ likely the dominant species ~~inof~~ non-crustal Fe  
with high [d-Fe]/[d-Al] ratios. The ~~fractions of mineral dust~~  $F_{\text{crust}}$  and ~~high temp FeOx~~  $F_{\text{anthro}}$  were evaluated ~~on the basis of using~~  
765 the [d-Fe]/[d-Al] ratios ~~and emission sources of in~~ aerosol particles, and their emission source samples. Approximately 80 %  
of d-Fe in TSP collected in spring, when numerous ~~events of~~ aerosol transport events from East Asia to the North Pacific  
occurred, originated from mineral particles. The high ~~fraction of mineral dust~~  $F_{\text{crust}}$  was attributed to the higher crustal- $F_{\text{sol}}\%$   
~~of crustal Fe~~ than ~~that of high temp FeOx anthro~~- $F_{\text{sol}}\%$ . The  $F_{\text{sol}}\%$  of submicron mineral dust (e.g., illite) was ~~known to be~~  
higher than ~~thatthose~~ of hematite and magnetite of the same size ~~under acidic conditions in solutions with pH higher than 1.7~~.  
770 Furthermore, the  $F_{\text{sol}}\%$  of fine aerosol particles increased with the decrease in aerosol pH, ~~indicatingwhich indicates~~ that the  
acidification of mineral particles played an important role in the supply of d-Fe to surface seawater in the North Pacific via  
atmospheric deposition. Thus, the source estimation of d-Fe ~~by~~ using the [d-Fe]/[d-Al] ratio is a powerful tool for  
estimatingestimation not only of the source of d-Fe in marine aerosols but also the dissolution processes of Fe in aerosol  
particles. The source estimation of d-Fe ~~by~~ using the [d-Fe]/[d-Al] ratio also has the advantage of being performed through a  
775 simple analytical method, in which Fe and Al are extracted by using MQultrapure water, and their concentrations are measured  
through ICP-MS. Therefore, this method can be easily conducted not only in future studies but also on aerosol samples



collected in previous [studies/research](#). Currently, data on the [d-Fe]/[d-Al] ratios of aerosols ~~that~~, [which](#) are strongly affected by anthropogenic Fe and emission sources associated with high-temperature combustion processes, are limited. Therefore, ~~collecting~~ [collection of](#) data on the [d-Fe]/[d-Al] ratios of these samples will enable us to identify the emission sources of d-Fe in marine aerosol particles with increased robustness.

780

**Data Availability** All quantitative data will be available at the ERAN database (<https://www.ied.tsukuba.ac.jp/database/00156.html>) with a doi: 10.34355/CRiED.U.Tsukuba.00156.

785

**Supplement.** The supplement related to this article is available online at XXXX.

**Author contributions.** The study was designed by K.S., A.S., and Y.T. Aerosol sampling was performed by K.S. and Y.Y. Major ion concentrations were determined by K.S., Y.Y., and C.M. Trace metal concentrations were measured by K.S., C.M., and M.K. The paper was written by K.S., and Y.T., and all authors were reviewed the manuscript before submission.

790

**Competing interests.** The authors declare that they have no conflict of interest.

**Financial support.** The studies were supported by Grant-in-Aid for JSPS Research Fellow (14J06437).

795 **Figure captions**

Figure 1: Sites (Higashi-Hiroshima) of size-fractionated aerosol sampling. Maps were visualized by Ocean Data View (Schlitzer, 2021).

Figure 2: Monthly variations and size distributions of (a)  $\text{Na}^+$ , (b)  $\text{Ca}^{2+}$ , (c)  $\text{Mg}^{2+}$ , (d)  $\text{K}^+$ , (e)  $\text{NH}_4^+$ , (f)  $\text{Cl}^-$ , (g)  $\text{NO}_3^-$ , (h)  $\text{SO}_4^{2-}$ , and (i)  $\text{nss-SO}_4^{2-}$ . The summation of all fractions corresponds to TSP concentration. (a) total Al and (b) total Fe concentrations. (c) Box plot of EF in each size fraction.

Figure 3: Monthly variation and size distributions of (a) d-Fe and (b)  $\text{Fe}_{\text{sol}}\%$ . (c) Box plot of  $\text{Fe}_{\text{sol}}\%$  in each size fraction. Monthly variation and size distributions of (d) d-Al and (e)  $\text{Al}_{\text{sol}}\%$ . (f) Box plot of  $\text{Al}_{\text{sol}}\%$  in each size fraction.

Figure 3: Monthly variations and size distributions of (a) total Al and (b) total Fe concentrations. (c) Box plot of  $\text{Fe}_{\text{sol}}\%$  in each size fraction.

805 Figure 4: Scatter plots of non-crystal Fe concentration with (a) Cu, (b) Zn, (c) Sb, and (d) Pb.  $\text{Fe}_{\text{sol}}\%$  and  $\text{Al}_{\text{sol}}\%$  in coarse aerosol particles with (a)  $[\text{nss-SO}_4^{2-}]/[\text{total Fe}]$  and  $[\text{nss-SO}_4^{2-}]/[\text{total Al}]$  and (b)  $[\text{NO}_3^-]/[\text{total Fe}]$  and  $[\text{NO}_3^-]/[\text{total Al}]$ . Scatter plots of  $\text{Fe}_{\text{sol}}\%$  and  $\text{Al}_{\text{sol}}\%$  in fine aerosol particles with (c)  $[\text{nss-SO}_4^{2-}]/[\text{total Fe}]$  and  $[\text{nss-SO}_4^{2-}]/[\text{total Al}]$ , (d)  $[\text{NO}_3^-]/[\text{total Fe}]$  and  $[\text{NO}_3^-]/[\text{total Al}]$  and (e) aerosol pH.

810 Figure 5: Scatter plots of non-crystal Fe concentration and Fe with (a) Zn, non-crystal Fe, (b) Sb, total V, (c) Pb, and (d) V, total Cu, (d) total Sb, and (e) total Pb concentrations in fine aerosol particles.

815 Figure 6: (a) Box plot of  $[\text{d-Fe}]/[\text{d-Al}]$  in emission source samples (Proton) and (Ligand) indicating proton- and ligand-promoted dissolutions. Scatter plots of the  $[\text{d-Fe}]/[\text{d-Al}]$  ratio with (b) the  $\text{Fe}_{\text{sol}}\%$  and (c) EF of Fe. Light blue circles and black squares in panels (b) and (c) represent the data on coarse and fine aerosol particles collected in Higashi-Hiroshima, respectively. Pink, yellow, light green, and gray regions show the typical ranges of the  $[\text{d-Fe}]/[\text{d-Al}]$  ratios of aluminosilicate glasses of coal combustion and MSWI, the proton- and ligand-promoted dissolution of mineral dust, and high-temp-FeOx, respectively. The regions were decided based on the box plots of panels (a).

Figure 7: Monthly variations of (a) non-crystal Fe fraction in TSP and (b) non-crystal Fe fraction in fine aerosol particles, (c) crystal- $\text{Fe}_{\text{sol}}\%$ , and (d) non-crystal  $\text{Fe}_{\text{sol}}\%$  when the  $[\text{d-Fe}]/[\text{d-Al}]$  ratio of non-crystal Fe is 2.08. The yellow shaded region shows the period when the air mass was mainly derived from Japan.

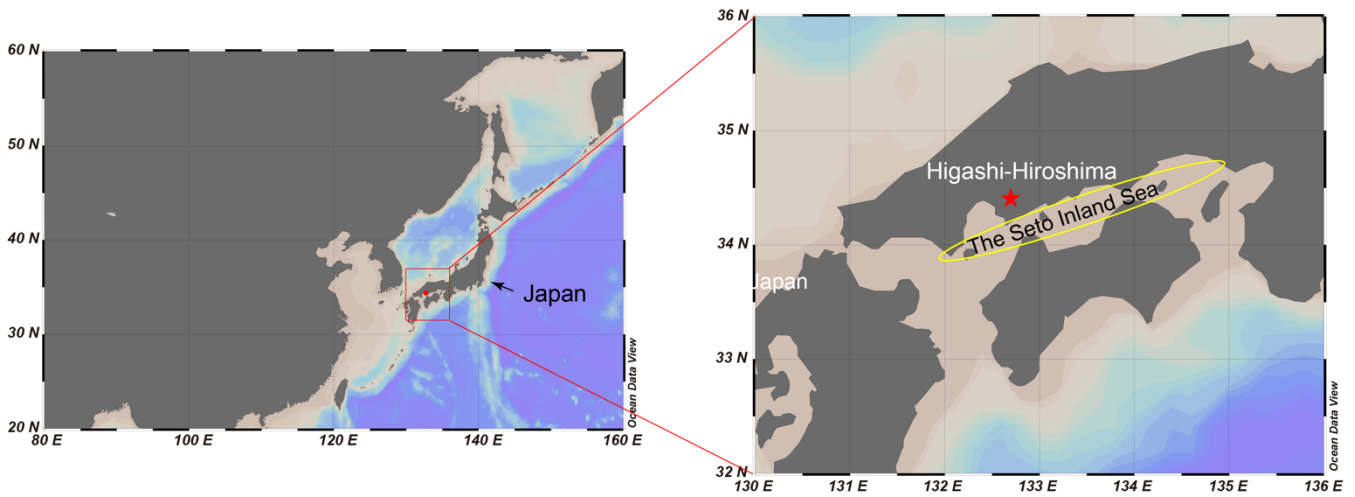
820 Figure 8: Scatter plots of the  $[\text{d-Fe}]/[\text{d-Al}]$  ratio with  $\text{Fe}_{\text{sol}}\%$  in (a) TSP samples and (b) size-fractionated aerosol particles collected in the marine atmosphere. (c) The fraction of non-crystal d-Fe in these samples was calculated using Equations 6 and 7. The  $[\text{d-Fe}]/[\text{d-Al}]$  ratios of mineral dust in the Pacific and Atlantic Oceans were the average ratios of Asian (0.238) and Saharan dusts (0.163), respectively. The  $[\text{d-Fe}]/[\text{d-Al}]$  ratio of non-crystal Fe was fixed at 2.08. The  $[\text{d-Fe}]/[\text{d-Al}]$  ratios of the TSP and size-fractionated aerosol samples were adapted from the works of Buck et al. (2006, 2010b), Shelley et al. (2018), Baker et al. (2020), and Sakata et al. (2022). The Fe isotopic ratio of TSP in the Atlantic Ocean was reported by Conway et al. (2019). Pink, yellow, light green, and gray regions in panels (a) and (b) show the typical  $[\text{d-Fe}]/[\text{d-Al}]$  ratios of coal/MSWI fly ash, proton- and ligand-promoted mineral dust dissolutions, and pyrogenic Fe oxides, respectively.

825

Figure 9: Non-crustal Fe fractions in the TSP samples collected from (a) the Pacific Ocean and (b) Atlantic Ocean. Non-crustal Fe fractions were calculated using the  $[d\text{-Fe}]/[d\text{-Al}]$  ratios reported by Buck et al. (2006, 2010b) and Shelley et al. (2018). The figures were described by Ocean Data View (Schlitzer, 2021).

Figures

835



840

Figure 1: Sites (Higashi-Hiroshima) of size-fractionated aerosol sampling. Maps were visualized by Ocean Data View (Schlitzer, 2021).

845

Figure 6

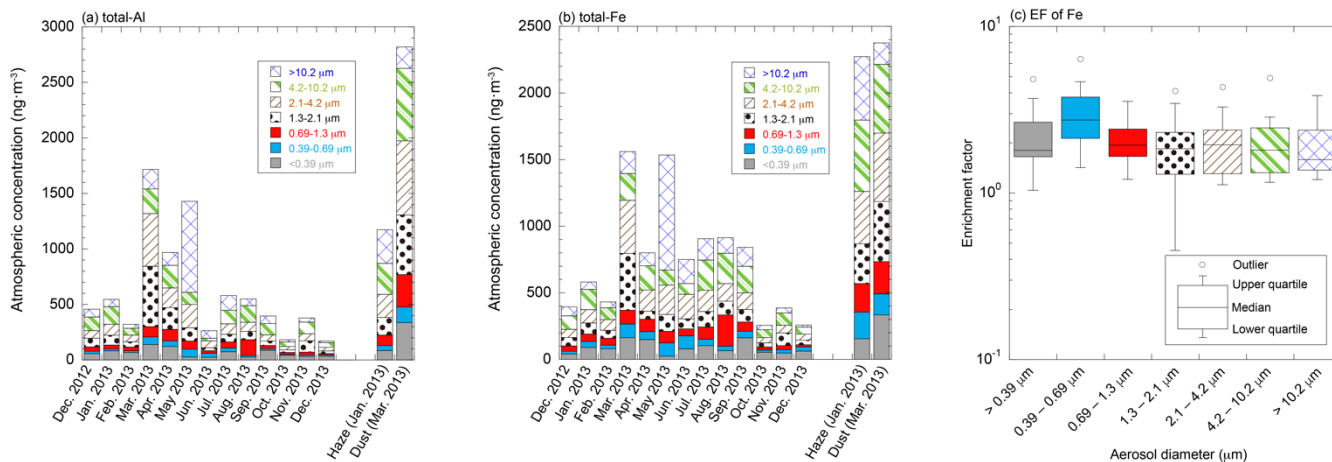
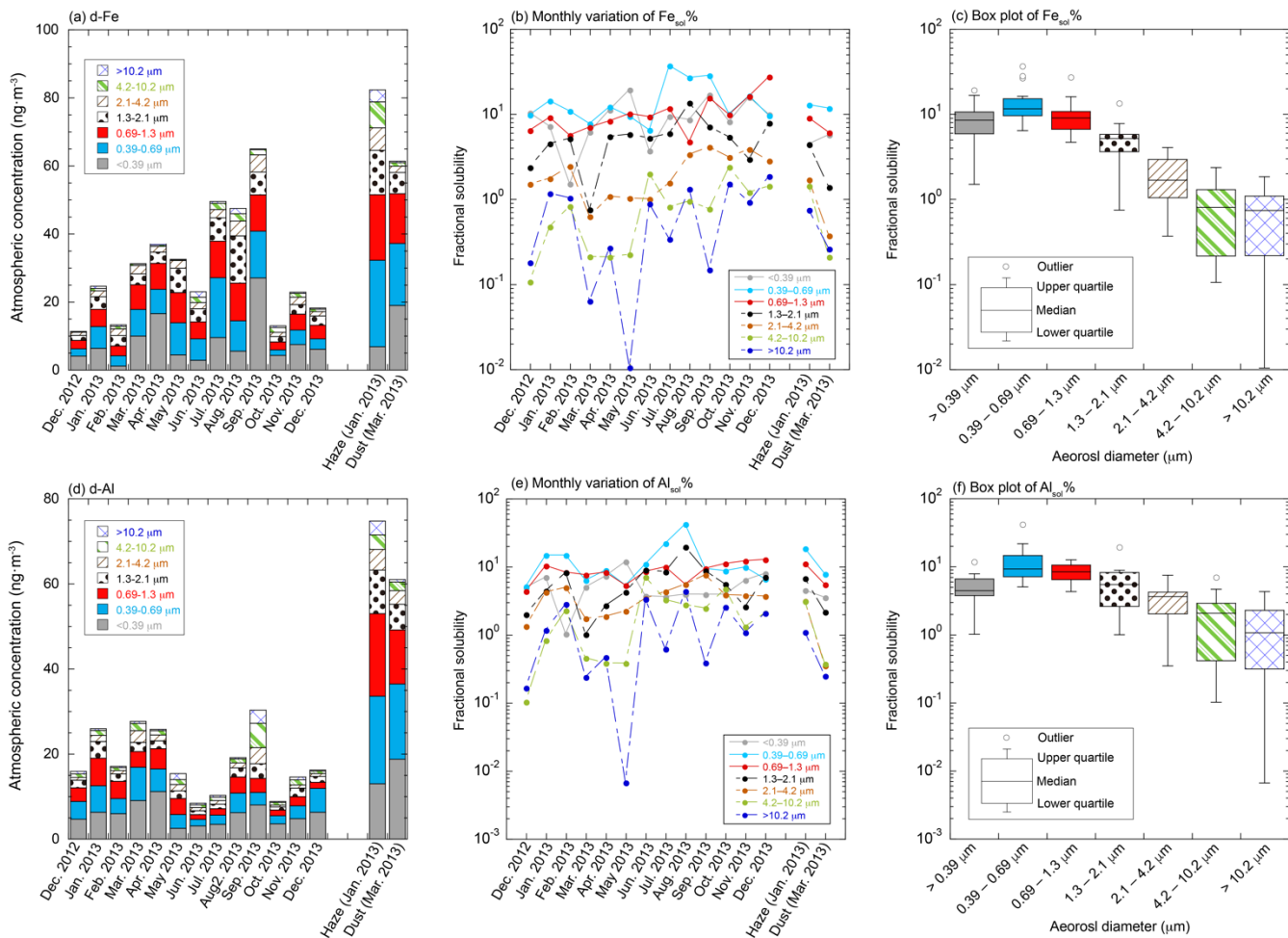
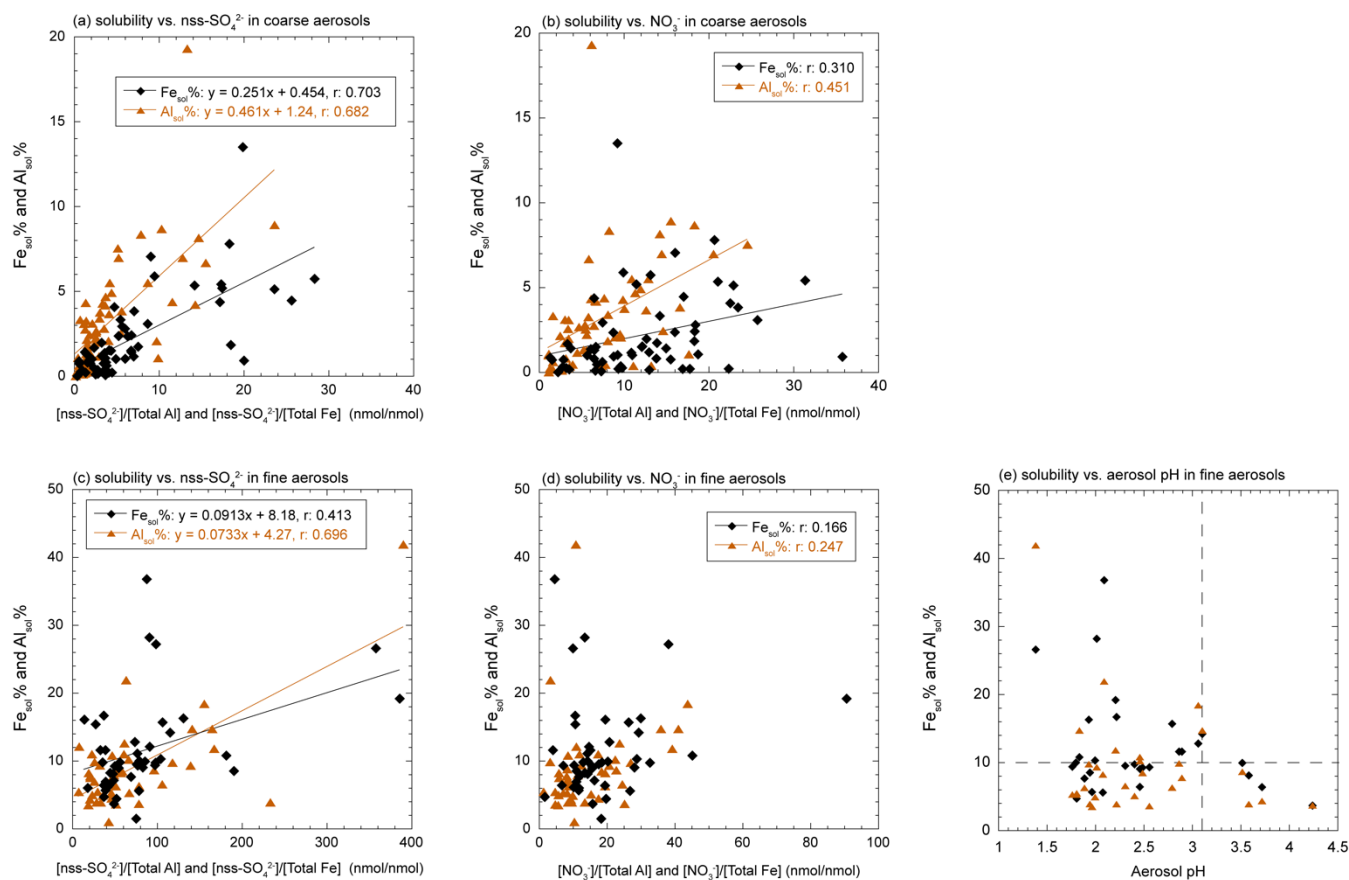


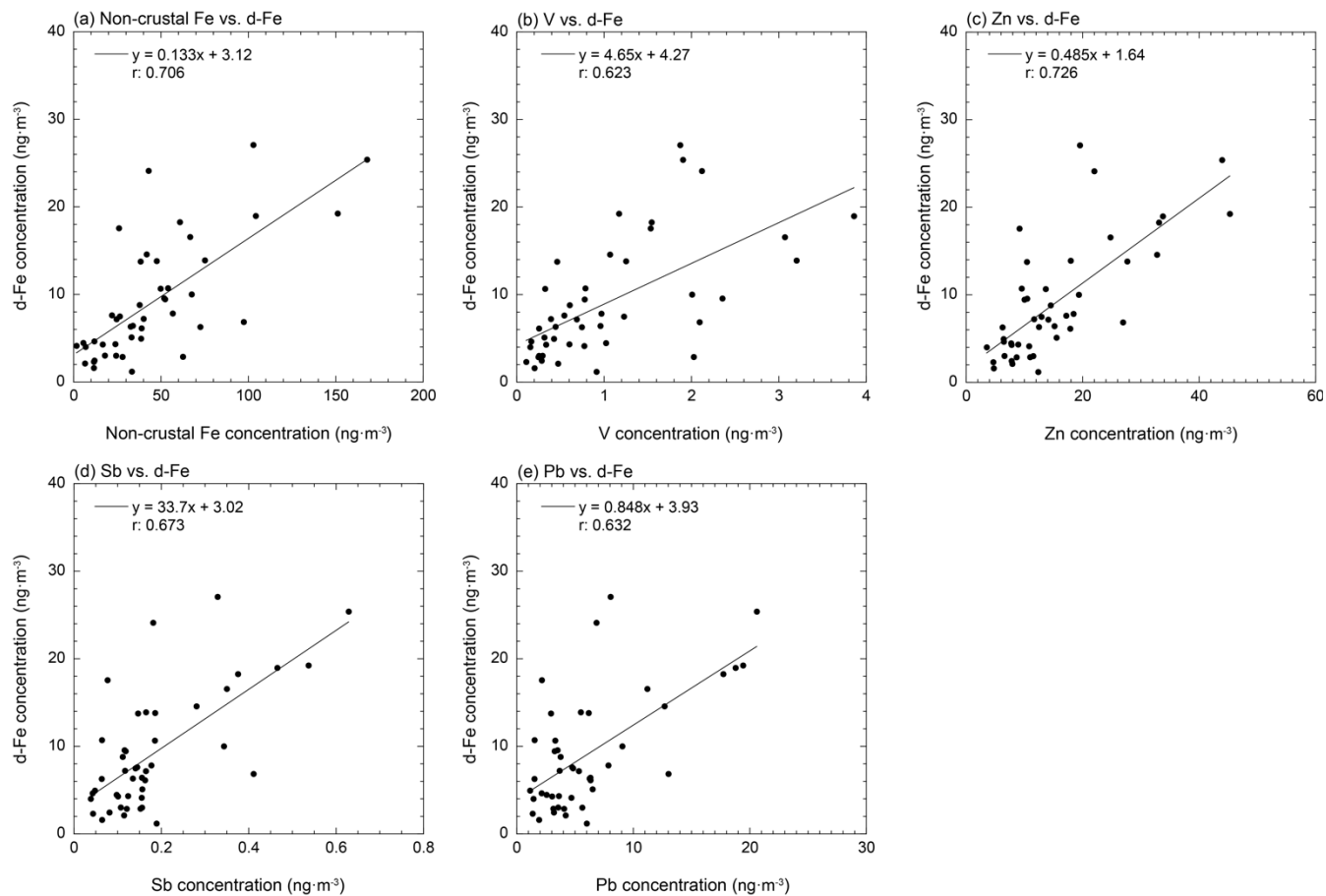
Figure 2: Monthly variations and size distributions of the (a) total Al and (b) total Fe concentrations. (c) Box plot of EF in each size fraction.



**Figure 3:** Monthly variation and size distributions of (a) d-Fe and (b) Fe<sub>sol</sub>%. (c) Box plot of Fe<sub>sol</sub>% in each size fraction. Monthly variation and size distributions of (d) d-Al and (e) Al<sub>sol</sub>%. (f) Box plot of Al<sub>sol</sub>% in each size fraction.

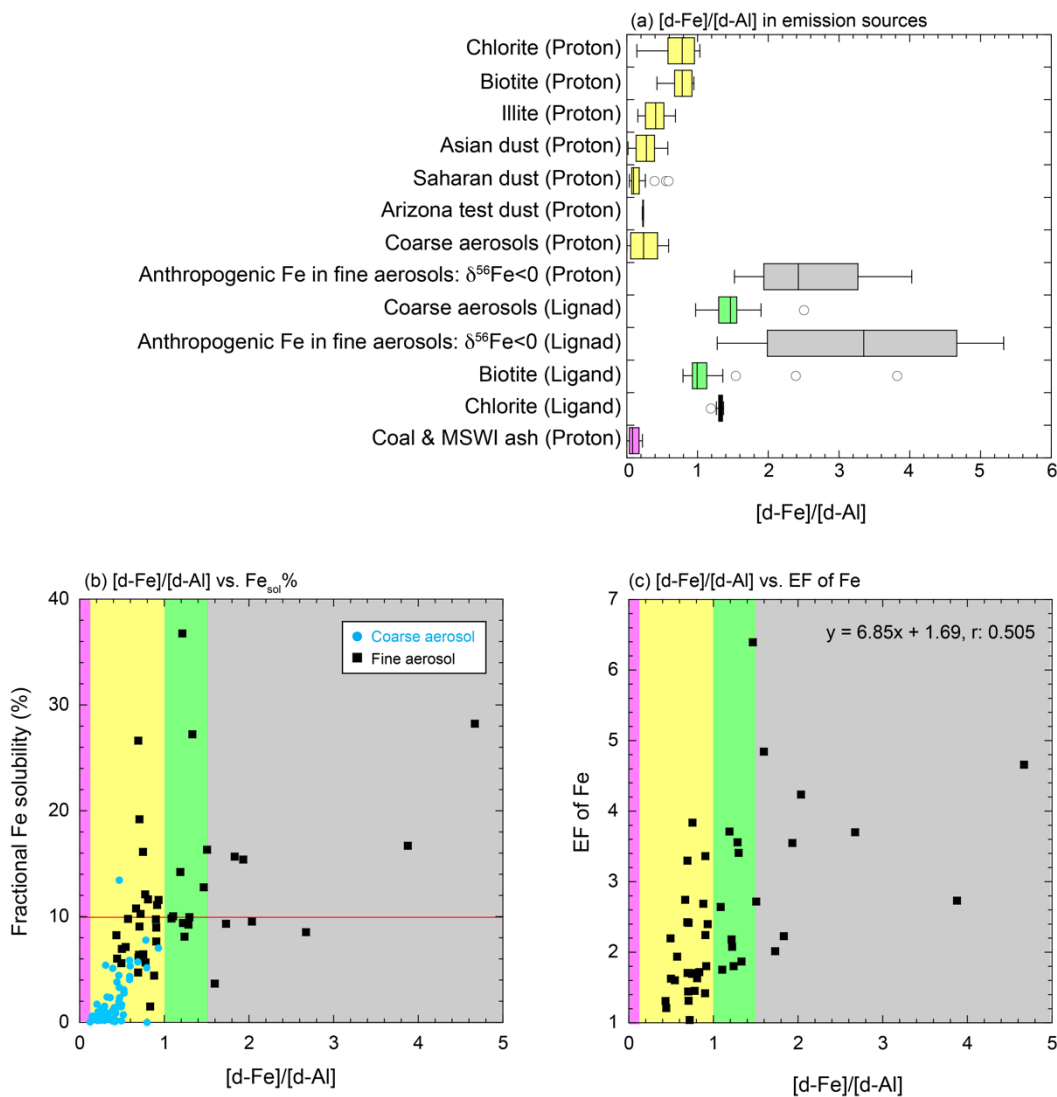


880 Figure 74: Scatter plots of  $\text{Fe}_{\text{sol}}\%$  and  $\text{Al}_{\text{sol}}\%$  in coarse aerosol particles with (a)  $[\text{nss-SO}_4^{2-}]/[\text{total Fe}]$  and  $[\text{nss-SO}_4^{2-}]/[\text{total Al}]$  and (b)  $[\text{NO}_3^-]/[\text{total Fe}]$  and  $[\text{NO}_3^-]/[\text{total Al}]$ . Scatter plots of  $\text{Fe}_{\text{sol}}\%$  and  $\text{Al}_{\text{sol}}\%$  in fine aerosol particles with (c)  $[\text{nss-SO}_4^{2-}]/[\text{total Fe}]$  and  $[\text{nss-SO}_4^{2-}]/[\text{total Al}]$ , (d)  $[\text{NO}_3^-]/[\text{total Fe}]$  and  $[\text{NO}_3^-]/[\text{total Al}]$  and (e) aerosol pH.



890 Figure 85: Scatter plots of d-Fe with (a) non-crustal Fe, (b) total V, (c) total Cu, (d) total Sb, and (e) total Pb concentrations in fine aerosol particles.

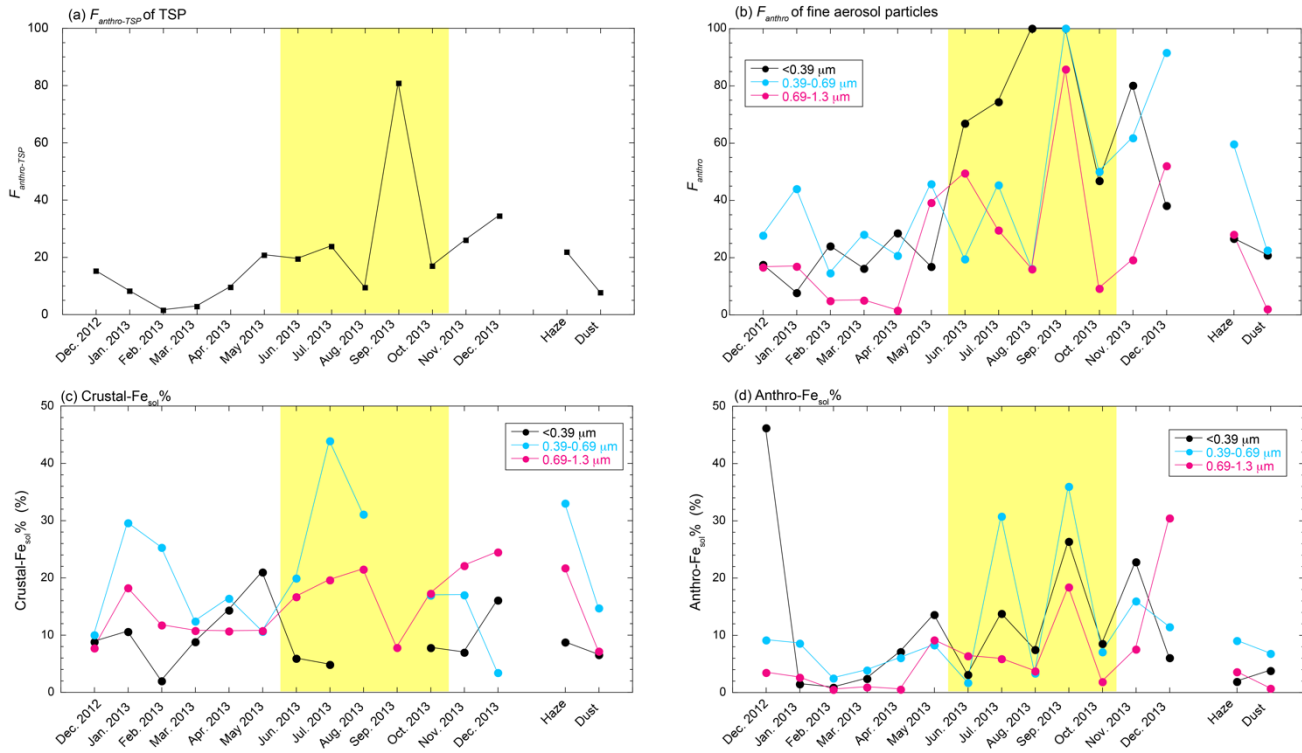




895

Figure 96: (a) Box plot of [d-Fe]/[d-Al] in emission source samples [P](Proton) and [L](Ligand) indicating proton-promoted and ligand-promoted dissolutions. Scatter plots of the [d-Fe]/[d-Al] ratio with (b) the  $\text{Fe}_{\text{sol}}\%$  and (c) EF of Fe. Light blue circles and black squares in panels (b) and (c) represent the data on coarse and fine aerosol particles collected in Higashi-Hiroshima, respectively. Pink, yellow, light green, and gray regions show the typical ranges of the [d-Fe]/[d-Al] ratios of aluminosilicate glasses of coal combustion and MSWI, the proton- and ligand-promoted dissolution of mineral dust, and high-temp-FeOx, respectively. The regions were decided based on the basis of the box plots of panels (a).

900



910

Figure 107: Monthly variations of (a) non-crustal Fe fraction in TSP and (b) non-crustal Fe fraction in fine aerosol particles, (c) crustal- $Fe_{sol}$ %, and (d) non-crustal  $Fe_{sol}$ % when the  $[d-Fe]/[d-Al]$  ratio of non-crustal Fe is 2.08.

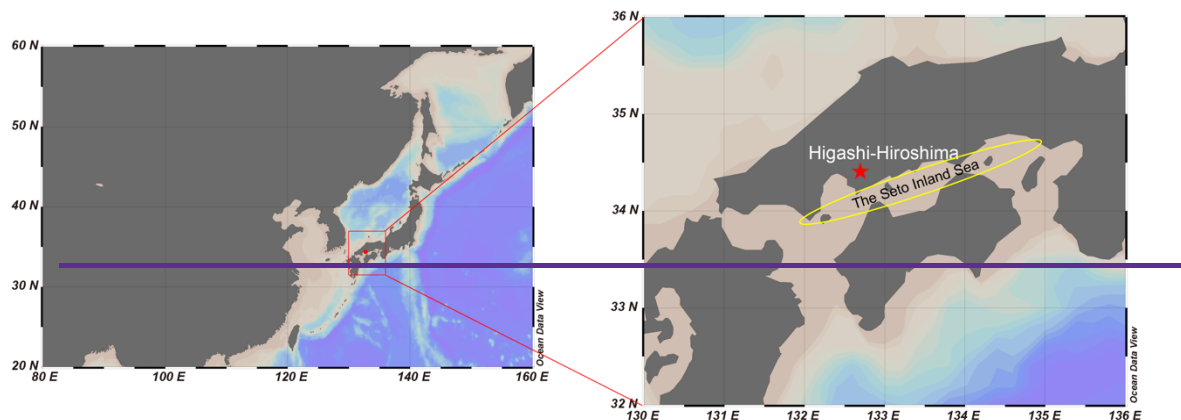
915

Figure 11: Scatter plots of The yellow shaded region shows the  $[d-Fe]/[d-Al]$  ratio with  $Fe_{sol}$ % in (a) TSP samples and (b) size-fractionated aerosol particles collected in the marine atmosphere. (c) The fraction of non crustal d Fe in these samples period when the air mass was calculated by using Equations 6 and 7. The  $[d-Fe]/[d-Al]$  ratios of mineral dust in the Pacific and Atlantic Oceans were the average ratios of Asian dust (0.238) and Saharan dust (0.163), respectively. The  $[d-Fe]/[d-Al]$  ratio of non-crustal Fe was fixed at 2.08. The  $[d-Fe]/[d-Al]$  ratios of TSP and size-fractionated aerosol samples were adapted mainly derived from Buck et al. (2006, 2010b), Shelley et al. (2018), Baker et al. (2020), and Sakata et al. (2022). The Fe isotopic ratio of TSP in the Atlantic Ocean was reported by Conway et al. (2019). Pink, yellow, light green, and gray regions in panels (a) and (b) show the typical  $[d-Fe]/[d-$

920

~~All ratios of coal/MSWI fly ash, proton-promoted and ligand-promoted mineral dust dissolution, and pyrogenic Fe oxides, respectively, Japan.~~

Figure 12: Non-crystal Fe fractions in TSP samples collected from (a) the Pacific Ocean and (b) Atlantic Ocean. Non-crystal Fe fractions were calculated by using reported  $[d\text{-Fe}]/[d\text{-Al}]$  ratios.



935 ~~Figure 1: Sites (Higashi Hiroshima) of size fractionated aerosol sampling. Maps were visualized by Ocean Data View (Schlitzer, 2021).~~

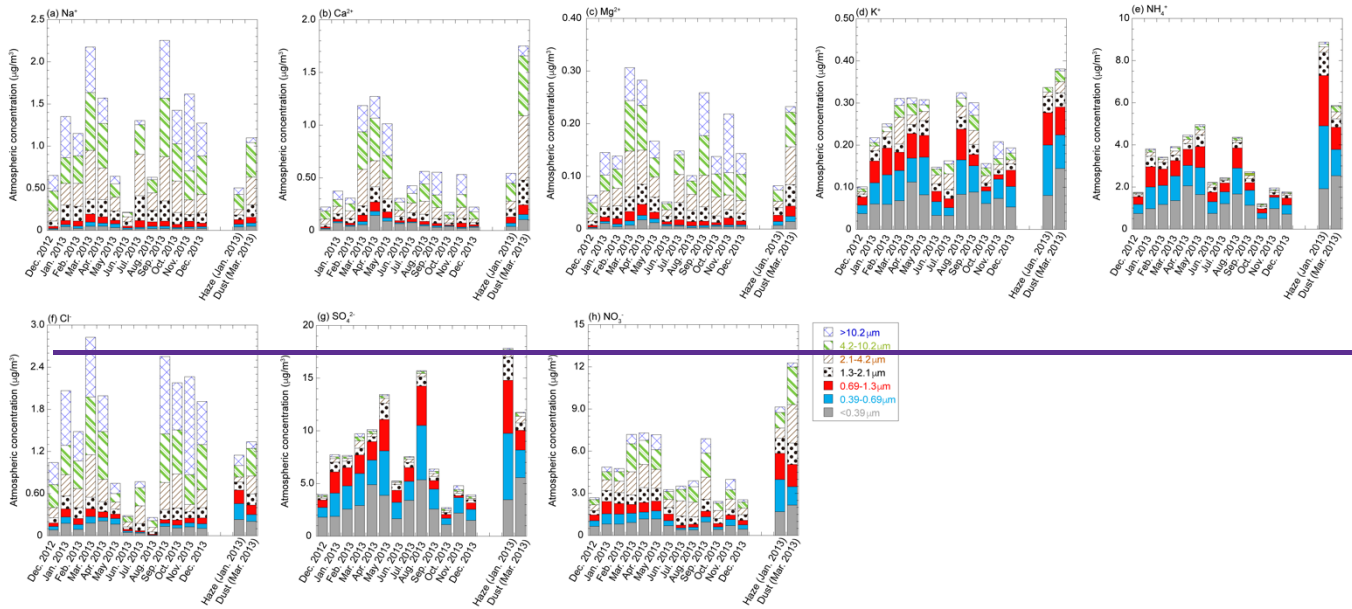


Figure 2: Monthly variations and size distributions of (a)  $\text{Na}^+$ , (b)  $\text{Ca}^{2+}$ , (c)  $\text{Mg}^{2+}$ , (d)  $\text{K}^+$ , (e)  $\text{NH}_4^+$ , (f)  $\text{Cl}^-$ , (g)  $\text{NO}_3^-$ , (h)  $\text{SO}_4^{2-}$ , and (i)  $\text{nss SO}_4^{2-}$ . The summation of all fractions corresponds to TSP concentration.

955

960

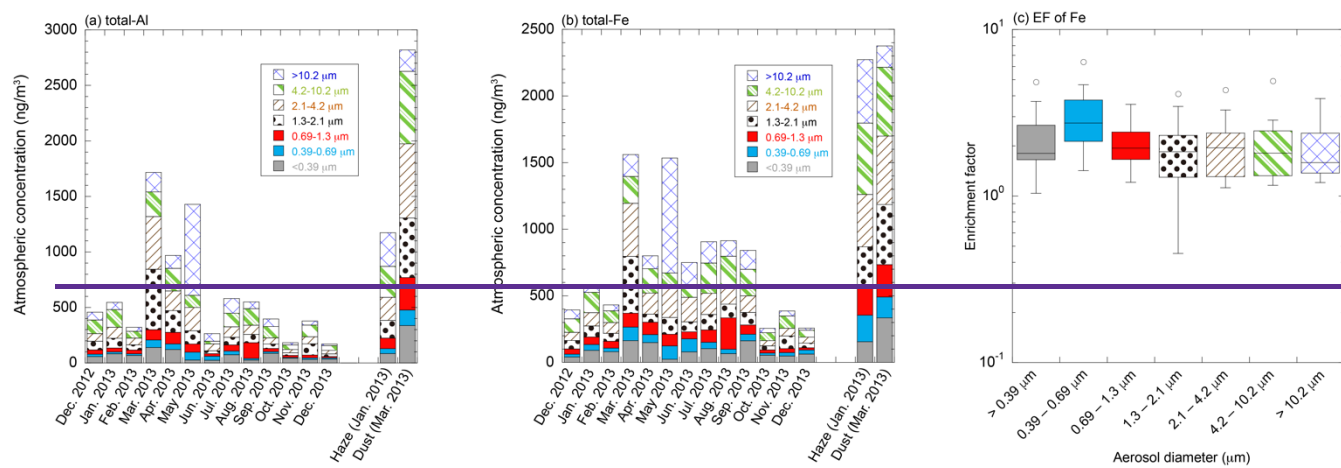


Figure 3: Monthly variations and size distributions of (a) total Al and (b) total Fe concentrations. (c) Box plot of  $Fe_{enr}\%$  in each size fraction.

965

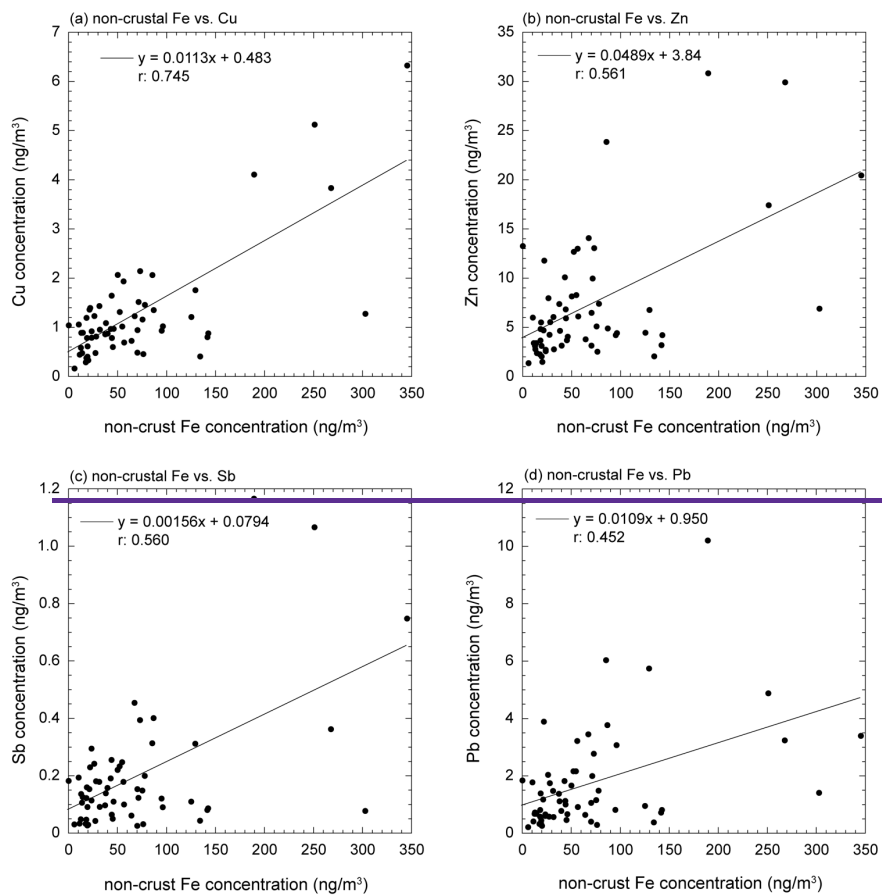
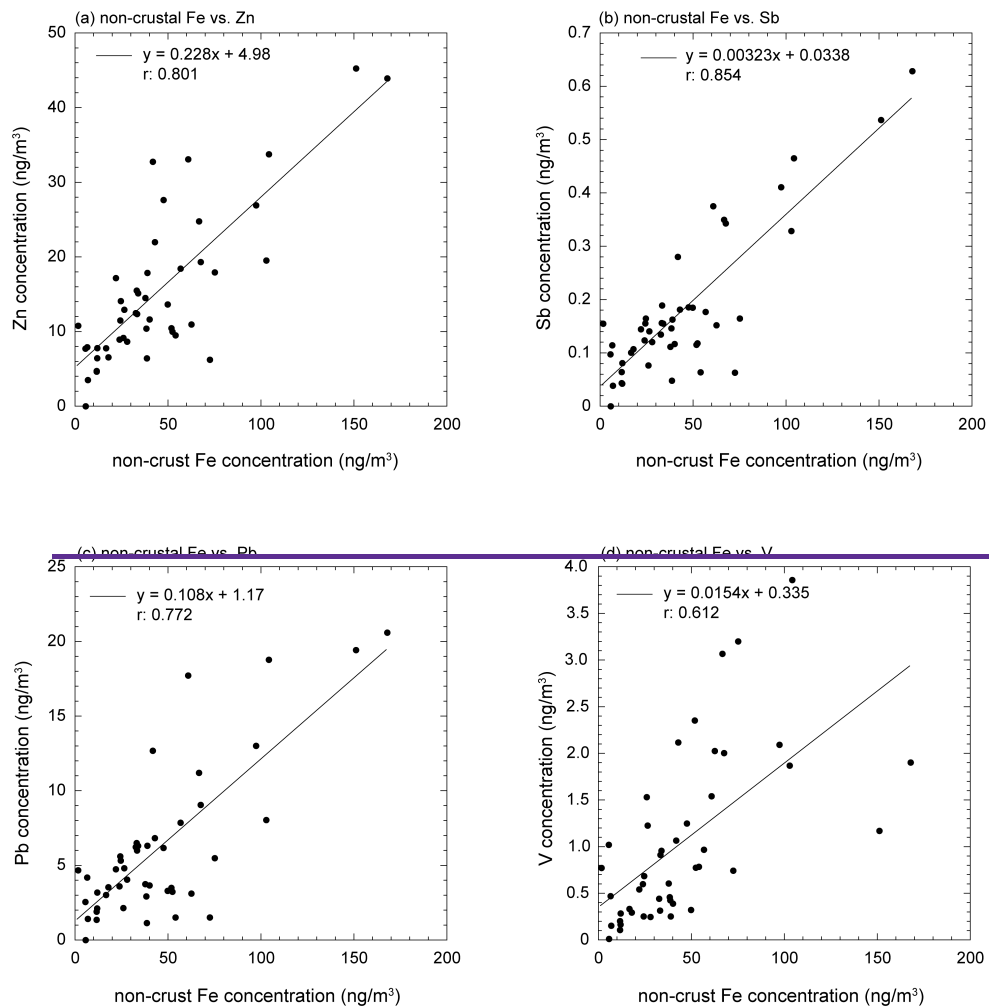


Figure 4: Scatter plots of non-crustal Fe concentration with (a) Cu, (b) Zn, (c) Sb, and (d) Pb in coarse aerosol particles.



980 Figure 5: Scatter plots of non-crustal Fe concentration with (a) Zn, (b) Sb, (c) Pb, and (d) V in fine aerosol particles.



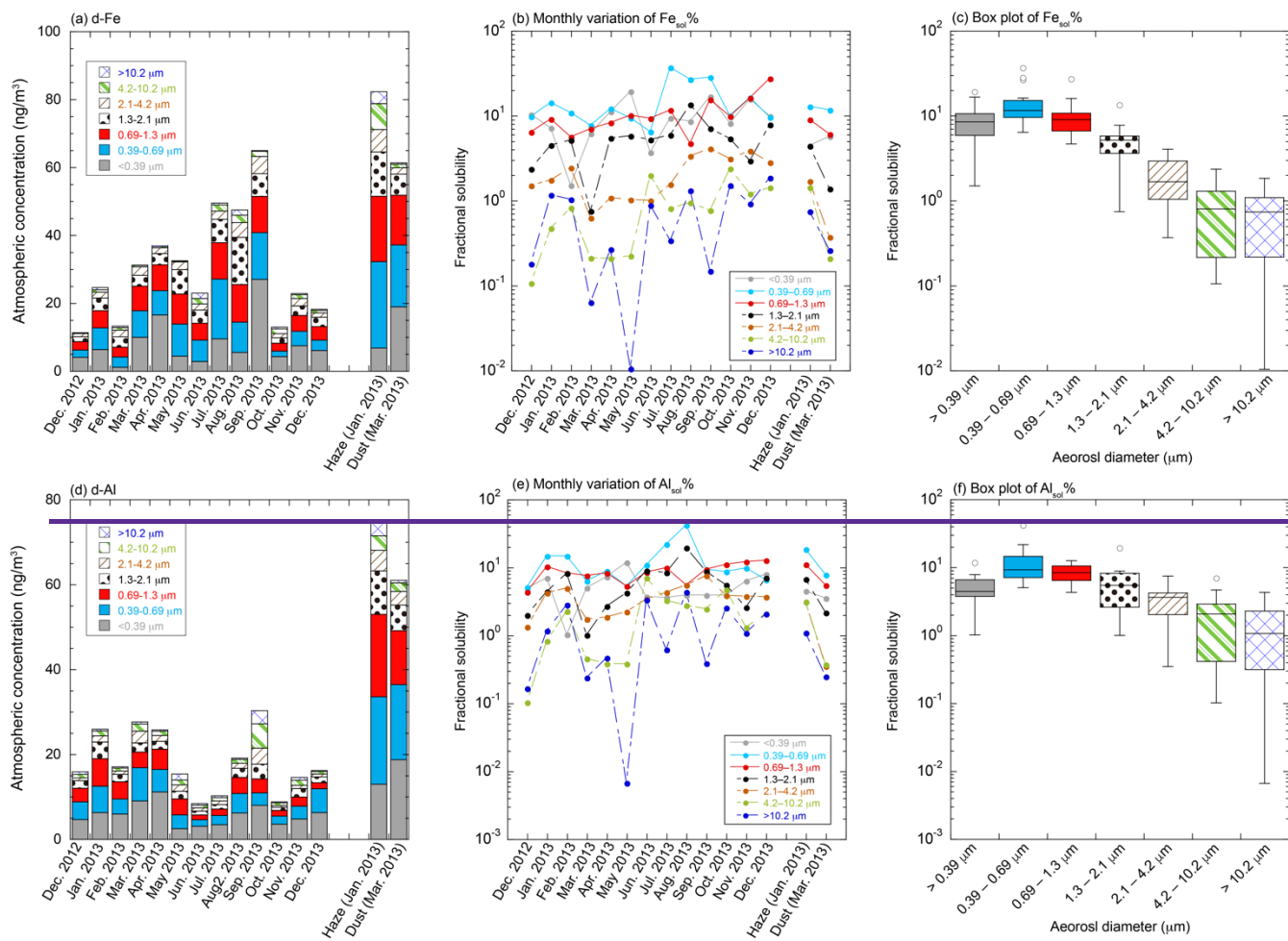
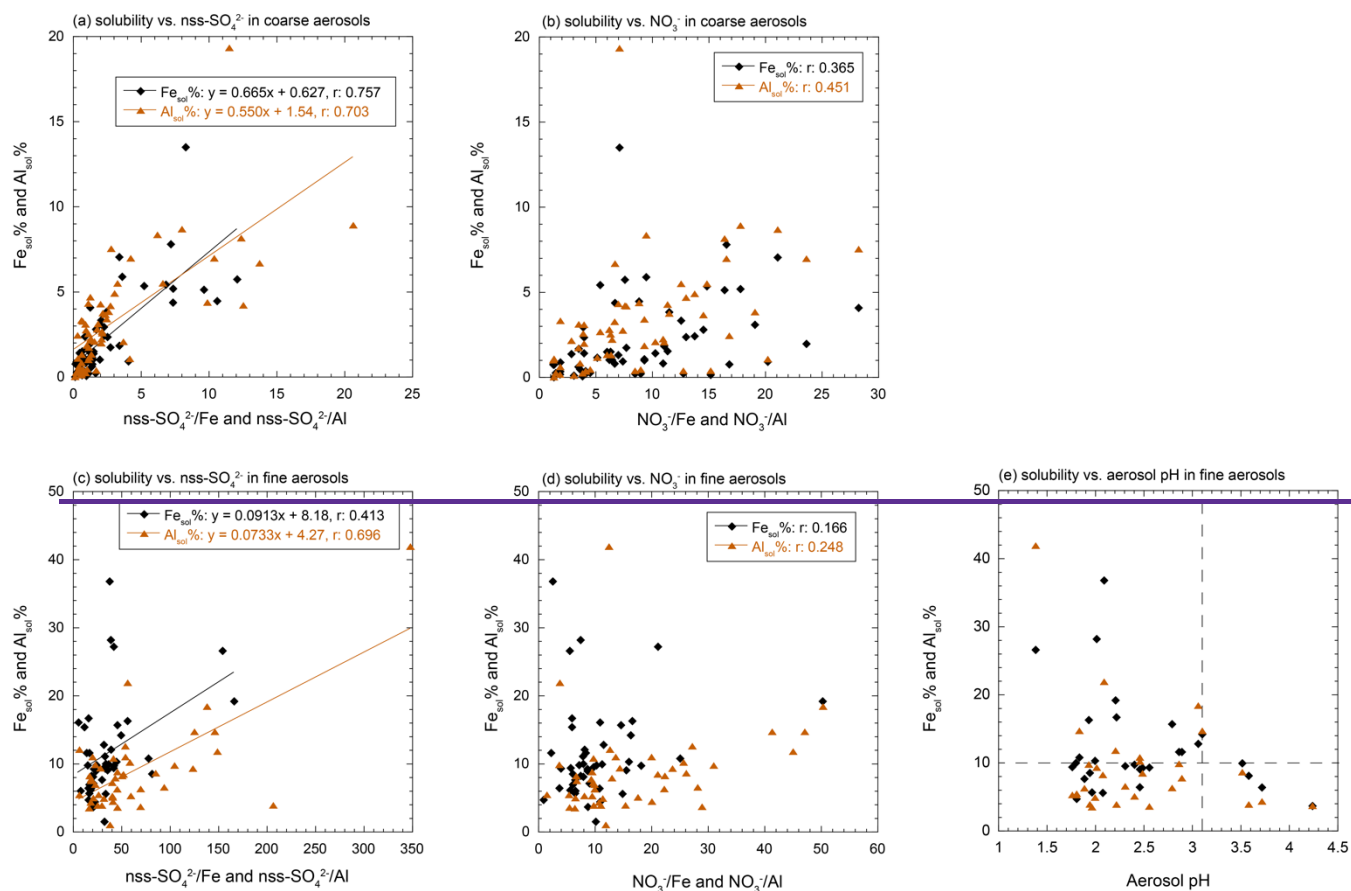


Figure 6: Monthly variation and size distributions of (a) d-Fe and (b) Fe<sub>sol</sub>%. (c) Box plot of Fe<sub>sol</sub>% in each size fraction. Monthly variation and size distributions of (d) d-Al and (e) Al<sub>sol</sub>%. (f) Box plot of Al<sub>sol</sub>% in each size fraction.

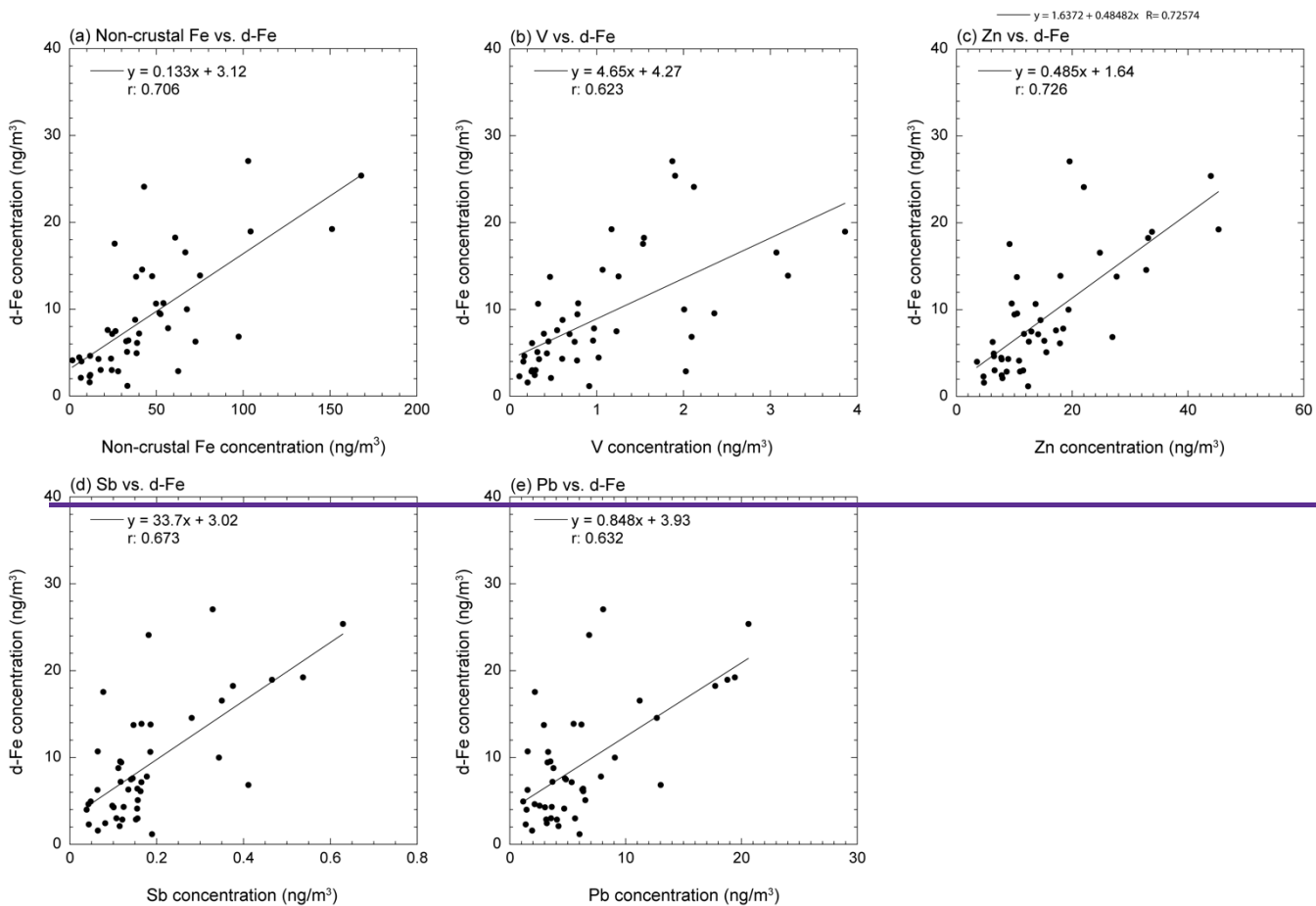
000



005

Figure 7: Scatter plots of Fe<sub>sol</sub>% and Al<sub>sol</sub>% in coarse aerosol particles with (a) nss-SO<sub>4</sub><sup>2-</sup>/Fe or Al and (b) NO<sub>3</sub><sup>-</sup>/Fe or Al. Scatter plots of Fe<sub>sol</sub>% and Al<sub>sol</sub>% in fine aerosol particles with (c) nss-SO<sub>4</sub><sup>2-</sup>/Fe or Al, (d) NO<sub>3</sub><sup>-</sup>/Fe or Al, and (e) aerosol pH.

010



015

Figure 8: Scatter plots of d-Fe with (a) non-crustal Fe, (b) total V, (c) total Cu, (d) total Sb, and (e) total Pb concentrations in fine aerosol particles.

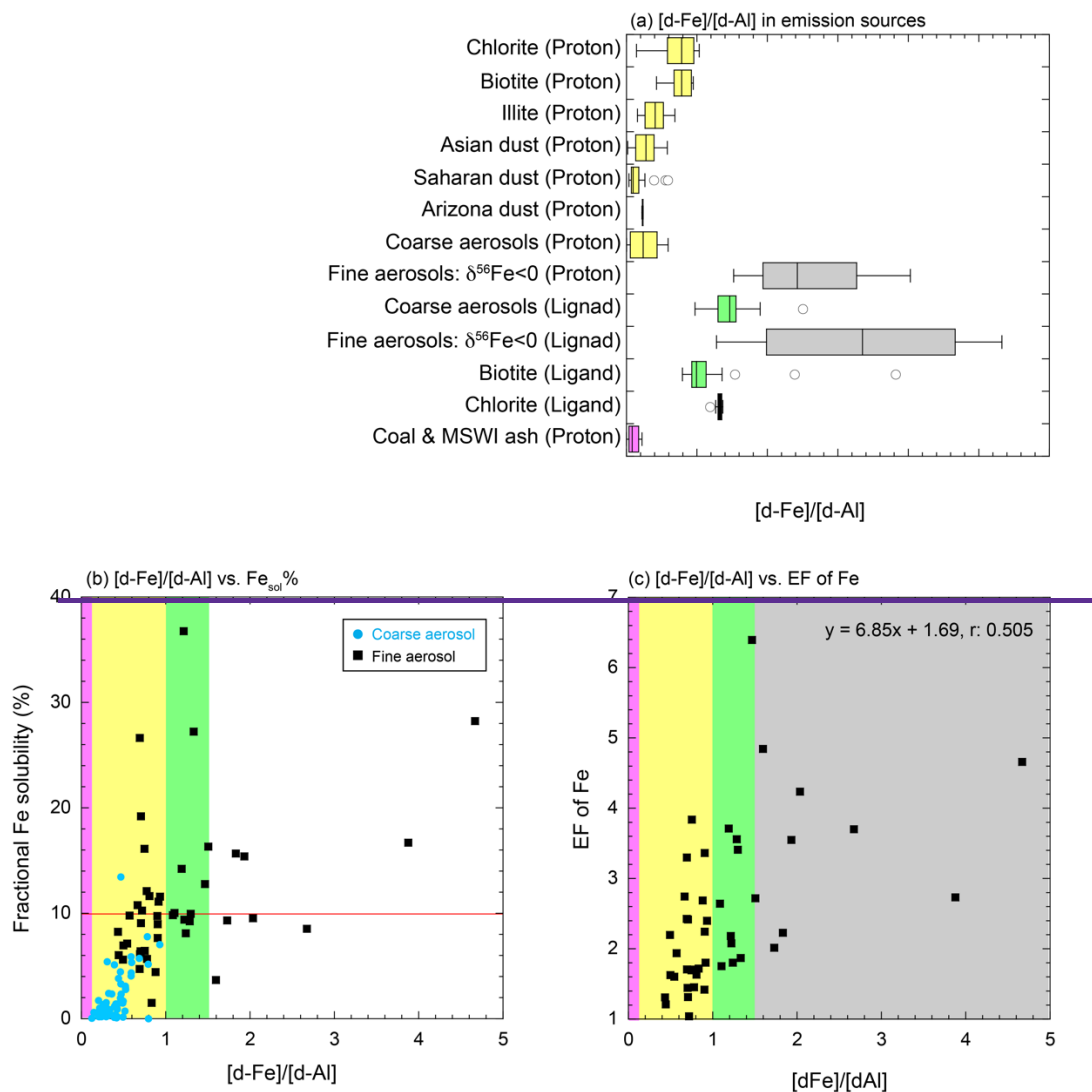
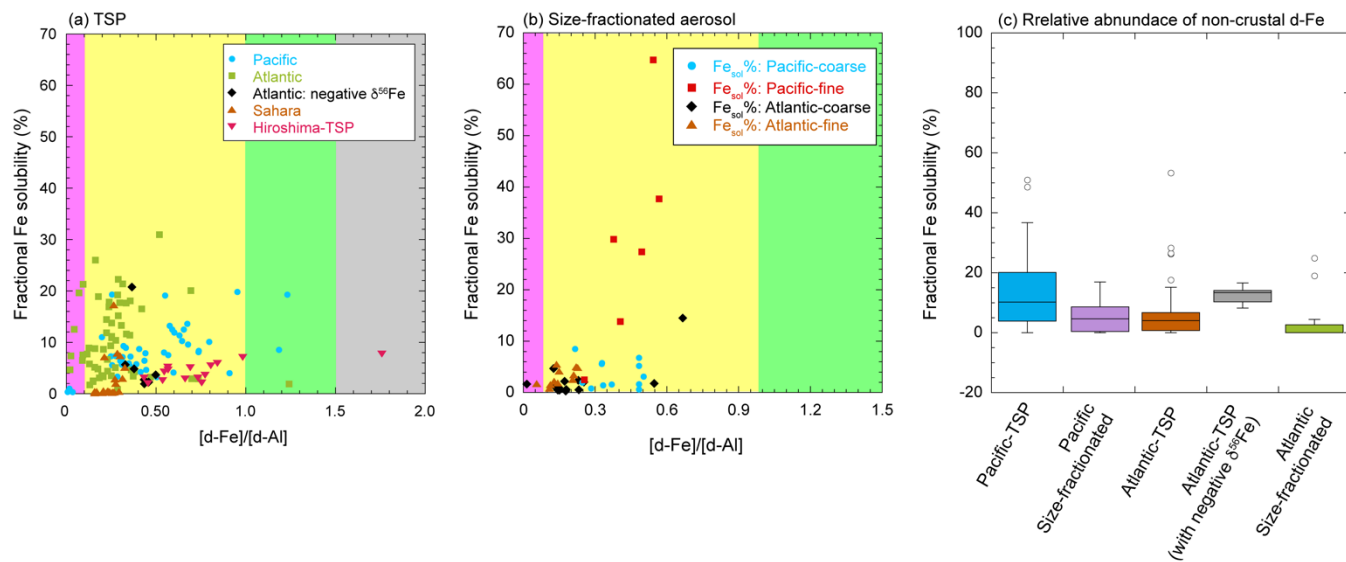


Figure 9: (a) Box plot of [d-Fe]/[d-Al] in emission source samples [P] and [L] indicating proton promoted and ligand promoted dissolutions. Scatter plots of



030

**Figure 8** [d-Fe]/[d-Al] ratio with (b) the  $\text{Fe}_{\text{sol}}\%$  and (c) EF of Fe. Light blue circles and black squares in panels (b) and (c) represent the data on coarse and fine aerosol particles collected in Higashi-Hiroshima, respectively. Pink, yellow, light green, and gray regions show the typical ranges of the [d-Fe]/[d-Al] ratios of aluminosilicate glasses of coal combustion and MSWI, the proton- and ligand-promoted dissolution of mineral dust, and high-temp FeOx, respectively. The regions were decided on the basis of the box plots of panels (a).

035

040

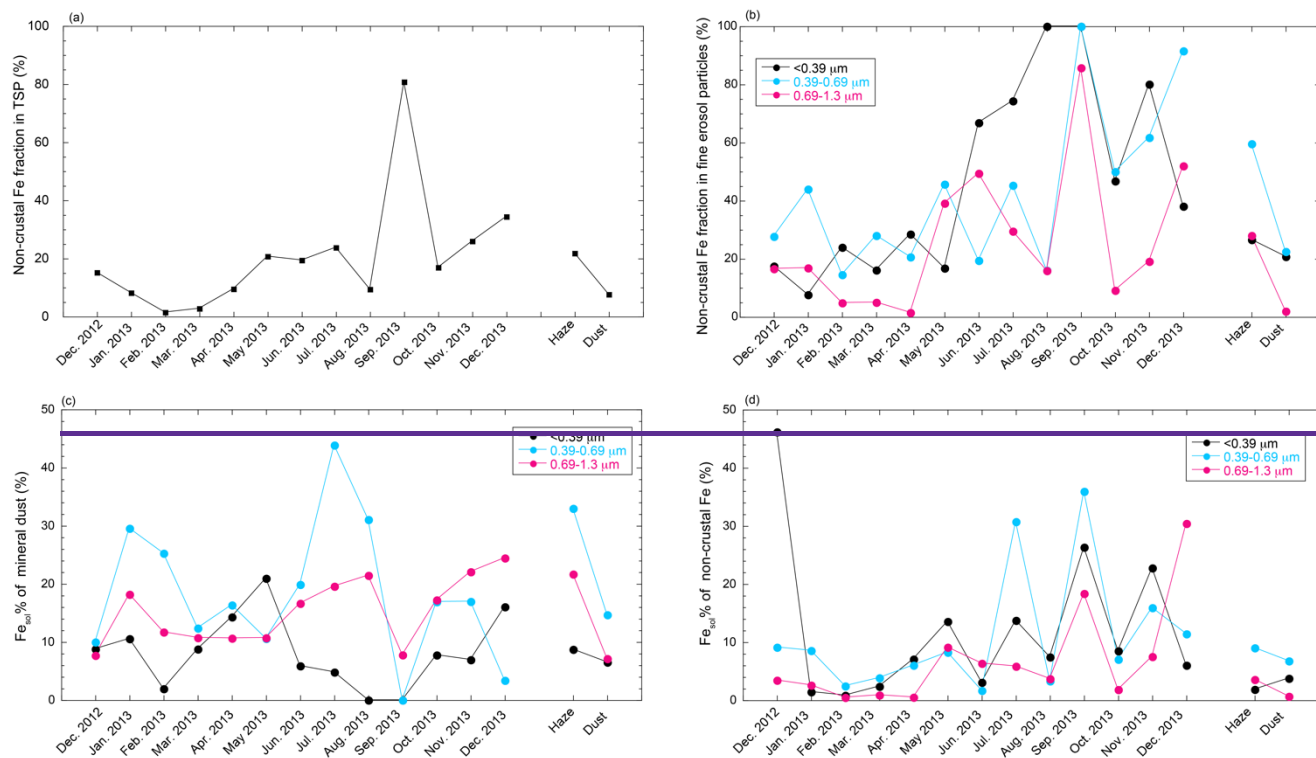


Figure 10: Monthly variations of (a) non-crystal Fe fraction in TSP and (b) non-crystal Fe fraction in fine aerosol particles, (c) crustal  $\text{Fe}_{\text{sol}}\%$ , and (d) non-crystal  $\text{Fe}_{\text{sol}}\%$  when the  $[\text{d Fe}]/[\text{d Al}]$  ratio of non-crystal Fe is 2.08.

045

050

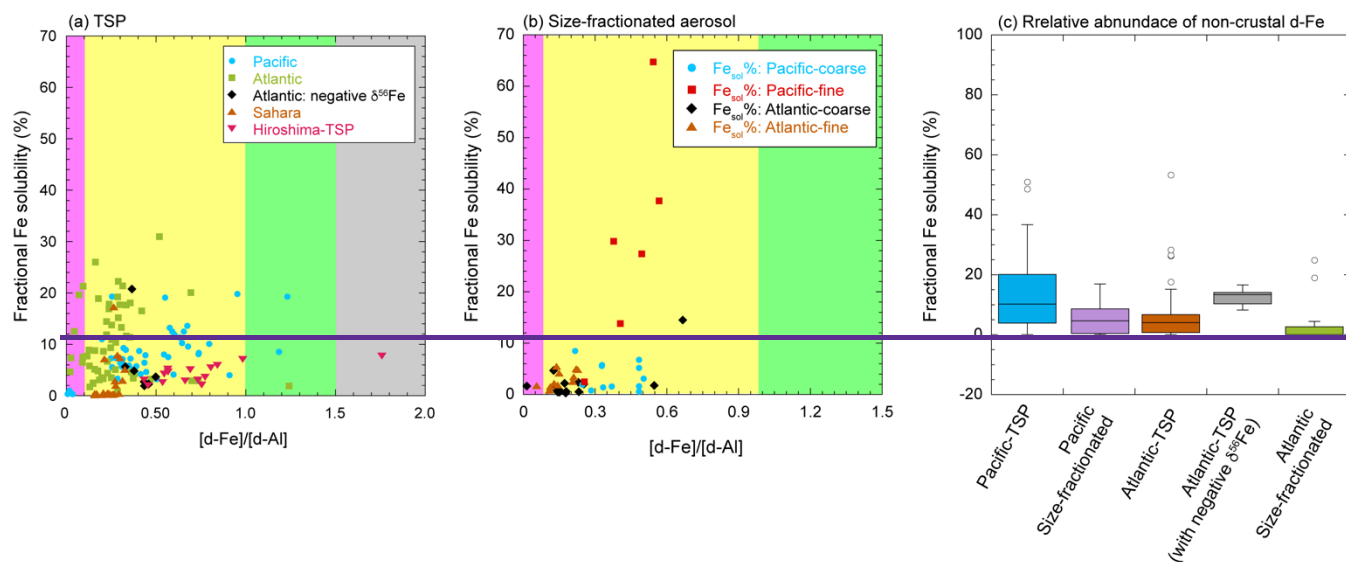


Figure 11: Scatter plots of the  $[\text{d-Fe}]/[\text{d-Al}]$  ratio with  $\text{Fe}_{\text{sol}}\%$  in (a) TSP samples and (b) size-fractionated aerosol particles collected in the marine atmosphere. (c) The fraction of non-crystal d-Fe in these samples was calculated by using Equations 6 and 7. The  $[\text{d-Fe}]/[\text{d-Al}]$  ratios of mineral dust in the Pacific and Atlantic Oceans were the average ratios of Asian dust (0.238) and Saharan dust (0.163), respectively. The  $[\text{d-Fe}]/[\text{d-Al}]$  ratio of non-crystal Fe was fixed at 2.08. The  $[\text{d-Fe}]/[\text{d-Al}]$  ratios of the TSP and size-fractionated aerosol samples were adapted from the works of Buck et al. (2006, 2010b), Shelley et al. (2018), Baker et al. (2020), and Sakata et al. (2022). The Fe isotopic ratio of TSP in the Atlantic Ocean was reported by Conway et al. (2019). Pink, yellow, light green, and gray regions in panels (a) and (b) show the typical  $[\text{d-Fe}]/[\text{d-Al}]$  ratios of coal/MSWI fly ash, proton-promoted and ligand-promoted mineral dust dissolution, and pyrogenic Fe oxides, respectively.

055

060

.065

.070

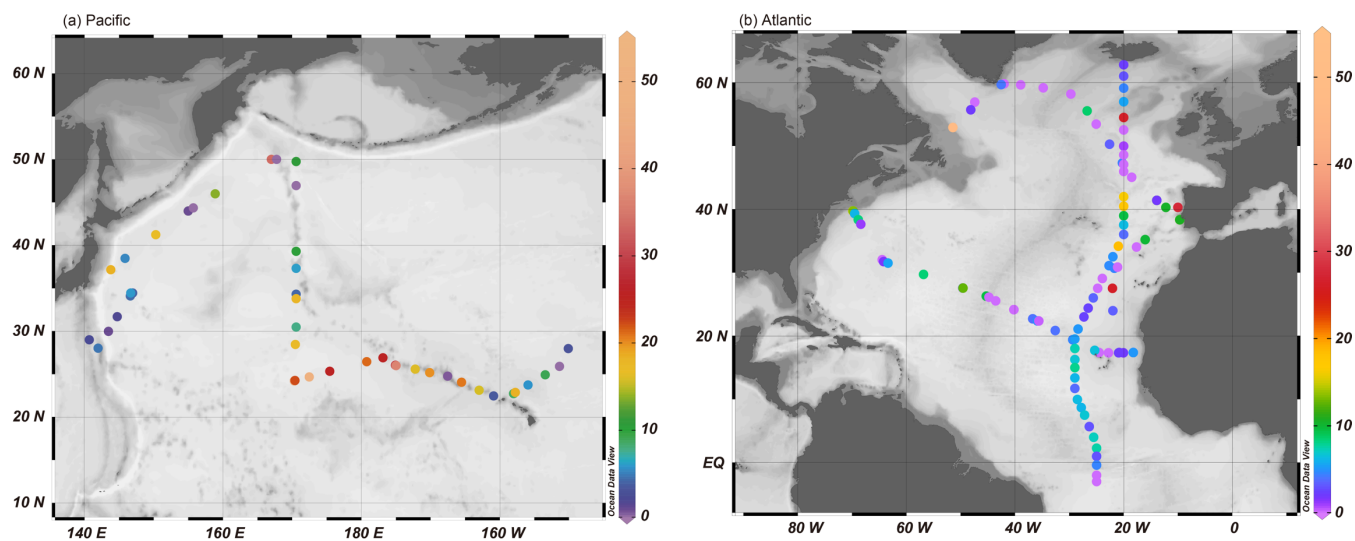


Figure 129: Non-crustal Fe fractions in the TSP samples collected from (a) the Pacific Ocean and (b) Atlantic Ocean. Non-crustal Fe fractions were calculated by using reported the  $[d\text{-Fe}]/[d\text{-Al}]$  ratios reported by Buck et al. (2006, 2010b) and Shelley et al. (2018). The figures were described by Ocean Data View (Schlitzer, 2021).

075



## References

- 080 Acker, J. G., Bricker, O. P.: The influence of pH on biotite dissolution and alteration kinetics at low temperature, *Geochim. Cosmochim. Acta*, 56, 3073–3092, [https://doi.org/10.1016/0016-7037\(92\)90290-Y](https://doi.org/10.1016/0016-7037(92)90290-Y), 1992.
- Adachi, K., Tainosho, Y.: Characterization of heavy metal particles embedded in tire dust, *Environ. Int.*, 30, 1009–1017, <https://doi.org/10.1016/j.envint.2004.04.004>, 2004.
- Akita, S., Maeda, T., Takeuchi, H.: Recovery of vanadium and nickel in fly ash from heavy oil, *J. Chem., Tech. Biotechnol.*, 62, 345–350, <https://doi.org/10.1002/jctb.280620406>, 1995.
- 085 Baker, A. R., and Jickells, T. D.: Atmospheric deposition of soluble trace elements along the Atlantic Meridional Transect (AMT), *Prog. Oceanogr.*, 158, 41–51, <http://dx.doi.org/10.1016/j.pocean.2016.10.002>, 2017.
- Baker, A. R., and Jickells, T. D.: Mineral particle size as a control on aerosol iron solubility, *Geophys. Res. Lett.*, 33, L17608, <https://doi.org/10.1029/2006GL026557>, 2006.
- 090 Baker, A. R., Li, M., Chance, R.: Trace metal fractional solubility in size-segregated aerosols from the tropical eastern Atlantic Ocean, *Global Biogeochem. Cy.*, 34, e2019GB006510, <https://doi.org/10.1029/2019GB006510>, 2020.
- ~~Baldo, C., Ito, A., Krom, M. D., Li, W., Jones, T., Drake, N., Ignatyev, K., Davidson, N., and Shi, Z.: Iron from coal combustion particles dissolved much faster than mineral dust under simulated atmospheric acidic condition. *Atmos. Chem. Phys.*, 22, 6045–6066, <https://doi.org/10.5194/aep-22-6045-2022>, 2022.~~
- 095 Bibi, I., Singh, B., and Silvester, E.: Dissolution of illite in saline-acidic solutions at 25 °C, *Geochim. Cosmochim. Acta*, 75, 3237–3249, <https://doi.org/10.1016/j.gca.2011.03.022>, 2011.
- Boyd, P. W., Jickells, T., Law, C. S., Blain, S., Boyle, E. A., Buesseler, K. O., Coale, K. H., Cullen, J. J., de Beear, H. J. W., Follows, M., Harvey, M., Lancelot, C., Levasseur, M., Owens, N. P. J., Pollard, R., Rivkin, R. B., Sarmiento, J., Schoemann, V., Smetacek, V., Takeda, S., Tsuda, A., Turner, S., and Watson, A. J.: Mesoscale iron enrichment experiments 1993–2005: Synthesis, and future directions, *Science*, 315, 612–617, <https://doi.org/10.1126/science.1131669>, 2007.
- 100 Brantley, S. L., Kubicki, J. D., White, A. F.: Kinetics of water-rock interaction, Springer, New York, <https://doi.org/10.1007/978-0-387-73563-4>, 2008.
- Bray, A. W., Oelkers, E. H., Bonneville, S., Wolff-Boenisch, D., Potts, N. J., Fones, G., and Benning, L. G.: The effect of pH, grain size, and organic ligands on biotite weathering rates, *Geochim. Cosmochim. Acta*, 164, 127–145, <http://dx.doi.org/10.1016/j.gca.2015.04.048>, 2015.
- 105 Buck, C. S., Landing, W. M., and Resing, J.: Pacific Ocean aerosols: Deposition and solubility of iron, aluminum, and other trace elements, *Mar. Chem.*, 157, 117–130, <http://dx.doi.org/10.1016/j.marchem.2013.09.005>, 2013.
- Buck, C. S., Landing, W. M., and Resing, J.: Particle size and aerosol iron solubility: A high-resolution analysis of Atlantic aerosols, *Mar. Chem.*, 120, 14–24, <https://doi.org/10.1016/j.marchem.2008.11.002>, 2010a.

- 110 Buck, C. S., Landing, W. M., Resing, J. A. and Lebon, G. T.: Aerosol iron and aluminum solubility in the northwest Pacific Ocean: Results from the 2002 IOC cruise, *Geochem. Geophys. Geosyst.*, 7, 4, Q04M07, <https://doi.org/10.1029/2005GC000977>, 2006.
- Buck, C. S., Landing, W. M., Resing, J. A., Measures, C. I.: The solubility and deposition of aerosol Fe and other trace elements in the North Atlantic Ocean: Observations from the A16N CLIVAR/CO<sub>2</sub> repeat hydrography section, *Mar. Chem.*, 120, 57–
- 115 70, <https://doi.org/10.1016/j.marchem.2008.08.003>, 2010b.
- [Cao, J. J., Chow, J. C., Watson, J. G., Wu, F., Han, Y. M., Jin, Z. D., Shen, Z. X., An, Z. S.: Size-differentiated source profiles for fugitive dust in the Chinese Loess Plateau, \*Atmos. Environ.\*, 42, 2261–2275, <https://doi.org/10.1016/j.atmosenv.2007.12.041>, 2008.](https://doi.org/10.1016/j.atmosenv.2007.12.041)
- Chance, R., Jickells, T. D., and Baker, A. R.: Atmospheric trace metal concentrations, solubility and deposition fluxes in
- 120 remote marine air over the south-east Atlantic. *Mar. Chem.*, 177, 45–56, <http://dx.doi.org/10.1016/j.marchem.2015.06.028>, 2015.
- Chang, C. Y., Wang, C. F., Mui, D. T., Chiang, H. L.: Application of methods (sequential extraction procedures and high-pressure digestion method) to fly ash particles to determine the element constituents: A case study for BCR-176. *J. Hazard. Mater.*, 163, 578–587, <https://doi.org/10.1016/j.jhazmat.2008.07.039>, 2009.
- 125 Chen, H. and Grassian, V. H.: Iron dissolution of dust source materials during simulated acidic processing: The effect of sulfuric, acetic, and oxalic acids, *Environ. Sci. Technol.*, 47, 1031210321, <https://doi.org/10.1021/es401285s>, 2013.
- Clegg, S. L., Pitzer, K. S., and Brimblecombe, P.: Thermodynamics of multicomponent, miscible, ionic solutions. II. Mixtures including unsymmetrical electrolyte. *J. Phys. Chem.*, 96, 9470–9479, <https://doi.org/10.1021/j100202a074>, 1992.
- [Clough, R., Lohan, M. C., Ussher, S. J., Nimmo, M., Worsfold, P. J.: Uncertainty associated with the leaching of aerosol filters for the determination of metals in aerosol particulate matter using collision/reaction cell ICP-MS detection, \*Talanta\*, 199, 425–430, <https://doi.org/10.1016/j.talanta.2019.02.067>, 2019.](https://doi.org/10.1016/j.talanta.2019.02.067)
- Conway, T. M., Hamilton D. S., Shelley, R. U., Aguilar-Islas, A. M., Landing, W. M., Mahowald, N. ., and John, S. G.: Tracing and constraining anthropogenic aerosol iron fluxes to the North Atlantic Ocean using iron isotopes, *Nature Commun.*, 10, 2628, <https://doi.org/10.1038/s41467-019-10457-w>, 2019.
- 135 Czech, T., Morphology and chemical composition of magnetic particles separated from coal fly ash, *Materials*, 15, 528, <https://doi.org/10.3390/ma15020528>, 2022.
- Desboeufs, K. V., Losno, R., Colin, J. L.: Factors influencing aerosol solubility during cloud processes, *Atmos. Environ.*, 35, 3529–3537, [https://doi.org/10.1016/S1352-2310\(00\)00472-6](https://doi.org/10.1016/S1352-2310(00)00472-6), 2001.
- [Ding, Z. L., Sun, J. M., Yang, S. L., Liu, T. S.: Geochemistry of the Pliocene red clay formation in the Chinese Loess Plateau and implications for its origin, source provenance and paleoclimate change, \*Geochim. Cosmochim. Acta\*, 65, 6, 901–913, \[https://doi.org/10.1016/S0016-7037\\(00\\)00571-8\]\(https://doi.org/10.1016/S0016-7037\(00\)00571-8\), 2001.](https://doi.org/10.1016/S0016-7037(00)00571-8)
- 140

- Duvall, R. M., Majestic, B. J., Shafer, M. M., Chuang, P. Y., Simoneit, B. R. T. Schauer, J. J.: The water-soluble fraction of carbon, sulfur, and crustal elements in Asian aerosols and Asian soils, *Atmos. Environ.*, 42, 5872–5884, <https://doi.org/10.1016/j.atmosenv.2008.03.028>, 2008.
- 145 ~~Echalar, F., Gaudichet, A., Cachier, H., Artaxo, P.: Aerosol emissions by tropical forest and savanna biomass burning: characteristic trace elements and fluxes. *Geophys. Res. Lett.*, 22, 3039–3042, <https://doi.org/10.1029/95GL03170>, 1995.~~
- Falkowski, P., Scholes, R. J., Boyle, E., Canadell, J., Canfield, D., Elser, J., Gruber, N., Hibbard, K., Hogberg, P., Linder, S., Mackenzie, F. T., Moore, B., Pedersen, T., Rosenthal, Y., Seitzinger, S., Smetacek, V., and Steffen, W.: The global carbon cycle: A test of our knowledge of earth as a system, *Science*, 290, 291–296, <https://doi.org/10.1126/science.290.5490.291>, 2000.
- 150 Fang, T., Guo, H., Zeng, L., Verma, V., Nenes, A., and Weber, R.: Highly Acidic Ambient Particles, Soluble Metals, and Oxidative Potential: A Link between Sulfate and Aerosol Toxicity, *Environ. Sci. Technol.*, 51, 2611–2620, <https://doi.org/10.1021/acs.est.6b06151>, 2017.
- ~~Finlayson Pitts, B. J.: The tropospheric chemistry of sea salt: A molecular level view of the chemistry of NaCl and NaBr, *Chem. Rev.*, 103, 4801–4822, <https://doi.org/10.1021/cr020653t>, 2003.~~
- 155 Fitzgerald, E., Ault, A. P., Zauscher, M. D., Mayol-Bracero, O. L., and Prather, K. A.: Comparison of the mixing state of long-range transported Asian and African mineral dust, *Atmos. Environ.*, 115, 19–25, <https://doi.org/10.1016/j.atmosenv.2015.04.031>, 2015.
- ~~Flament, P., Mattielli, N., Aimez, L., Choël, M., Deboudt, K., de Jong, J., Rimetz-Planchon, J., Weis, D.: Iron isotopic fractionation in industrial emissions and urban aerosols, *Chemosphere*, 73, 1793–1798, <https://doi.org/10.1016/j.chemosphere.2008.08.042>, 2008.~~
- 160 Fomenko, E. V., Anshits, N. N., Solovyov, L. A., Knyazev, Y. V., Semenov, S. V., Bayukov, O. A., Anshits, A. G.: Magnetic fractions of PM<sub>2.5</sub>, PM<sub>2.5–10</sub>, PM<sub>10</sub> from coal fly ash as environmental pollutants, *ACS Omega*, 6, 20076–20085, <https://doi.org/10.1021/acsomega.1c03187>, 2021.
- 165 Friese, E., and Ebel, A.: Temperature dependent thermodynamic model of the system H<sup>+</sup>–NH<sub>4</sub><sup>+</sup>–Na<sup>+</sup>–SO<sub>4</sub><sup>2-</sup>–NO<sub>3</sub><sup>-</sup>–Cl–H<sub>2</sub>O. *J. Phys. Chem. A*, 114, 11595–11631, <https://doi.org/10.1021/jp101041j>, 2010.
- ~~Fu, X., Wang, T., Wang, S., Zhang, L., Cai, S., Xing, J., Hao, J.: Anthropogenic emissions of hydrogen chloride and fine particulate chloride in China, *Environ. Sci. Technol.*, 52, 1644–1654, <https://doi.org/10.1021/acs.est.7b05030>, 2018.~~
- 170 Furuya, K., Miyajima, Y., Chiba, T., Kikuchi, T.: Elemental characterization of particle size-density separated coal fly ash by spectrophotometry, inductively coupled plasma emission spectrometry, and scanning electron microscopy-energy dispersive X-ray analysis. *Environ. Sci. Technol.*, 21, 898–903, <https://doi.org/10.1021/es00163a008>, 1987.
- Gao, Y., Marsay, C. M., Yu, S., Fan, S., Mukherjee, P., Buck, C. S., Landing, W. M.: Particle-size variability of aerosol iron and impact on iron solubility and dry deposition fluxes to the Arctic Ocean, *Sci. Rep.*, 9, 16653, <https://doi.org/10.1038/s41598-019-52468-z>, 2019.

- 175 Gietl, J. K., Lawrence, R., Thorpe, A. J., Harrison, R. M.: Identification of brake wear particles and derivation of a quantitative tracer for brake dust at a major road. *Atmos. Environ.*, 44, 141–146, <https://doi.org/10.1016/j.atmosenv.2009.10.016>, 2010.
- Gitari, W. M., Fatoba, O. O., Petrik, L. F., Vadapalli, V. R. K.: Leaching characteristics of selected south African fly ashes: Effect of pH on the release of major and trace species, *J. Environ. Sci. Health A*, 44, 206–220, <https://doi.org/10.1080/10934520802539897>, 2009.
- 180 Guo, H., Nenes, A., Weber, R. J.: The underappreciated role of nonvolatile cations in aerosol ammonium-sulfate molar ratios. *Atmos. Chem. Phys.*, 18, 17307–17323, <https://doi.org/10.5194/acp-18-17307-2018>, 2018
- Halle, L. L., Palmqvist, A., Kampmann, K., Jensen, A., Hansen, T., Khan, F. R.: Tire wear particle and leachate exposures from a pristine and road-worn tire to *Hyalella azteca*: Comparison of chemical content and biological effects, *Aquat. Toxicol.*, 232, <https://doi.org/10.1016/j.aquatox.2021.105769>, 2021.
- 185 Hansen, L. D., Silberman, D., Fisher, G. L.: Crystalline components of stack-collected, size-fractionated coal fly ash, *Environ. Sci. Technol.*, 15, 1057–1062, <https://doi.org/10.1021/es00091a004>, 1981.
- Harrison, R. M., Allan, J., Carruthers, D., Heal, M. R., Lewis, A. C., Marnier, B., Murrells, T., Williams, A.: Non-exhaust vehicle emissions of particulate matter and VOC from road traffic: A review, *Atmos. Environ.*, 262, 118592, <https://doi.org/10.1016/j.atmosenv.2021.118592>, 2021.
- 190 Hsieh, C. C., Chen, H. Y., and Ho, T. Y.: The effect of aerosol size on Fe solubility and deposition flux: A case study in the East China Sea. *Mar. Chem.*, 241, 104106, <https://doi.org/10.1016/j.marchem.2022.104106>, 2022.
- Huang, S. J., Chang, C. Y., Mui, D. T., Chang, F. C., Lee, M. Y., Wang, C. F.: Sequential extraction for evaluating the leaching behavior of selected elements in municipal solid waste incineration fly ash. *J. Hazard. Mater.*, 149, 180–188, <https://doi.org/10.1016/j.jhazmat.2007.03.067>, 2007.
- 195 Iijima, A., Sato, K., Yano, K., Tago, H., Kato, M., Kimura, H., Furuta, N.: Particle size and composition distribution analysis of automotive brake abrasion dusts for the evaluation of antimony sources of airborne particulate matter, *Atmos. Environ.*, 41, 4908–4919, <https://doi.org/10.1016/j.atmosenv.2007.02.005>, 2007.
- Ito, A., and Shi, Z.: Delivery of anthropogenic bioavailable iron from mineral dust and combustion aerosols to the ocean, *Atmos. Chem. Phys.*, 16, 85–99, <https://doi.org/10.5194/acp-16-85-2016>, 2016.
- 200 Ito, A., Myriokefalitakis, S., Kanakidou, M., Mahowald, N. M., Scanza, R. A., Hamilton, D. S., Baker, A. R., Jickells, T., Sarin, M., Bikina, S., Gao, Y., Shelley, R. U., Buck, C. S., Landing, W. M., Bowie, A. R., Perron, M. M. G., GÜieu, C., Meskhidze, N., Johnson, M. S., Feng, Y., Kok, J. F., Nenes, A., Duce, R. A.: Pyrogenic iron: The missing link to high iron solubility in aerosols. *Sci. Adv.*, 5, eaau7671, <https://doi.org/10.1126/sciadv.aau7671>, 2019.
- Ito, A., Ye, Y., Baldo, C., Shi, Z.: Ocean fertilization by pyrogenic aerosol iron, *npj Clim. Atmos. Sci.*, 4, 30, <https://doi.org/10.1038/s41612-021-00185-8>, 2021.
- 205 Jeong, G. Y., Achterberg, E. P.: Chemistry and mineralogy of clay minerals in Asian and Saharan dusts and the implications for iron supply to the oceans. *Atmos. Chem. Phys.*, 14, 12415–12428, <https://doi.org/10.5194/acp-14-12415-2014>, 2014.

- Jeong, G. Y., Nousiainen, T.: TEM analysis of the internal structures and mineralogy of Asian dust particles and the implications for optical modeling, *Atmos. Chem. Phys.* 14, 7233–7254, <https://doi.org/10.5194/acp-14-7233-2014>, 2014.
- 210 Jeong, G. Y.: Mineralogy and geochemistry of Asian dust: dependence on migration path, fractionation, and reactions with polluted air, *Atmos. Chem. Phys.*, 20, 7411–7428, <https://doi.org/10.5194/acp-20-7411-2020>, 2020.
- Jickells, T. D., An, Z. S., Andersen, K. K., Baker, A. R., Bergametti, G., Brooks, N., Cao, J. J., Boyd, P. W., Duce, R. A., Hunter, K. A., Kawahata, H., Kubilay, N., laRoche, J., Liss, P. S., Mahowald, N., Prospero, J. M., Ridgwell, A. J., Tegen, I., and Torres, R.: Global iron connections between desert dust, ocean biogeochemistry, and climate. *Science*, 308, 67–71, 215 <https://doi.org/10.1126/science.1105959>, 2005.
- Jickells, T. D., Baker, A. R., Chance, R.: Atmospheric transport of trace elements and nutrients to the oceans, *Phil. Trans. R. Soc. A*, 374, 20150286, <http://dx.doi.org/10.1098/rsta.2015.0286>, 2016.
- Journet, E., Desboeufs, K. V., Caquineau, S., Colin, J. L.: Mineralogy as a critical factor of dust iron solubility, *Geophys. Res. Lett.*, 35, L07805, <https://doi.org/10.1029/2007GL031589>, 2008.
- 220 Kajino, M., Hagino, H., Fujitani, Y., Morikawa, T., Fukui, T., Onishi, K., Okuda, T., Kajikawa, T., Igarashi, Y.: Modeling transition metals in East Asia and Japan and its emission sources, *GeoHealth*, 4, e2020GH00259, <https://doi.org/10.1029/2020GH000259>, 2020.
- Kakavas, S., Patoulias, D., Zakoura, M., Nenes, A., Pandis, S. N.: Size-resolved aerosol pH over Europe during summer, *Atmos. Chem. Phys.*, 21, 799–811, <https://doi.org/10.5194/acp-21-799-2021>, 2021.
- 225 Karydis, V. A., Tsimpidi, A. P., Pozzer, A., Astitha, M., Lelieveld, J.: Effect of mineral dust on global atmospheric nitrate concentrations, *Atmos. Chem. Phys.*, 16, 1491–1509, <https://doi.org/10.5194/acp-16-1491-2016>, 2016.
- Kim, A. G., Kazonich, G., Dahlberg, M.: Relative solubility of cations in class F fly ash, *Environ. Sci. Technol.*, 37, 4507–4511, <https://doi.org/10.1021/es0263691>, 2003.
- Kodama, H., Schnitzer, M.: Dissolution of chlorite minerals by fulvic acid, *Can. J. Soil Sci.*, 53, 240–243, 230 <https://doi.org/10.4141/cjss73-036>, 1973.
- Komonweeraket, K., Cetin, B., Aydilek, A. H., Benson, C. H., Edil, T. B.: Effects of pH on the leaching mechanisms of elements from fly ash mixed soils, *Fuel*, 140, 788–802, <http://dx.doi.org/10.1016/j.fuel.2014.09.068>, 2015.
- Kukier, U., Ishak, C. F., Sumner, M. E., Miller, W. P.: Composition and element solubility of magnetic and non-magnetic fly ash fractions, *Environ. Pollut.*, 123, 255–266, [https://doi.org/10.1016/S0269-7491\(02\)00376-7](https://doi.org/10.1016/S0269-7491(02)00376-7), 2003.
- 235 Kurisu, M., Adachi, K., Sakata, K., and Takahashi, Y.: Stable isotope ratios of combustion iron produced by evaporation in a steel plant, *ACS Earth Space Chem.*, 3, 588–598, <https://doi.org/10.1021/acsearthspacechem.8b00171>, 2019.
- Kurisu, M., Sakata, K., Miyamoto, C., Takaku, Y., Iizuka, T., Takahashi, Y.: Variation of iron isotope ratios in anthropogenic materials emitted through combustion processes, *Chem. Lett.*, 45, 970–972, <https://doi.org/10.1246/cl.160451>, 2016b.
- Kurisu, M., Sakata, K., Uematsu, M., Ito, A., and Takahashi, Y.: Contribution of combustion Fe in marine aerosols over the 240 northwestern Pacific estimated by Fe stable isotope ratios, *Atmos. Chem. Phys.*, 21, 16027–16050, <https://doi.org/10.5194/acp-21-16027-2021>, 2021.

- Kurusu, M., Takahashi, Y., Iizuka, T., and Uematsu, M.: Very low isotope ratio of iron in fine aerosols related to its contribution to the surface ocean, *J. Geophys. Res. Atmos.*, 121, 11119–11136, <https://doi.org/10.1002/2016JD024957>, 2016a.
- Li, R., Zhang, H., Wang, F., He, Y., Huang, C., Luo, L., Dong, S., Jia, X., Tang, M.: Mass fractions, solubility, speciation and isotopic compositions of iron in coal and municipal waste fly ash, *Sci. Total Environ.*, 838, 155974, <http://dx.doi.org/10.1016/j.scitotenv.2022.155974>, 2022.
- Li, S., Zhang, B., Wu, D., Li, Z., Chu, S. Q., Ding, X., Tang, X., Chen, J., Li, Q.: Magnetic particles unintentionally emitted from anthropogenic sources: Iron and steel plants, *Environ. Sci. Technol., Lett.*, 8, 295–300, <https://doi.org/10.1021/acs.estlett.1c00164>, 2021.
- 250 Li, W., Xu, L., Liu, X., Zhang, J., Lin, Y., Yao, X., Gao, H., Zhang, D., Chen, J., Wang, W., Harrison, R. M., Zhang, X., Shao, L., Fu, P., Nenes, A., and Shi, Z.: Air pollution-aerosol interactions produce more bioavailable iron for ocean ecosystems. *Sci. Adv.*, 3, e1601749, <https://doi.org/10.1126/sciadv.1601749>, 2017.
- ~~Liu, Y., Fan, Lin, Q., Chen, Bi, X., Zhao, J., Ling, Z., Hong, Zhang, G., Yang, Y., Peng, L., Lian, X., Fu, Y., Li, W. M., Chen, X. D., Miller, M., Ou, J., Tang, M., Wang, M., Wei, X.: Modeling the impact of chlorine emissions from coal combustion and prescribed waste incineration on tropospheric ozone., Peng, P., Sheng, G., Zhou, Z. In-cloud formation of secondary species in iron-containing particles, *Atmos. Chem. Phys.*, 19, 1195–1206. <https://doi.org/10.5194/acp-19-1195-2019>, 2019.~~
- 255 ~~Liu, L., Li, W., Lin, Q., Wang, Y., Zhang, J., Zhu, Y., Yuan, Q., Zhou, S., Zhang, D., Baldo, C., Shi, Z.: Size-dependent aerosol iron solubility in an urban atmosphere, *NPJ Clim. Atmos. Sci.*, 5, 54, <https://doi.org/10.1038/s41612-022-00277-z>, 2022.~~
- 260 ~~Liu, L., Zhang, J., Xu, L., Yuan, Q., Chen, J., Shi, Z., Sun, Y., Fu, P., Wang, Z., Zhang, D., Li, W.: Cloud scavenging of anthropogenic refractory particles at a mountain site in North China, *Atmos. Chem. Phys.*, 18, 2709–2724, <https://doi.org/10.5194/acp-18-2709-2018>, 2018.~~
- ~~Liu, X., Turner, J. R., Hand, J. L., Schichtel, B. A., Martin, R. V.: A global-scale mineral dust equation, *J. Geophys. Res. Atmos.*, 127, e2022JD036937, <https://doi.org/10.1029/2022JD036937>, 2022.~~
- Lowson, R. T., Comarmond, J., Rajaratnam, G., Brown, P. L.: The kinetics of the dissolution of chlorite as a function of pH and at 25°C, *Geochim. Cosmochim. Acta*, 69, 1687–1699, <https://doi.org/10.1016/j.gca.2004.09.028>, 2005.
- Mahowald, N. M., Engelstaedter, S., Luo, C., Sealy, A., Artaxo, P., Benitez-Nelson, C., Bonnet, S., Chen, Y., Chuang, P. Y., Cohen, D. D., Dulac, F., Herut, B., Johansen, A. M., Kubilay, N., Losno, R., Maenhaut, W., Paytan, A., Prospero, J. M., Shank, L. M., Siefert, R. L.: Atmospheric iron deposition: Global distribution, variability and human perturbations. *Annu. Rev. Mar. Sci.* 1, 245–278, <https://doi.org/10.1146/annurev.marine.010908.163727>, 2009.
- 270 Mahowald, N. M., Hamilton, D. S., Mackey, K. R. M., Moore, J. K., Baker, A. R., Scanza, R. A. and Zhang, Y.: Aerosol trace metal leaching and impacts on marine microorganisms, *Nat. Commun.*, 9(1), 1–15, <https://doi.org/10.1038/s41467-018-04970-7>, 2018.
- Marcotte, A. R., Anbar, A. D., Majestic, B. J., Herckes, P.: Mineral dust and iron solubility: Effects of composition, particles size, and surface area, *Atmos.*, 11, 533, <https://doi.org/10.3390/atmos11050533>, 2020.

- 275 Martin, J. H., and Fitzwater, S. E.: Iron deficiency limits phytoplankton growth in the north-west Pacific subarctic, *Nature*, 331, 341–343, <https://doi.org/10.1126/science.1105959>, 1988.
- Martin, J. H., Coale, K. H., Johnson, K. S., Fitzwater, S. E., Gordon, R. M., Tanner, S. J., Hunter, C. N., Elrod, V. A., Nowicki, J. L., Coley, T. L., Barber, R. T., Lindley, S., Watson, A. J., van Scoy, K., Law, C. S., Liddicoat, M. I., Lng, R., Stanton, T., Stockel, J., Collings, C., Anderson, A., Bidigare, R., Ondrusek, M., Latasa, M., Millero, F. J., Lee, K., Yao, W., Zhang, J. Z.
- 280 Friederich, G., Sakamoto, C., Chavez, F., Buck, K., Kolber, Z., Greene, R., Falkowski, P., Chisholm, S. W., Hoge, F., Swift, R., Yungel, J., Turner, S., Nightingale, P., Hatton, A., Liss, P., Tindale, N. W. Testing the iron hypothesis in ecosystems of the equatorial Pacific Ocean. *Nature*, 371, 123–129, <https://doi.org/10.1038/371123a0>, 1994.
- Martin, J. H.: Glacial-interglacial CO<sub>2</sub> change: The iron hypothesis, *Paleoceanogr.*, 5, 1, 1–13, <https://doi.org/10.1029/PA005i001p00001>, 1990.
- 285 Martínez-García, A., Rosell-Melé, A., Geibert, W., Gersonde, R., Masqué, P., Gaspari, V., Barbante, C.: Links between iron supply, marine productivity, sea surface temperature, and CO<sub>2</sub>, over the last 1.1 Ma, *Paleoceanogr.*, 24, PA1207, <https://doi.org/10.1029/2008PA001657>, 2009.
- Martínez-García, A., Rosell-Melé, A., Jaccard, S. L., Geibert, W., Sigman, D. M., Haug, G. H.: Southern Ocean dust-climate coupling over the past four million years, *Nature*, 476, 312–316, <https://doi.org/10.1038/nature10310>, 2011.
- 290 Martínez-García, A., Sigman, D. M., Ren, H., Anderson, R. F., Straub, M., Hodell, D. A., Jaccard, S. L., Eglinton, T. I., Haug, G. H.: Iron fertilization of the subantarctic Ocean during the last ice age. *Science*, 343, 1347–1350, <https://doi.org/10.1126/science.1246848>, 2014.
- ~~Maters, E. C., Mulholland, D. S., Flament, P., de Jong, J., Mattielli, N., Deboudt, K., Dhont, G., Bychkov, E.: Laboratory study of iron isotope fractionation during dissolution of mineral dust and industrial ash in simulate cloud water, *Chemosphere*, 299, 134472, <https://doi.org/10.1016/j.chemosphere.2022.134472>, 2022.~~
- 295 McDaniel, M. F. M., Ingall, E. D., Morton, Castorina, E., Weber, R. J., Shelley, R. U., Landing, W. M., Longo, A. F., Feng, Y., Lai, B.: Relationship between atmospheric aerosol mineral surface area and iron solubility, *ACS Earth Space Chem.*, 3, 2443–2451, <https://doi.org/10.1021/acsearthspacechem.9b00152>, 2019.
- ~~Mead, C., Herekes, P., Majestic, B. J., Anbar, A.D.: Source apportionment of aerosol iron in the marine environment using iron isotope analysis, *Geophys. Res. Lett.*, 40, 5722–5727, <https://doi.org/10.1002/2013GL057713>, 2013.~~
- ~~Miyamoto, C., Sakata, K., Yamakawa, Y., and Takahashi, Y.: Determination of calcium and sulfate species in aerosols associated with the conversion of its species through reaction processes in the atmosphere and its influence on cloud condensation nucleie activation. *Atmos. Environ.*, 223, 117193, <https://doi.org/10.1016/j.atmosenv.2019.117193>, 2020.~~
- 300 Moore, C. M., Mills, M. M., Arrigo, K. R., Berman-Frank, I., Bopp, L., Boyd, P. W., Galbraith, E. D., Geider, R. J., Guieu, C., Jaccard, S. L., Jickells, T. D., La Roche, J., Lenton, T. M., Mahowald, N. M., Marañón, E., Marinov, I., Moore, J. K., Nakatsuka, T., Oeschies, A., Saito, M. A., Thingsted, T. F., Tsuda, A., and Ulloa, O.: Processes and patterns of oceanic nutrient limitation, *Nature Geosci.*, 6, 701–710, <https://doi.org/10.1038/ngeo1765>, 2013.
- 305

- Nishikawa, M., Batdorj, D., Ukachi, M., Onishi, K., Nagano, K., Mori, I., Matsui, I. and Sano, T.: Preparation and chemical characterisation of an Asian mineral dust certified reference material. *Anal. Method.*, 5, 4088–4095, <https://doi.org/10.1039/C3AY40435H>, 2013.
- 310 Nozaki, Y.: Elemental Distribution, in: *Encyclopedia of Ocean Sciences*, edited by: Steele, J. H., Thorpe, S. A., and Turekian, K. K., Academic, San Diego, *Encyclopedia of Ocean Sciences*, 840–845, <https://doi.org/10.1006/rwos.2001.0402>, 2001.
- Nriagu, J. O., and Pacyna, J. M.: Quantitative assessment of worldwide contamination of air, water and soils by trace metals, *Nature*, 333, 134–139, <https://doi.org/10.1038/333134a0>, 1988.
- 315 Oakes, M., Ingall, E. D., Lai, B., Shafer, M. M., Hays, M. D., Liu, Z. G., Russell, A. G., Weber, R. J.: Iron solubility related to particle sulfur content in source emission and ambient fine particles, *Environ. Sci. Technol.*, 46, 6637–6644, <https://doi.org/10.1021/es300701c>, 2012.
- Pacyna, J. M., Pacyna, E.G.: An Assessment of Global and Regional Emissions of Trace Metals to the Atmosphere from Anthropogenic Sources Worldwide. *Environmental Research*, 9, 269–298, <https://doi.org/10.1139/a01-012>, 2001.
- 320 Paris, R. and Desboeufs, K. V.: Effect of atmospheric organic complexation on iron-bearing dust solubility, *Atmos. Chem. Phys.*, 13, 4895–4905, <https://doi.org/10.5194/acp-134895-2013>, 2013.
- Praharaj, T., Powell, M. A., Hart, B. R., Tripathy, S.: Leachability of elements from sub-bituminous coal fly ash from India. *Environ. Int.*, 27, 609–615, [https://doi.org/10.1016/S0160-4120\(01\)00118-0](https://doi.org/10.1016/S0160-4120(01)00118-0), 2002.
- Pye, H. O. T., Nenes, A., Alexander, B., Ault, A. P., Barth, M. C., Clegg, S. L., Collett Jr., J. L., Fahey, K. M., Hennigan, C. J., Herrmann, H., Kanakidou, M., Kelly, J. T., Ku, I. T., McNeill, V. F., Riemer, N., Schaefer, T., Shi, G., Tilgner, A., Walker, J. T., Wang, T., Weber, R., Xing, J., Zaveri, R. A., Zuend, A.: The acidity of atmospheric particles and clouds. *Atmos. Chem. Phys.*, 20, 4809–4888, <https://doi.org/10.5194/acp-20-4809-2020>, 2020.
- Rivera, N., Kaur, N., Hesterberg, D., Ward, C. R., Austin, R. E., Duckworth, O. W.: Chemical composition, speciation and elemental associations in coal fly ash samples related to the Kingston ash spill, *Energy Fuels*, 29, 954–967, <https://doi.org/10.1021/ef501258m>, 2015.
- 330 Sakata, K., Kurisu, M., Takeichi, Y., Sakaguchi, A., Tanimoto, H., Tamenori, Y., Matsuki, A., Takahashi, Y.: Iron (Fe) speciation in size-fractionated aerosol particles in the Pacific Ocean: The role of organic complexation of Fe with humic-like substances in controlling Fe solubility, *Atmos. Chem. Phys.*, 22, 9461–9482, <https://doi.org/10.5194/acp-22-9461-2022>, 2022.
- Sakata, K., Kurisu, M., Tanimoto, H., Sakaguchi, A., Uematsu, M., Miyamoto, C., and Takahashi, Y.: Custom-made PTFE filters for ultra-clean size-fractionated aerosol sampling for trace metals, *Mar. Chem.*, 206, 100–108, <https://doi.org/10.1016/j.marchem.2018.09.009>, 2018.
- 335 Sakata, K., Sakaguchi, A., Yokoyama, Y., Terada, Y., Takahashi, Y.: Lead speciation studies on coarse and fine aerosol particles by bulk and micro X-ray absorption fine structure spectroscopy. *Geochem. J.*, 51, 215–225, <https://doi.org/10.2343/geochemj.2.0456>, 2017.



- 340 Sakata, K., Sakaguchi, A., Tanimizu, M., Takaku, Y., Yokoyama, Y., and Takahashi, Y.: Identification of sources of lead in the atmosphere using X-ray absorption near-edge structure (XANES) spectroscopy, *J. Environ. Sci.*, 26, 343–352, [https://doi.org/10.1016/S1001-0742\(13\)60430-1](https://doi.org/10.1016/S1001-0742(13)60430-1), 2014.
- Sakata, M., Kurata, M., Tanaka, N.: Estimating contribution from municipal solid waste incineration to trace metal concentrations in Japanese urban atmosphere using lead as a marker element, *Geochem. J.*, 34, 23–32, <https://doi.org/10.2343/geochemj.34.23>, 2000.
- 345 Schlitzer, R.: Ocean Data View, <https://odv.awi.de> (last access: 4 November 2022), 2021.
- Schroth, A. W., Crusius, J., Sholkovitz, E. R., and Bostick, B. C.: Iron solubility driven by speciation in dust sources to the ocean, *Nature Geosci.*, 2, 337–340, <https://doi.org/10.1038/ngeo501>, 2009.
- Sedwick, P. N., Sholkovitz, E. R., Church, T. M.: Impact of anthropogenic combustion emissions on the fractional solubility of aerosol iron: Evidence from the Sargasso Sea, *Geochem. Geophys. Geosyst.*, 8, Q10Q06, <https://doi.org/10.1029/2007GC001586>, 2007.
- 350 Seidel, A., Zimmels, Y.: Mechanism and kinetics of aluminium and iron leaching from coal fly ash by sulfuric acid. *Chem. Eng. Sci.*, 53, 3535–3852, [https://doi.org/10.1016/S0009-2509\(98\)00201-2](https://doi.org/10.1016/S0009-2509(98)00201-2), 1998.
- Shah, V., Jacob, D. J., Moch, J. M., Wang, X., Zhai, S.: Global modelling of cloud water acidity, precipitation acidity, and acid inputs to ecosystems, *Atmos. Chem. Phys.*, 20, <https://doi.org/10.5194/acp-20-12223-2020>, 2020.
- 355 Shelley, R. U., Landing, W. M., Ussher, S. J., Planquette, H., and Sarthou, G.: Regional trends in the fractional solubility of Fe and other metals from North Atlantic aerosols (GEOTRACES cruises GA01 and GA03) following a two-stage leach, *Biogeosci.*, 15, 2271–2288, <https://doi.org/10.5194/bg-15-2271-2018>, 2018.
- Shi, Z. B., Woodhouse, M. T., Carslaw, K. S., Krom, M. D., Mann, G. W., Baker, A. R., Savov, I., Fones, G. R., Brooks, B., Drake, N., Jickells, T. D., Benning, L. G.: Minor effect of physical size sorting on iron solubility of transported mineral dust, *Atmos. Chem. Phys.*, <https://doi.org/10.5194/acp-11-8459-2011>, 11, 8459–8469, 2011.
- 360 Sholkovitz, E. R., Sedwick, P. N., and Church, T. M.: Influence of anthropogenic combustion emissions on the deposition of soluble aerosol iron to the ocean: Empirical estimates for island sites in the North Atlantic, *Geochim. Cosmochim. Acta*, 73, 14, 3981–4003, <https://doi.org/10.1016/j.gca.2009.04.029>, 2009.
- 365 Sholkovitz, E. R., Sedwick, P. N., Church, T. M., Baker, A. R., Powell, C. F.: Fractional solubility of aerosol iron: Synthesis of a global-scale data set, *Geochim. Cosmochim. Acta*, 89, 173–189, <http://dx.doi.org/10.1016/j.gca.2012.04.022>, 2012.
- Shupert, L. A., Ebbs, S. D., Lawrence, J., Gibson, D. J., Filip, P.: Dissolution of copper and iron from automotive brake pad wear debris enhances growth and accumulation by the invasive macrophyte *Salvinia molesta* Mitchell, *Chemosphere*, 92, 45–51, <http://dx.doi.org/10.1016/j.chemosphere.2013.03.002>, 2013.
- 370 Simoneit, B. R. T.: Biomass burning — a review of organic tracers for smoke from incomplete combustion, *Appl. Geochem.*, 17, 129–162, [https://doi.org/10.1016/S0883-2927\(01\)00061-0](https://doi.org/10.1016/S0883-2927(01)00061-0), 2002.
- Song, Q., Osada, K.: Seasonal variation of aerosol acidity in Nagoya, Japan and factors affecting it, *Atmos. Environ.*, 5, 200062, <https://doi.org/10.1016/j.aea.2020.100062>, 2020.

- Stein, A. F., Draxler, R. R., Rolph, G. D., Stunder, B. J. B., Cohen, M. D. and Ngan, F.: Noaa's hysplit atmospheric transport and dispersion modeling system, *Bull. Am. Meteorol. Soc.*, 96, 2059–2077, <https://doi.org/10.1175/BAMS-D-14-00110.1>, 2015.
- Sullivan, R. C., Guazzotti, S. A., Sodeman, D. A., and Prather, K. A.: Direct observations of the atmospheric processing of Asian mineral dust, *Atmos. Chem. Phys.*, 7, 1213–1236, <https://doi.org/10.5194/acp-7-1213-2007>, 2007a. ~~2007.~~
- ~~Sullivan, R. C., Guazzotti, S. A., Sodeman, D. A., Tang, Y., Carmichael, G. R., Prather, K. A.: Mineral dust is a sink for chlorine in the marine boundary layer, *Atmos. Environ.*, 41, 7166–7179, <https://doi.org/10.1016/j.atmosenv.2007.05.047>, 2007b.~~
- Tagliabue, A., Bowie, A. R., Boyd, P. W., Buck, K. N., Johnson, K. S., Saito, M. A.: The integral role of iron in ocean biogeochemistry, *Nature*, 543, 51–59, <https://doi.org/10.1038/nature21058>, 2017.
- ~~Takahashi Y, Furukawa, T., Kanai, Y., Uematsu, M., Zheng, G., Marcus, M. A.: Seasonal changes in Fe species and soluble Fe concentration in the atmosphere in the Northwest Pacific region based on the analysis of aerosols collected in Tsukuba, Japan, *Atmos. Chem. Phys.*, 13, 7695–7710, <https://doi.org/10.5194/acp-13-7695-2013>, 2013.~~
- Takahashi, Y., Higashi, M., Furukawa, T., and Mitsunobu, S.: Change of iron species and iron solubility in Asian dust during the long-range transport from western China to Japan, *Atmos. Chem. Phys.*, 11, 11237–11252, <https://doi.org/10.5194/acp-11-11237-2011>, 2011.
- Tao, Y., Murphy, J. G.: The mechanisms responsible for the interactions among oxalate, pH, and Fe dissolution in PM<sub>2.5</sub>, *ACS Earth Space Chem.*, 3, 2259–2265, <https://doi.org/10.1021/acsearthspacechem.9b00172>, 2019b.
- Tao, Y., Murphy, J. G.: The sensitivity of PM<sub>2.5</sub> acidity to meteorological parameters and chemical composition changes: 10-year records from six Canadian monitoring sites, *Atmos. Chem. Phys.*, 19, 9309–9320, <https://doi.org/10.5194/acp-19-9309-2019>, 2019a.
- Taylor, S. R.: Abundance of chemical elements in the continental crust: a new table, [https://doi.org/10.1016/0016-7037\(64\)90129-2](https://doi.org/10.1016/0016-7037(64)90129-2), *Geochim. Cosmochim. Acta*, 28, 1273–1285, 1964.
- Tian., S., Pan, Y., Liu, Z., Wen, T., Wang, Y.: Size-resolved aerosol chemical analysis of extreme haze pollution events during early 2013 in urban Beijing, China, <https://doi.org/10.1016/j.jhazmat.2014.07.023>, *J. Hazard. Mater.*, 279, 452–460, 2014.
- ~~Tobo, Y., Zhang, D., Matsuki, A., Iwasaka, Y.: Asian dust particles converted into aqueous droplets under remote marine atmospheric conditions, *Proc. Natl. Acad. Sci. U.S.A.*, 107, 17905–17910, <https://doi.org/10.1073/pnas.1008235107>, 2010.~~
- ~~Uematsu, M.; Duce, R. A., Prospero, J. M., Chen, L., Merrill, J. T., McDonald, R. L.: Transport of mineral aerosol from Asia over the north Pacific Ocean. *J. Geophys. Res.*, 88, 5343–5352, <https://doi.org/10.1029/JC088iC09p05343>, 1983.~~
- Uno, I., Stake, S., Carmichael, G. R., Tang, Y., Wang, Z., Takemura, T., Sugimoto, N., Shimizu, A., Murayama, T., Cahill, T. A., Cliff, S., Uematsu, M., Ohta, S., Quinn, P. K., Bates, T. S.: Numerical study of Asian dust transport during the springtime of 2001 simulated with the Chemical Weather Forecasting System (CFORS) model, *J. Geophys. Res.*, 109, D19S24, <https://doi.org/10.1029/2003JD004222>, 2004.
- Wählén, P., Berkowicz, R., Palmgren, F.: Characterisation of traffic-generated particulate matter in Copenhagen, *Atmos. Environ.*, 40, 2151–2159, <https://doi.org/10.1016/j.atmosenv.2005.11.049>, 2006.

- Wang, Y.S., Yao, L., Wang, L.L., Liu, Z.R., Ji, D.S., Tang, G.Q., Zhang, J., Sun, Y., Hu, B., Xin, J. Y.: Mechanism for the formation of the January 2013 heavy haze pollution episode over central and eastern China, *Sci. China Earth Sci.*, 57, 1, 14-25, <https://doi.org/10.1007/s11430-013-4773-4>, 2014.
- Wang, Z., Fu, H., Zhang, L., Song, W., and Chen, J.: Ligand-promoted photoreductive dissolution of goethite by atmospheric low-molecular dicarboxylates, *J. Phys. Chem. A*, 121, 16471656, <https://doi.org/10.1021/acs.jpca.6b09160>, 2017.
- ~~Wang, Z., Wang, T., Fu, H., Zhang, L., Tang, M., George, C., Grassian, V. H., Chen, J.: Enhanced heterogeneous uptake of sulfur dioxide on mineral particles through modification of iron speciation during simulated cloud processing, *Atmos. Chem. Phys.*, 19, <https://doi.org/10.5194/acp-19-12569-2019>, 2019.~~
- ~~Zhang, H., Li, R., Dong, S., Wang, F., Zhu, Y., Meng, H., Huang, C., Ren, Y., Wang, X., Hu, X., Li, T., Peng, C., Zhang, G., Xue, L., Wang, X., Tang, M.: Abundance and fractional solubility of aerosol iron during winter at a coastal city in Northern China: Similarities and contrasts between fine and coarse particles *J. Geophys. Res. Atmos.*, 127, e2021JD036070, <https://doi.org/10.1029/2021JD036070>, 2022.~~
- ~~Zhang, H., Li, R., Huang, C., Wu, C., Wang, G., Cao, C., Li, J., Li, X., Dong, S., Wang, F., Li, T., Chen, Y., Zhang, G., Ren, Y., Chen, Q., Huang, R. J., Chen, S., Xue, T., Wang, X., Tang, M.: Seasonal variation of aerosol iron solubility in coarse and fine particles at an inland city in northwestern China, *Atmos. Chem. Phys.*, 23, 3543–3559, <https://doi.org/10.5194/acp-23-3543-2023>, 2023.~~
- ~~J., Wu, F., Huang, R., Cao, J., Han, Y., Ge, S., Xie, Y., Xue, G., Wang, X.: Chemical characteristics of airborne particles in Xi'an inland China during dust storm episodes: Implications for heterogeneous formation of ammonium nitrate and enhancement of N deposition, *Environ. Pollut.*, 244, 877–884, <https://doi.org/10.1016/j.envpol.2018.10.019>, 2019.~~
- ~~Wu, C., Zhang, G., Wang, G., Lv, S., Li, D., Liu, L., Li, J., Liu, S., Du, W., Meng, J., Qiao, L., Zhou, M., Huang, C., Wang, H.: Efficient heterogeneous formation of ammonium nitrate on the saline mineral particle surface in the atmosphere of East Asia during dust storm periods, *Environ. Sci. Technol.*, 54, 15622–156320, <https://dx.doi.org/10.1021/acs.est.0c04544>, 2020.~~
- ~~Yu, J., Yan, C., Liu, Y., Li, X., Zhou, T., Zheng, M.: Potassium: a tracer for biomass burning in Beijing? *Aerosol Air Qual. Res.*, 18, 2447–2459, <https://doi.org/10.4209/aaqr.2017.11.0536>, 2018.~~
- Zhang, L., Wang, Q., Sata, A., Ninomiya, Y., Yamashita, T.: Interactions among inherent minerals during coal combustion and their impacts on the emission of PM<sub>10</sub>. 2. Emission of submicrometer-sized particles, *Energy Fuels*, 21, 766–777, <https://doi.org/10.1021/ef060308x>, 2007.
- Zhu, Q., Liu, Y., Shao, T., Tang, Y.: Transport of Asian aerosols to the Pacific Ocean, *Atmos. Res.*, 234, 104735, <https://doi.org/10.1016/j.atmosres.2019.104735>, 2020.
- Zhu, Y., Li, W., Lin, Q., Yuan, Q., Liu, L., Zhang, J., Zhang, Y., Shao, L., Niu, H., Yang, S., Shi, Z.: Iron solubility in fine particles associated with secondary acidic aerosols in east China, *Environ. Pollut.*, 264, 114769, <https://doi.org/10.1016/j.envpol.2020.114769>, 2020.

- 440 Zhu, Y., Li, W., Wang, Y., Zhang, J., Liu, L., Xu, L., Xu, J., Shi, J., Shao, L., Fu, P., Zhang, D., Shi, Z.: Sources and processes of iron aerosols in a megacity in Eastern China, *Atmos. Chem. Phys.*, 22, 2191–2202, <https://doi.org/10.5194/acp-22-2191-2022>, 2022.
- Zuo, P., Huang, Y., Liu, P., Zhang, J., Yang, H., Liu, L., Bi, J., Lu, D., Zhang, Q., Liu, Q., Jiang, G.: Stable iron isotopic signature reveals multiple sources of magnetic particulate matter in the 2021 Beijing sandstorms, *Environ. Sci. Technol. Lett.*, 9, 299–305, <https://doi.org/10.1021/acs.estlett.2c00144>, 2022.
- 445